

**EXPERIMENTAL INVESTIGATION OF TAILWATER EFFECT ON THE
ENERGY DISSIPATION THROUGH SCREENS**

**A THESIS SUBMITTED TO
THE GRADUATE SCHOOL OF NATURAL AND APPLIED SCIENCES
OF
MIDDLE EAST TECHNICAL UNIVERSITY**

BY

VEDAT ASLANKARA

**IN PARTIAL FULFILLMENT OF THE REQUIREMENTS
FOR
THE DEGREE OF MASTER OF SCIENCE
IN
CIVIL ENGINEERING**

SEPTEMBER 2007

**EXPERIMENTAL INVESTIGATION OF TAILWATER EFFECT ON THE
ENERGY DISSIPATION THROUGH SCREENS**

submitted by **VEDAT ASLANKARA** in partial fulfillment of the requirements for
the degree of **Mater of Science in Civil Engineering Department, Middle East
Technical University** by,

Prof. Dr. Canan ÖZGEN
Dean, Graduate School of **Natural and Applied Sciences**

Prof. Dr. Güney ÖZCEBE
Head of Department, **Civil Engineering**

Assoc. Prof. Dr. Zafer BOZKUŞ
Supervisor, **Civil Engineering Dept., METU**

Prof. Dr. Metin GER
Co-Supervisor, **Civil Engineering Dept., METU**

Examining Committee Members

Assoc. Prof. Dr. İsmail AYDIN (METU, CE)

Assoc. Prof. Dr. Zafer BOZKUŞ (METU, CE)

Prof. Dr. Metin GER (METU, CE)

Assist. Prof. Dr. Şahnaz TİĞREK (METU, CE)

Assoc. Prof. Dr. M. Ali KÖKPINAR (DSİ)

Date: 05.09.2007

I hereby declare that all information in this document has been obtained and presented in accordance with academic rules and ethical conduct. I also declare that, as required by these rules and conduct, I have fully cited and referenced all material and results that are not original to this work.

Name, Last name :Vedat ASLANKARA

Signature :

ABSTRACT

EXPERIMENTAL INVESTIGATION OF TAILWATER EFFECT ON THE ENERGY DISSIPATION THROUGH SCREENS

Aslankara, Vedat

M.Sc., Department of Civil Engineering

Supervisor: Assoc. Prof. Dr. Zafer Bozkuş

Co-Supervisor: Prof. Dr. Metin Ger

September 2007, 87 pages

Previous studies have shown that screens may be utilized efficiently for dissipating the energy of water. For the present study, a series of experimental works are executed to investigate the tailwater and multiple screen effects on the energy dissipation through screens. Water flowing beneath a sliding gate is used to simulate the flow downstream of a hydraulic structure. In the present study, one double screen and two double screen arrangements with porosity of 40% and inclination angle of 90 degree is used. A tailwater gate structure is used to adjust the tailwater depth. The major parameters for the present study are upstream flow depth, tailwater gate height, location of the screen together with the supercritical upstream flow Froude number for a range covering from 5.0 to 22.5. The gate opening simulating a hydraulic structure is adjusted at heights of 2 cm and 3 cm during the study. The results of the experiments show that the tailwater depth has no significant additional contribution on the energy dissipation, whereas multiple screen arrangement dissipates more energy as compared to one double screen arrangement.

Keywords: Screen, energy dissipation, multiple screen, tailwater depth, hydraulic jump, supercritical flow.

ÖZ

ELEKLERLE ENERJİ KIRILIMINA KUYRUKSUYU ETKİSİNİN DENEYSEL OLARAK ARAŞTIRILMASI

Aslankara, Vedat

Yüksek Lisans, İnşaat Mühendisliği Bölümü

Tez Danışmanı: Doç. Dr. Zafer Bozkuş

Yardımcı Tez Danışmanı: Prof. Dr. Metin Ger

Eylül 2007, 87 sayfa

Yakın geçmişte yapılan çalışmalar elek kullanılmasının suyun fazla enerjisini sönmölemek için etkili bir yol olduğunu göstermiştir. Bu çalışma için, eleklerle enerji kırılımına kuyruksuyu ve birden fazla elek kullanılmasının etkilerini araştırmak amacıyla bir dizi deney yapılmıştır. Bir hidrolik yapının mansabında gerçekleşen akışı göstermek için sürgülü bir kapakla kontrol edilen su akışı kullanılmıştır. Bu çalışmada %40 boşluk oranına sahip dikey olarak yerleştirilen çiftli elekler, bir çiftli elek ve iki çiftli elek düzenlerinde kullanılmıştır. Kuyruksuyu akım derinliğini kontrol etmek için bir kuyruksuyu kapağı kullanılmıştır. Bu çalışmanın ana parametreleri memba su derinliği, kuyruksuyu kapak yüksekliği, eleğin yeri ve 5.0 ile 22.5 arasında değişen memba akımının Froude sayısıdır. Araştırma süresince hidrolik bir yapının benzeşimini sağlayan kapağın açıklık değerleri 2 cm ve 3 cm olarak kullanılmıştır. Deney sonuçları, kuyruksuyu akım derinliğinin enerji kırılımı üzerine dikkate değer artı bir getirisi olmadığını fakat iki çiftli elek düzeninin bir çiftli elek düzenine kıyasla daha fazla enerji kıldığını göstermektedir.

Anahtar Sözcükler : Elek, enerji kırılımı, çoklu elek, kuyruksuyu akım derinliği, hidrolik sıçrama, süperkritik akım.

To my family...

ACKNOWLEDGMENTS

I would like to express my deepest gratitude and appreciation to Assoc. Prof. Dr. Zafer Bozkuş for his guidance and support throughout my whole thesis study.

I would like to thank Prof. Dr. Metin Ger for his constructive discussions during my study.

I owe special thanks to my fiancée Çiğdem Aksungur for her academic and non-academic guidance and trust.

Finally, I would like to express my deepest gratitude to my family for their love, understanding, trust and invaluable support throughout my whole life.

TABLE OF CONTENTS

ABSTRACT	iv
ÖZ	v
DEDICATION	vi
ACKNOWLEDGMENTS	vii
TABLE OF CONTENTS	viii
LIST OF TABLES	x
LIST OF FIGURES	xi
LIST OF SYMBOLS	xiv
CHAPTER	
1. INTRODUCTION.....	1
2. LITERATURE REVIEW.....	3
3. CONCEPTUAL FRAME.....	7
3.1 THEORETICAL ASPECT	7
3.1.1 ONE DOUBLE SCREEN ARRANGEMENT	7
3.1.2 TWO DOUBLE SCREEN ARRANGEMENT	13
3.2 DIMENSIONAL ANALYSIS	16
4. LABORATORY WORK	20
4.1 EXPERIMENTAL SETUP	20
4.1.1 GATES	22
4.1.2 SCREENS	23
4.1.3 ORIFICE METER.....	24
4.2 EXPERIMENTAL PROCEDURE	25

viii

5. RESULTS AND DISCUSSIONS	28
5.1 INTRODUCTION	28
5.2 PERFORMANCE OF THE SYSTEM	29
5.2.1 PERFORMANCE OF THE SYSTEM AT LARGE.....	29
5.2.2 COMPARISON OF THE PRESENT DATA WITH THAT OF PREVIOUS STUDIES.....	39
5.2.3 COMPARISON OF SYSTEM PERFORMANCES BETWEEN ODSA AND TDSA.....	43
5.3 PERFORMANCE OF THE SCREENS.....	47
5.3.1 PERFORMANCE OF THE SCREENS AT LARGE.....	47
5.4 SYSTEM EFFICIENCIES.....	58
5.4.1 COMPARISON OF SYSTEM EFFICIENCIES OF ODSA AND TDSA	62
5.5 SCREEN EFFICIENCIES	64
6. CONCLUSIONS AND RECOMMENDATIONS	68
REFERENCES.....	71
APPENDICES	
A. ORIFICE METER DETAILS	73
B. UNCERTAINTY ANALYSIS OF EXPERIMENTAL DATA.....	76
B.1 UNCERTAINTY ANALYSIS FOR Q.....	77
B.2 UNCERTAINTY ANALYSIS FOR ΔE_{GC1}	78
B.3 UNCERTAINTY ANALYSIS FOR S.....	80
C. EXPERIMENTAL DATA	82

LIST OF TABLES

Table 4.1 The range of the experiments for ODSA	25
Table 4.2 X values and gate openings for ODSA	25
Table 4.3 The range of the experiments for TDSA.....	26
Table 4.4 X values and gate openings for TDSA	26
Table 5.1 Reference key for ODSA	28
Table 5.2 Reference key for TDSA	28
Table C.1 Experimental Data with ODSA.....	82
Table C.2 Experimental Data with TDSA	86

LIST OF FIGURES

Figure 2.1 Plan view of different types of screen arrangements.....	6
Figure 3.1 General sketch and energy loss definitions of the flow for Case 1	9
Figure 3.2 General sketch and energy loss definitions of the flow for Case 2	9
Figure 3.3 General sketch of the flow for Case 3	13
Figure 3.4 General sketch and energy loss definitions for Case 1 in TDSA	14
Figure 3.5 General sketch and energy loss definitions for Case 2 in TDSA	14
Figure 4.1 Side view of the setup.....	22
Figure 4.2 A general view of the setup	22
Figure 4.3 Front and plan views of the double screen with a porosity of 40%.....	24
Figure 5.1 $\Delta E_{GC1}/E_G$ vs. Fr_G for ODSA and its best fit curve.....	31
Figure 5.2a $\Delta E_{GC1}/E_G$ vs. Fr_G for ODSA with different h_t/d and their best fit curves	32
Figure 5.2b $\Delta E_{GC1}/E_G$ vs. Fr_G for ODSA with different h_t/d and their best fit curves	32
Figure 5.3 $\Delta E_{GC1}/E_G$ vs. Fr_G for ODSA with different t/d at $X/d = 99$	33
Figure 5.4 $\Delta E_{GC1}/E_G$ vs. Fr_G for ODSA with different t/d at $X/d = 66$	33
Figure 5.5 $\Delta E_{GC1}/E_G$ vs. Fr_G for ODSA with different X/d for $t/d = 2D$	34
Figure 5.6 $\Delta E_{GC1}/E_G$ vs. Fr_G for ODSA with different X/d for $t/d = 1.33D$	34
Figure 5.7 $\Delta E_{GC1}/E_G$ vs. Fr_G for TDSA and its best fit curve	35
Figure 5.8 $\Delta E_{GC1}/E_G$ vs. Fr_G for TDSA for $t/d = 2D$	36
Figure 5.9 $\Delta E_{GC1}/E_G$ vs. Fr_G for TDSA for $t/d = 1.33D$	36
Figure 5.10 $\Delta E_{GC1}/E_G$ vs. Fr_G for TDSA at $X_1/d = 66$	37
Figure 5.11 $\Delta E_{GC1}/E_G$ vs. Fr_G for TDSA at $X_1/d = 99$	37
Figure 5.12 $\Delta E_{GC1}/E_G$ vs. Fr_G for TDSA at $X_1/d = 149$	38
Figure 5.13 $\Delta E_{GC1}/E_G$ vs. Fr_G for TDSA with different t/d values	38
Figure 5.14 $\Delta E_{GC1}/E_G$ vs. Fr_G for TDSA with different X_1/d values	39
Figure 5.15 Data of previous studies and its curve based on Equation 5.1	41
Figure 5.16 Data of previous studies and its curve based on Equation 5.5	41

Figure 5.17 Data of all studies and its best fit curve.....	42
Figure 5.18 Çakır (2003) and ODSA data and its best fit curve.....	42
Figure 5.19 Çakır (2003) and TDSA data and its best fit curve	43
Figure 5.20 All the present data with ODSA and TDSA and their best fit curves. ...	44
Figure 5.21 The present data with ODSA and TDSA for $t/d = 1.33D$	45
Figure 5.22 The present data with ODSA and TDSA for $t/d = 2D$	45
Figure 5.23 The present data with ODSA and TDSA at $X_1/d = 66$	46
Figure 5.24 The present data with ODSA and TDSA at $X_1/d = 99$	46
Figure 5.25 S/E_G vs. Fr_G for the ODSA data and its best fit curve.....	48
Figure 5.26 S/E_G vs. Fr_G for the ODSA data at $X/d = 66$	48
Figure 5.27 S/E_G vs. Fr_G for the ODSA data at $X/d = 99$	49
Figure 5.28 S/E_G vs. Fr_G for the ODSA data for $t/d = 1.33D$	49
Figure 5.29 S/E_G vs. Fr_G for the ODSA data for $t/d = 2D$	50
Figure 5.30 S/E_A and $\Delta E_{AC1}/E_A$ vs. Fr_A for $t/d=2D$, $X/d=99$ and $h_t/d=0$	52
Figure 5.31 S/E_A and $\Delta E_{AC1}/E_A$ vs. Fr_A for $t/d=2D$, $X/d=99$ and $h_t/d=1.5\sim 2.7$	52
Figure 5.32 S/E_A and $\Delta E_{AC1}/E_A$ vs. Fr_A for $t/d=2D$, $X/d=99$ and $h_t/d=3.25\sim 6.9$	53
Figure 5.33 S/E_A and $\Delta E_{AC1}/E_A$ vs. Fr_A for $t/d=2D$, $X/d=66$ and $h_t/d=0$	53
Figure 5.34 S/E_A and $\Delta E_{AC1}/E_A$ vs. Fr_A for $t/d=2D$, $X/d=66$ and $h_t/d=2.1$	54
Figure 5.35 S/E_A and $\Delta E_{AC1}/E_A$ vs. Fr_A for $t/d=2D$, $X/d=66$ and $h_t/d=3.9\sim 4.5$	54
Figure 5.36 S/E_A and $\Delta E_{AC1}/E_A$ vs. Fr_A for $t/d=1.33D$, $X/d=66$ and $h_t/d=0$	55
Figure 5.37 S/E_A and $\Delta E_{AC1}/E_A$ vs. Fr_A for $t/d=1.33D$, $X/d=66$ and $h_t/d=1.4$	55
Figure 5.38 S/E_A and $\Delta E_{AC1}/E_A$ vs. Fr_A for $t/d=1.33D$, $X/d=66$ and $h_t/d=3.0$	56
Figure 5.39 S/E_A and $\Delta E_{AC1}/E_A$ vs. Fr_A for $t/d=1.33D$, $X/d=99$ and $h_t/d=0$	56
Figure 5.40 S/E_A and $\Delta E_{AC1}/E_A$ vs. Fr_A for $t/d=1.33D$, $X/d=99$ and $h_t/d=1.4\sim 2.6$	57
Figure 5.41 S/E_A and $\Delta E_{AC1}/E_A$ vs. Fr_A for $t/d=1.33D$, $X/d=99$ and $h_t/d=3.0$	57
Figure 5.42 η_{sys} vs. Fr_G for ODSA with different h_t/d	58
Figure 5.43 η_{sys} vs. Fr_G for ODSA with different h_t/d at $X/d=66$	59
Figure 5.44 η_{sys} vs. Fr_G for ODSA with different h_t/d at $X/d=99$	59
Figure 5.45 η_{sys} vs. Fr_G for ODSA with different h_t/d for $t/d=1.33D$	60
Figure 5.46 η_{sys} vs. Fr_G for ODSA with different h_t/d for $t/d=2D$	60

Figure 5.47 η_{sys} vs. Fr_G for TDSA	61
Figure 5.48 η_{sys} vs. Fr_G for TDSA with different t/d	61
Figure 5.49 η_{sys} vs. Fr_G for TDSA with different X_1/d	62
Figure 5.50 η_{sys} vs. Fr_G for ODSA and TDSA and their best fit curves	63
Figure 5.51 η_{scr} vs. Fr_G for ODSA	65
Figure 5.52 η_{scr} vs. Fr_G for ODSA with different h_t/d at $X/d = 66$	65
Figure 5.53 η_{scr} vs. Fr_G for ODSA with different h_t/d at $X/d = 99$	66
Figure 5.54 η_{scr} vs. Fr_G for ODSA with different h_t/d for $t/d = 1.33D$	66
Figure 5.55 η_{scr} vs. Fr_G for ODSA with different h_t/d for $t/d = 2D$	67
Figure A.1 Orifice-meter details	74
Figure A.2 Variation of C_o with respect to Reynolds number	75
Figure B.1 Relative Uncertainty for Q_j values vs. Re	78
Figure B.2 $\delta\Delta E_{GC}/\Delta E_{GC}$ vs. Fr_G for the present data	79
Figure B.3 $\delta S/S$ vs. Fr_G for the present data	81

LIST OF SYMBOLS

A_0	area of Section 0 of the orifice-meter
A_1	area of Section 1 of the orifice-meter
A_2	area of Section 2 of the orifice-meter
C_0	discharge coefficient of the orifice-meter
C_C	contraction coefficient of the orifice-meter
C_V	contraction coefficient of vena contracta
d	gate opening
D	a symbol to denote double screen configuration
D_0	orifice throat diameter
D_1	pipe diameter in which the orifice meter is mounted
D_{hole}	diameters of the screen holes
E_G	energy at section G
Fr_A	Froude number at Section A
Fr_B	Froude number at Section B
Fr_{C1}	Froude number at Section C_1
Fr_{C2}	Froude number at Section C_2
Fr_E	Froude number at Section E
Fr_G	Froude number at Section G
g	gravitational acceleration
h_L	head loss through the orifice-meter
h_t	tailwater gate height
k	distance between the screens of the double screen
L	theoretical length of a full jump
p	porosity of the screen
p_1	pressure at Section 1 of the orifice-meter
p_2	pressure at Section 2 of the orifice-meter
Q	flow rate

Q_{ideal}	ideal discharge for the orifice-meter
rms	root mean square
Re	Reynolds number
S	energy dissipated due to screen
t	thickness of the screen
V_1	velocity at Section 1 of the orifice-meter
V_2	velocity at Section 2 of the orifice-meter
V_A	average velocity at Section A
V_B	average velocity at Section B
V_{C1}	average velocity at Section C_1
V_{C2}	average velocity at Section C_2
V_E	average velocity at Section E
V_G	average velocity at Section G
w	width of the channel
X_1	distance between the first screen and the gate
X_2	distance between the second screen and the gate
x	distance from the upstream end of the pseudo-jump to the screen
y_A	water depth at Section A
y_{A2}	conjugate depth of y_A
y_B	water depth at Section B
y_{C1}	water depth at Section C_1
y_{C2}	water depth at Section C_2
y_G	water depth at Section G
ΔE_{AB}	energy loss between Sections A and B
ΔE_{AC1}	energy loss between Sections A and C_1
ΔE_{AC2}	energy loss between Sections A and C_2
ΔE_{GC1}	energy loss between Sections G and C_1
ΔE_{GC2}	energy loss between Sections G and C_2
ΔE_{jA}	energy loss due to a full jump at Section A

ΔE_{jG}	energy loss due to a full jump at Section G
α	a non-dimensional parameter defined in Equation 3.3
β	a non-dimensional parameter defined in Equation 3.2
ϕ	diameter ratio of the Sections 0 and 1 for the orifice-meter
γ	specific weight of water
η_{scr}	screen efficiency
η_{sys}	system efficiency
μ	dynamic viscosity of water
ρ	density of water

CHAPTER 1

INTRODUCTION

Control of the velocity and hence the energy of the water flowing downstream of hydraulic structures is one of the main concerns of hydraulic engineers. As water moves through the environment, it may cause erosion and scour which can affect the stability adversely and hence the life time of structures if the excessive energy of the flow is not dissipated.

Flow control structures are used widely in order to keep this excess energy under control; even benefit from it in some cases. These control structures should meet some functional requirements; enough capacity to deliver the design discharge safely and dissipating the necessary amount of energy to protect hydraulic structure and downstream channel from localized erosion and scour.

Stilling basins are the most commonly used control structures. In recent years, an alternative method has been introduced to dissipate the excessive energy of water downstream of small hydraulic structures, that is, the implementation of screens.

Screens or porous baffles have been used in the past for various purposes. The recent studies have shown them to be efficient tools also as an energy dissipater. In order to increase the efficiency, that is, the energy dissipation capability, different models of screens are tested in order to broaden the view on the performance of screens as an alternative method for energy dissipation. Laboratory work done so far suggests that the screens or porous baffles might be useful for energy dissipation downstream of small hydraulic structures.

The present study in a way is a continuation of the previous studies on the energy dissipation of different models of screens. This time, laboratory work and analysis have been performed to investigate mainly the tailwater effect and also secondarily multiple screen effect on the energy dissipation through screens.

Dimensional analysis shows that relative location of the screen, Froude number of the upstream flow, relative tailwater gate height and relative thickness of the screen are the major non-dimensional parameters.

In the present study, experiments are conducted according to the non-dimensional parameters specified in dimensional analysis for a range of Froude numbers from 5.0 to 22.5. Vertically placed one double screen and two double screen arrangements with porosity of 40% are used. A tailwater gate structure is used to adjust the tailwater depth. Moreover, the sliding gate opening simulating a hydraulic structure is adjusted at heights of $d=2$ cm and $d=3$ cm during the study. This height appears in non dimensional terms of X/d , t/d and h_t/d , relative distance for screen location, relative screen thickness, and relative tailwater gate height, respectively. The range of those parameters in the study is varied for X/d from 66 to 149, for t/d from 1.33D to 2D and for h_t/d from 0.0 to 6.9.

In Chapter II, a brief summary of the previous works for different screen configurations as energy dissipaters are presented. In Chapter III, conceptual frame for the present study is introduced. In Chapter IV, the details of the experimental setup and procedure are given. The experimental results with discussions are described in Chapter V. Finally, conclusions of the analysis are drawn in Chapter VI.

CHAPTER 2

LITERATURE REVIEW

The pioneering study on the topic of using screen-type energy dissipaters downstream of small hydraulic structures was introduced by Rajaratnam and Hurlig (2000). Follow up studies were performed by Çakır (2003), Balkış (2004) and Güngör (2005) whose results were published by Bozkuş et al.(2004, 2005, 2006, 2007). The present study, in a way, is a continuation of the studies on the energy dissipation in order to broaden the view on the performance of screens by testing multiple screens' energy dissipative capability on the energy dissipation characteristics taking into consideration the tailwater effect. Above mentioned recent studies are summarized below.

The laboratory experiments by Rajaratnam and Hurlig (2000) on the energy dissipation through screens or porous baffles showed that screens with a porosity of 40% could be effective energy dissipaters. Two series of experiments were conducted in two different horizontal rectangular channels. They performed the main series of experiments in a horizontal rectangular channel 0.45 m wide, 0.43 m deep, and 6.3 m long. A headtank provided flow with a sharp-edged sluice gate. They controlled the tailwater depth by a tailgate located downstream end of the flume. A second series of experiments was performed in another rectangular channel, 0.305 m wide, 0.7 m deep and 6 m long with a sluice gate fitted with a streamlined bottom to produce a supercritical stream with a depth equal to the gate opening. The overall range of supercritical Froude numbers covered in both channels was from 4 to 13. The flow leaving the screen was also supercritical with reduced Froude number. The screen was placed perpendicularly across the flume 1.25 m away from the gate. Three types of screen arrangements, namely, double, single and triangular made of

hard plastic with approximately square holes (of 5 mm sides) were used. The effect of screens resulted in free hydraulic jumps, forced hydraulic jumps, and in some cases submerged jumps. Results showed that energy dissipation by screens was larger than that produced by the conventional hydraulic jump at the same Froude number.

Another investigation on the subject was executed by Çakır (2003). A horizontal rectangular channel with the dimensions of 7.5 m length, 29 cm width and 70 cm height was used. A pressurized tank with a sliding gate was used to simulate a small hydraulic structure. The porosity, thickness and location of the screens are the major parameters together with the supercritical upstream flow Froude number ranging from 4 to 18. Vertical screens made of Plexiglas with the porosities of 20%, 40%, 50%, and 60% were used. The location of the screens was arranged up to 100 times the upstream flow depth. The 2cm, 4cm and 4D (two screens arranged to form a 2cm gap between them) arrangements are constructed using single 1cm thick plexiglas screens (arrangements A, B and C in Figure 2.1). This study also showed that screens could be used as effective energy dissipaters below hydraulic structures.

A follow up investigation on the subject was performed by Balkış (2004). For this case another parameter, inclination of the screen was introduced. The experiments were executed in the same channel as Çakır's (2003). The thickness, location and inclination of the screens are the major parameters together with the supercritical upstream flow Froude number with a range from 5 to 24. The porosity of the screen used in the experiments was 40%. And the inclinations of the screen were tested at the angles of 60°, 75° and 90°. The location of the screens was arranged up to 100 times the upstream flow depth. The 2cm, 4cm and 4D arrangements are constructed using single 1cm thick Plexiglas screens (arrangements A, B and C in Figure 2.1). This study showed that inclination of the screens did not have any further positive effect on the energy dissipation compared to vertically placed screens.

Most recent investigation was performed by Güngör (2005). The experiments were executed in the same channel as Çakır's (2003). For this case triangular screen arrangement was introduced. The inclination angle of the screens was 60 degree. The location of screens and the supercritical upstream flow Froude number with a range from 7.5 to 25.5 are the major parameters. The porosity of the screen used in the experiments was 40%. The gate opening simulating a hydraulic structure was adjusted with various heights of 1 cm, 1.25 cm, 1.6 cm, 1.7 cm, 2 cm, 2.5 cm, 2.7 cm, 3.2 cm and 3.3 cm during the study. The results of the experiments showed that the triangular screen configuration with the same pore geometry has no significant additional contribution on the energy dissipation as compared to vertically placed screens.

Findings of Çakır's study (2003) were presented and published by Bozkuş et al. (2004 and 2007). The conclusions drawn were as follows;

- The porosity of 40% is the optimum porosity for screen-type energy dissipaters, as already noted by Rajaratnam and Hurtig (2000),
- The system performance, $\Delta E_{GC} / E_G$, increases with increasing Froude number,

where E_G is the specific energy just downstream of the gate and ΔE_{GC} is the energy loss between just downstream of the gate and vena contracta point downstream of the screen

- As Froude number increases, system efficiency decreases
- Double screens dissipate more energy than single screens
- Screens were found to be more efficient as energy dissipater than traditional hydraulic jump stilling basins for downstream of small hydraulic structures.

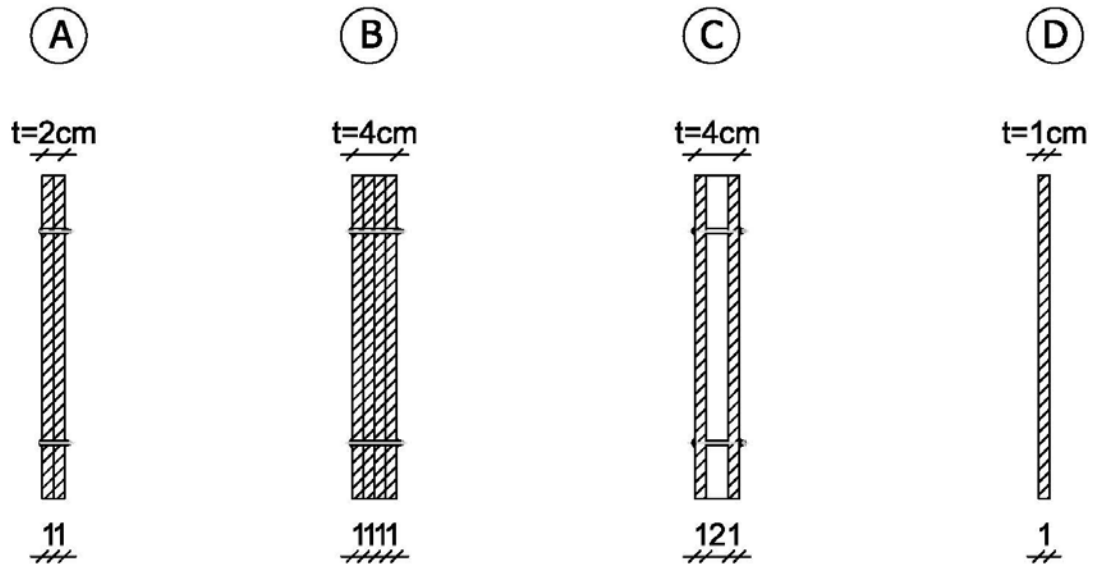


Figure 2.1 Plan view of different types of screen arrangements

CHAPTER 3

CONCEPTUAL FRAME

In the present study, a gate beneath pressurized tank is used to simulate the flow conditions downstream of a small hydraulic structure. The main goal of the study, as stated previously, is to investigate the tailwater and multiple screen effect on the energy dissipation through screens. A tailwater gate structure is introduced as a control structure at the most downstream location to maintain a subcritical flow subsequent to the impingement on the screen. An undular hydraulic jump occurs after passing by the screen because of the presence of the tailwater gate structure. Two double screen arrangement is used to investigate the multiple screen effect on the same experimental setup so that an undular jump occurs again after passing by the second screen.

3.1 THEORETICAL ASPECT

3.1.1 ONE DOUBLE SCREEN ARRANGEMENT

To observe the effect of screens and the tailwater gate structure on the behavior of flow downstream of a gate, several preliminary experiments were performed. It is observed that a supercritical flow may show three distinct behaviors when it encounters a screen with a tailwater gate control downstream. The theoretical framework was constructed using those flow forms. The one double screen arrangement will be called with the abbreviation ODSA thereafter.

CASE 1:

Placing the screen on the channel may generate a full hydraulic jump having the length L far upstream of the screen, Figure 3.1. As shown in the figure, the screen falls in the fully subcritical region. In the laboratory, data collection for each experiment series is always initiated at the highest upstream flow Froude number and highest tail water gate height attainable, for a specified sliding gate opening and position of the screen. Then the tailwater gate is lowered step by step in each data set until it is horizontal and the Froude number of the upstream flow is decreased at this stage. It is observed that flow conditions at Case 1 changes into flow conditions at Case 2 as the tailwater gate is lowered for the same upstream flow Froude number.

CASE 2:

The screen may lead to a pseudo hydraulic jump, just upstream of the screen, Figure 3.2. That is, a jump occurs at the screen and its length is not enough for the jump to be considered a complete hydraulic jump. For this case, energy dissipation through the screen turns out to be much higher than the first case. That is, the effectiveness of the screens is much higher in the second case than in the first case.

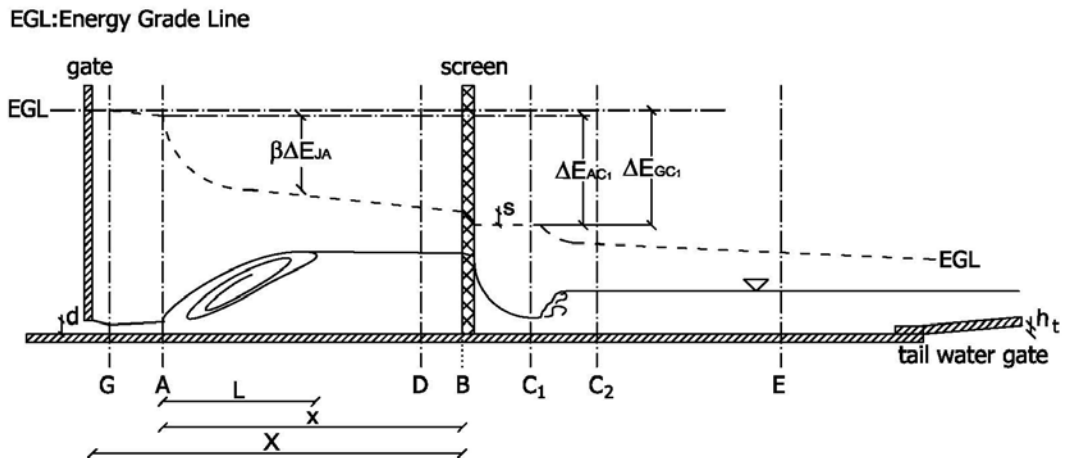


Figure 3.1 General sketch and energy loss definitions of the flow for Case 1

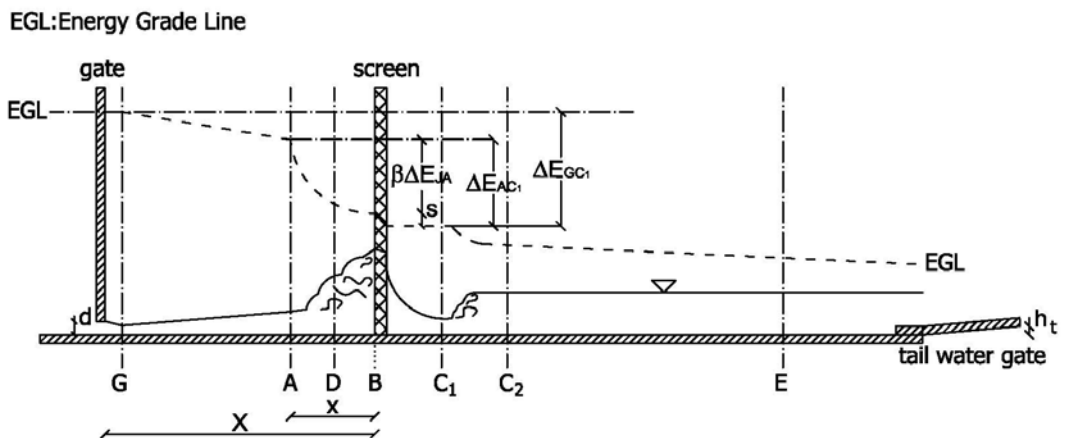


Figure 3.2 General sketch and energy loss definitions of the flow for Case 2

For the analysis of the first two cases the following conceptual frame is constructed. The approach employed for the energy loss computations is the same as that of Çakır (2003).

The definition of all the variables involved in the analysis presented below is depicted in Figures 3.1 and 3.2.

The energy loss between section A and the screen, ΔE_{AB} , is computed by using the below expressions.

$$\Delta E_{AB} = \beta \Delta E_{JA} \quad (3.1)$$

where ΔE_{JA} is designated as the energy loss due to a full jump if there were one occurred at section A and β was defined by Çakır (2003) as

$$\beta = e^{(1-\frac{1}{\alpha})} \quad (3.2)$$

$$\alpha = \frac{x}{L} \quad (3.3)$$

$$\text{For } L > x, \quad 0 < \beta < 1 \quad (3.4)$$

$$\text{For } L \leq x, \quad \beta = 1 \quad (3.5)$$

The length of a fully formed jump, L , is calculated after French (1986), as

$$L = 9.75 y_A (Fr_A - 1)^{1.01} \quad (3.6)$$

where

$$Fr_A = \frac{V_A}{\sqrt{g y_A}} \quad (3.7)$$

in which y_A , Fr_A , V_A are the flow depth, Froude number and flow velocity respectively at section A and g is the gravitational acceleration. On the other hand, energy loss for a complete hydraulic jump can be expressed by

$$\Delta E_{JA} = \left(y_A + \frac{V_A^2}{2g} \right) - \left(y_{A2} + \frac{V_{A2}^2}{2g} \right) \quad (3.8)$$

where y_A is the flow depth at section A, V_A is the velocity at section A, y_{A2} is the subcritical sequent depth of flow and V_{A2} is the velocity at the section where y_{A2} occurs.

The effectiveness of the screen is analyzed either by calculating the system loss, ΔE_{GC1} or by calculating the energy loss through the screen, S. Furthermore, system efficiency η_{sys} and screen efficiency η_{scr} are defined based on those quantities.

The system loss, ΔE_{GC1} is calculated, as

$$\Delta E_{GC1} = \left(y_G + \frac{V_G^2}{2g} \right) - \left(y_{C1} + \frac{V_{C1}^2}{2g} \right) \quad (3.9)$$

$$y_G = C_V \cdot d \quad (3.10)$$

with $C_V=0.610$ after Rajaratnam and Subramanya (1967)

The energy loss at the screen, S, is calculated, as

$$S = \Delta E_{AC1} - \Delta E_{AB} \quad (3.11)$$

that is,

$$S = \left(y_A + \frac{V_A^2}{2g} \right) - \left(y_{C1} + \frac{V_{C1}^2}{2g} \right) - \beta \Delta E_{jA} \quad (3.12)$$

where y_{C1} and V_{C1} are the flow depth and velocity respectively at Section C_1 .

Efficiency of the system is calculated as

$$\eta_{sys} = \frac{\Delta E_{GC_1} - \Delta E_{jG}}{\Delta E_{jG}} \quad (3.13)$$

where ΔE_{jG} is defined as energy loss due to a hypothetical full jump that could have formed at section G.

Efficiency of the screen is calculated as

$$\eta_{scr} = \frac{S}{\Delta E_{jG}} \quad (3.14)$$

CASE 3:

The screen may lead to a submerged hydraulic jump when upstream flow Froude number is relatively low or the tailwater depth is relatively high, Figure 3.3. That is, a submerged jump occurs as soon as the flow leaves the headtank and the screen is in the fully subcritical region. For this case, energy dissipation turns out to be lower than the second case. Therefore, the present study focuses mainly on the first two cases for ODSA. However, the third case is also included for the completeness of the study.

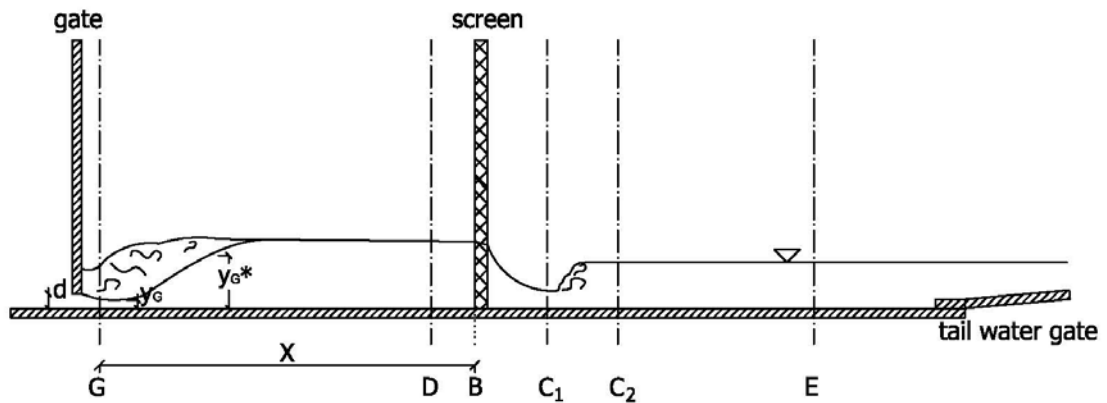


Figure 3.3 General sketch of the flow for Case 3

3.1.2 TWO DOUBLE SCREEN ARRANGEMENT

To observe the effect of multiple screens on the behavior of flow downstream of a gate, several preliminary experiments were performed. It is observed that a supercritical flow may show two distinct behaviors when it encounters multiple screens with a tailwater gate control downstream. The theoretical framework was constructed using those flow forms. The two double screen arrangement will be called with the abbreviation TDSA thereafter.

CASE 1:

Placing two screens on the channel may generate a full hydraulic jump having the length L far upstream of the screen, Figure 3.4. In other words, the screens are in the fully subcritical region. It is observed that by placing two screens, a pseudo jump with one screen and same upstream flow Froude number, may change into a free jump so the screens fall in the fully subcritical region.

CASE 2:

The screens may lead to a submerged hydraulic jump when upstream flow Froude number is below 19, Figure 3.5. That is, a submerged jump occurs as soon as the flow leaves the headtank and the screens are in the fully subcritical region. The present study focuses mainly on the second case for TDSA, because the first case occurs only at very high upstream flow Froude numbers.

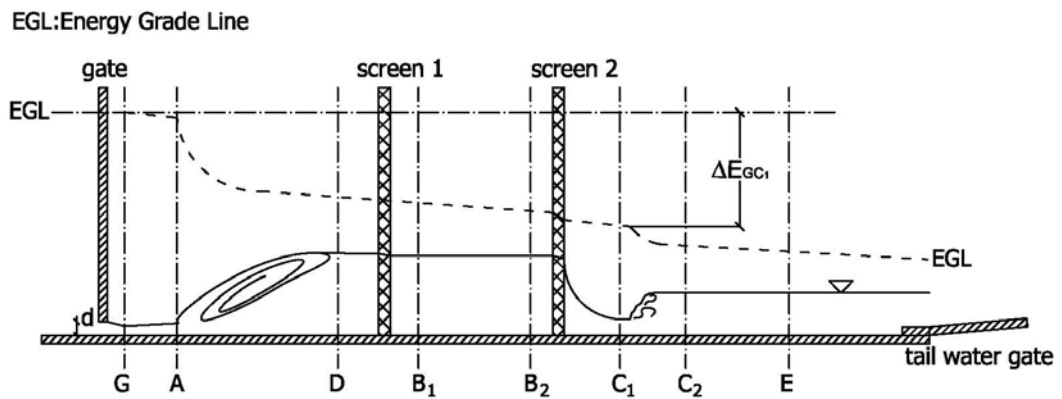


Figure 3.4 General sketch and energy loss definitions for Case 1 in TDSA

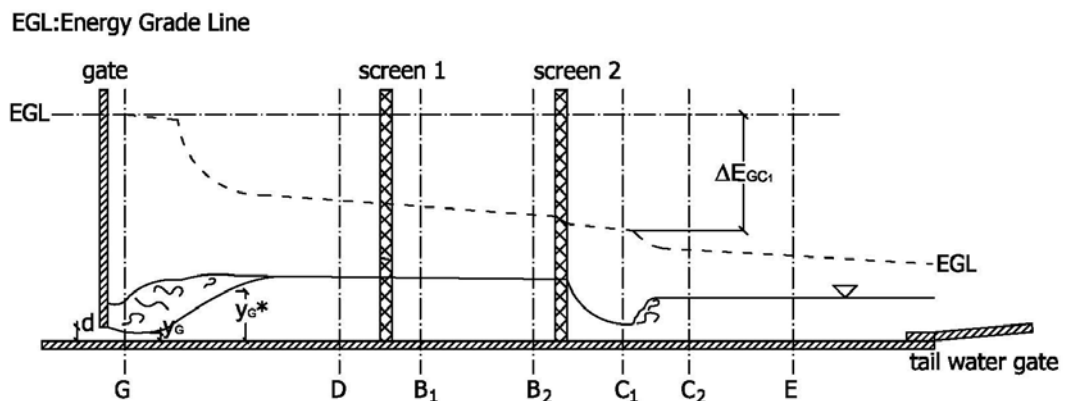


Figure 3.5 General sketch and energy loss definitions for Case 2 in TDSA

For the analysis of both of the two cases the following conceptual frame is constructed. The approach employed for the energy loss computations is the same as that of Çakır (2003) with some exceptions.

The definition of all the variables involved in the analysis presented below is depicted in Figures 3.4 and 3.5.

The energy loss between section A and the screen is not computed because the gate is submerged and the location of the jump can not be determined exactly.

The effectiveness of the screens is not analyzed because the flow parameters at section A can not be determined. Therefore, only the system efficiency η_{sys} is calculated.

The system loss, ΔE_{GC1} is calculated, as

$$\Delta E_{GC1} = \left(y_G^* + \frac{V_G^2}{2g} \right) - \left(y_{C1} + \frac{V_{C1}^2}{2g} \right) \quad (3.15)$$

$$y_G = C_v \cdot d \quad (3.16)$$

$$V_G = Q / y_G \quad (3.17)$$

with $C_v=0.610$

where y_G^* is the water depth at section G, y_{C1} and V_{C1} are the flow depth and velocity respectively at Section C_1 .

Efficiency of the system is calculated as

$$\eta_{sys} = \frac{\Delta E_{GC_1} - \Delta E_{jG}}{\Delta E_{jG}} \quad (3.18)$$

where ΔE_{jG} is defined as energy loss due to a full free hypothetical jump that could have formed at section G with the same upstream flow Froude number as computed using flow depth y_G .

3.2 DIMENSIONAL ANALYSIS

The screen energy loss, S, as the dependent variable can be expressed as a function of the independent variables in the phenomena as follows:

$$S = f_1(Q, d, w, y_G, y_A, y_C, y_t, x, X, p, k, t, g, \rho, \mu, \theta) \quad (3.19)$$

in which

S: the screen loss or the energy head dissipated due to screen, [L],

Q: discharge, [L^3T^{-1}],

d: gate opening, [L],

w: width of the channel, [L],

y_A : water depth at Section A, [L],

y_C : water depth at Section C, [L],

y_G : water depth at Section G, [L],

y_t : tailwater depth, [L],

x: the distance from the upstream end of the pseudo-jump to the screen, [L],

X: distance between the screen and the gate, [L],

p: porosity of the screen,

k: distance between the screens of the double screens, [L],

t: thickness of the screen, [L],

g: gravitational acceleration, [LT⁻²],

ρ : density of water, [ML⁻³],

μ : dynamic viscosity of water, [ML⁻¹T⁻¹]

θ : inclination angle,

Recalling the fact that the slug length L and Fr_C, Froude number at section C, are functions of

$$L = f_2(g, w, Q, y_A) \quad (3.20)$$

$$Fr_C = f_3(g, w, Q, y_C) \quad (3.21)$$

Equation 3.19 can be rewritten by replacing y_A and y_C by L and Fr_C respectively.

$$S = f_4(Q, d, w, y_G, y_t, L, Fr_C, x, X, p, k, t, g, \rho, \mu, \theta) \quad (3.22)$$

After choosing, y_G, g and ρ as repeating variables, the dimensional analysis is performed and following non-dimensional form is obtained:

$$\frac{S}{y_G} = f_5\left(\frac{w}{y_G}, \frac{y_t}{y_G}, Fr_G, \frac{L}{y_G}, Fr_C, \frac{x}{y_G}, \frac{X}{y_G}, p, \frac{k}{y_G}, \frac{t}{y_G}, \frac{d}{y_G}, Re, \theta\right) \quad (3.23)$$

where Re is the Reynolds number.

In addition, recalling the fact that E_G, energy at section G, having the length dimension is a function of

$$E_G = f_6(g, y_G, d, w, Q) \quad (3.24)$$

After choosing y_G , g as repeating variables, the dimensional analysis is performed and following non-dimensional form is obtained:

$$\frac{E_G}{y_G} = f_7\left(\frac{w}{y_G}, Fr_G, \frac{d}{y_G}\right) \quad (3.25)$$

As seen from Equation (3.25), $\frac{E_G}{y_G}$ is a function of $\frac{w}{y_G}$. Therefore, Equation

(3.23) can be rewritten by replacing $\frac{w}{y_G}$ with $\frac{E_G}{y_G}$

$$\frac{S}{y_G} = f_8\left(\frac{E_G}{y_G}, \frac{y_t}{y_G}, Fr_G, \frac{L}{y_G}, Fr_C, \frac{x}{y_G}, \frac{X}{y_G}, p, \frac{k}{y_G}, \frac{t}{y_G}, \frac{d}{y_G}, Re, \theta\right) \quad (3.26)$$

The above equation can be put in a more convenient form such that

$$\frac{S}{E_G} = f_9\left(Fr_G, \frac{x}{L}, \frac{y_t}{d}, \frac{X}{d}, \frac{k}{d}, \frac{t}{d}, \left|\theta, p, Fr_C, \frac{E_G}{d}, \frac{x}{d}, C_v, Re\right|\right) \quad (3.27)$$

in which $\frac{x}{L}$ was defined as α in Equation 3.3.

As Çakır (2003) stated;

“The three of the last seven parameters namely Fr_C , $\frac{E_G}{d}$, and $\frac{x}{d}$ are beyond the scope of this study. C_v , which is defined as $\frac{y_G}{d}$ is a constant. Since the magnitude of Fr_G is relatively high in the range covered during the experiments of this free surface flow study in which gravitational effects are more dominant, the importance of the Reynolds number is secondary, thus it is assumed to be negligible.”

In addition, the findings of Rajaratnam and Hurtig (2000) and Çakır (2003) showed that porosity of 40% is the most efficient porosity for screens as energy dissipaters. Therefore, the porosity is dropped out as a variable and 40% of porosity (optimum porosity) is chosen for the present study. Moreover, since Güngör's (2005) study showed that the triangular screens has no significant further positive effect on energy dissipation, only vertical screens were used for this study. Furthermore, as Çakır's (2003) and Balkış' (2004) studies proved that double screens arrangement dissipate more energy than single screens, only double screens were used. Thus, p , θ and k can be dropped out of the equation as variables.

Then, Equation (3.27) can further be reduced into the following form

$$\frac{S}{E_G} = f_{10}\left(Fr_G, \alpha, \frac{t}{d}, \frac{y_t}{d}, \frac{X}{d}\right) \quad (3.28)$$

in which y_t is a function of tailwater gate height h_t

$$\frac{S}{E_G} = f_{11}\left(Fr_G, \alpha, \frac{t}{d}, \frac{h_t}{d}, \frac{X}{d}\right) \quad (3.29)$$

That is, the present experimental study is carried out by taking into account the following dimensionless parameters: $Fr_G, \alpha, \frac{t}{d}, \frac{h_t}{d}, \frac{X}{d}$.

CHAPTER 4

LABORATORY WORK

In this chapter, the details of the experimental setup and procedure are described in accordance with the conceptual frame.

4.1 EXPERIMENTAL SETUP

The experiments are conducted on a horizontal rectangular channel of 7.5 m long, 29 cm wide and 70 cm deep. A constant head tank is used to supply water. A 206 mm inside diameter pipe connected to that tank is utilized to carry water to a pressurized tank having a sliding gate at its bottom. In addition, a valve is placed on the pipe in order to adjust the discharge, and a tailwater gate structure is used to adjust the tailwater depth during the study. For the discharge measurements, an orifice meter is installed on the pipe. Moreover, for flow depth measurements, a mobile point gage is operated. The value of 40% is chosen for the porosity of the screens since Çakır's study proved that 40% is the most efficient porosity of the screens as an energy dissipater. Since Balkış (2004) study showed that there is no significant effect of inclination on the system's energy dissipation and Güngör's (2005) study showed that the triangular screen configuration with the same pore geometry has no significant additional contribution on the energy dissipation as compared to vertically placed screens, in this study laboratory work and analysis have been performed to investigate the tailwater effect and multiple screen effect on the energy dissipation through screens.. A detailed schematic view of the channel and the setup is shown in Figures 4.1 and 4.2.

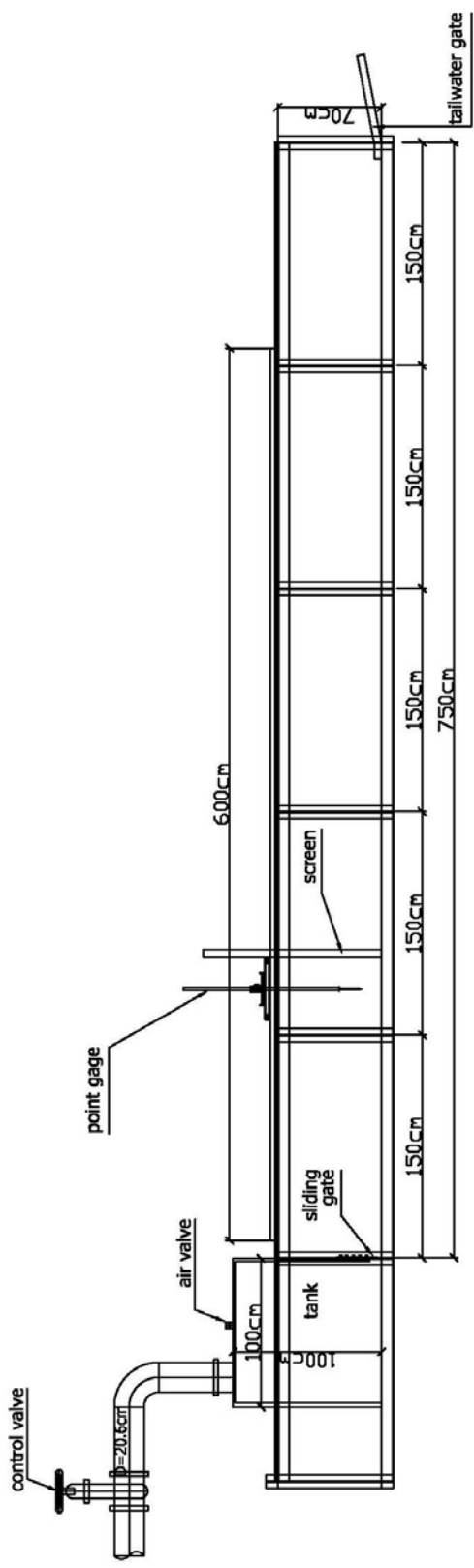


Figure 4.1 Side view of the experimental setup

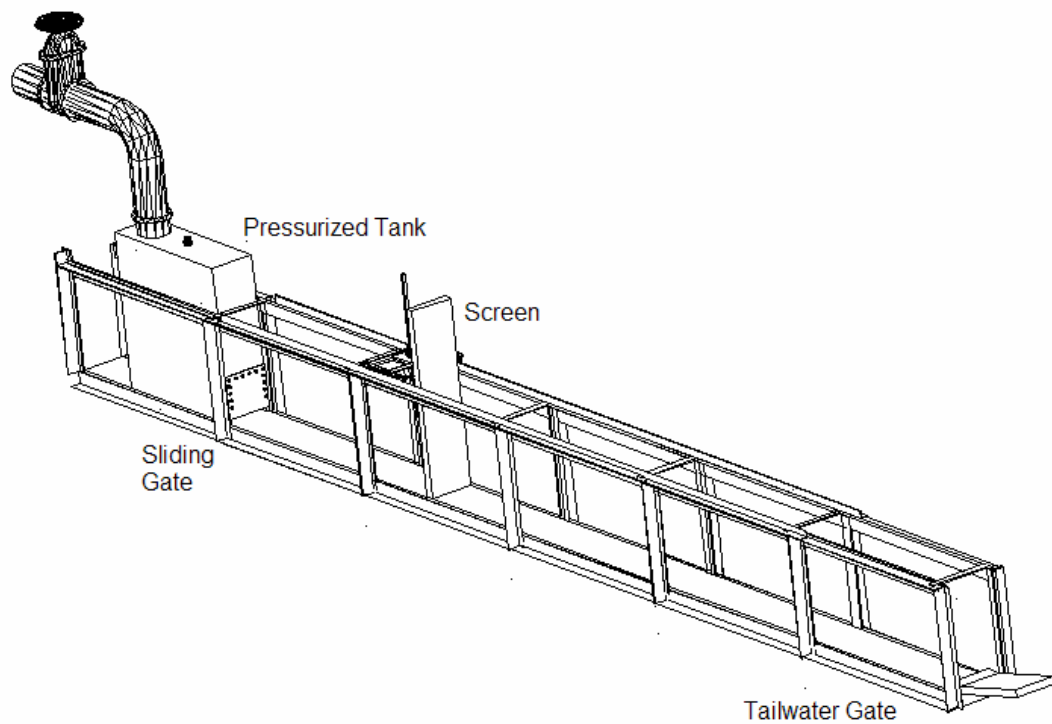


Figure 4.2 A general view of the setup

4.1.1 GATES

The sliding gate located at the bottom of the pressurized tank acts like a sluice gate and ensures the upstream supercritical flow conditions necessitated for the study. Froude number range covered during the study is from 5.0 to 22.5. The gate opening is adjusted at heights of 2.0 cm and 3.0 cm during the study. All the initial energy calculations are done with respect to the depth at vena contracta. The velocity head is based on the depth which is computed by using contraction coefficient and flow depth is measured using a point gage as specified in conceptual frame chapter.

The tailwater gate located at the end of the channel acts as an over flow weir and controls the downstream flow depth. Tailwater gate mechanism formed a step downstream of the flow. This in turn created a downstream control resulting in a

subcritical flow. Consequently, supercritical flow leaving the screen encounters subcritical flow forming another secondary jump.

4.1.2 SCREENS

The material used for screens is Plexiglas, which is chosen for its easy handling property. The thickness of the screens is 1 cm and they have a porosity of 40%, which is achieved by drilling 1 cm diameter holes arranged with a uniform triangular mesh. During the study, experiments with only double screen arrangement (two screens set so that 2 cm gap between them is formed) are conducted since Balkış' (2004) and Çakırs' (2003) works proved that double screen arrangement dissipates the energy more than single screen arrangement does, Figure 4.3. For the stability purpose, screens are fixed at the bottom of the channel by means of screws. In the present work, two screen arrangements are used, which are one double screen and two double screen arrangements. In one double screen arrangement, the effects of the relative screen position, X/d , the relative screen thickness, t/d and the relative tailwater depth y_t/d are examined by changing the height of the sliding gate opening, the location of the screen, and the height of the tailwater gate. In two double screen arrangement, the effects of the relative screen position, X/d , and the relative screen thickness, t/d are examined by changing the height of the sliding gate opening, and the locations of the screens.

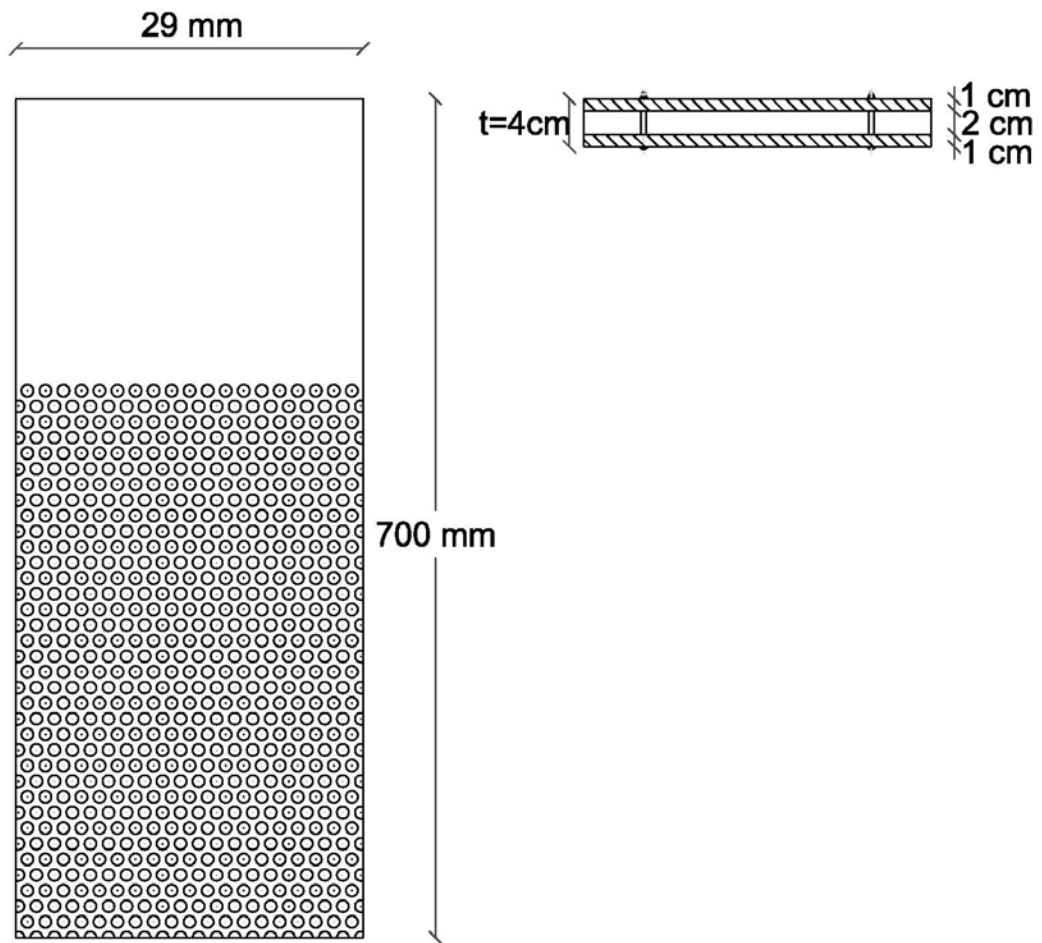


Figure 4.3 Front and plan views of the double screen with a porosity of 40%

4.1.3 ORIFICE METER

An orifice meter whose design is made according to the Institution of Turkish Standards (TSE) specifications is constructed on the pipe serving as a link between the constant head tank and the pressurized tank. A 30 degree inclined mercury manometer, used for the discharge measurements, is connected to the orifice meter. The details of TSE requirements are given in Appendix A including a detailed drawing and correction coefficient chart for the orifice meter.

4.2 EXPERIMENTAL PROCEDURE

Table 4.1 shows all of the experimental runs performed for the one double screen arrangement. The X values and gate openings are determined as given in Table 4.2 for one double screen arrangement. Table 4.3 shows all of the experimental runs performed for the two double screen arrangement. The X values and gate openings are determined as given in Table 4.4 for two double screen arrangement. These particular tests were selected according to all X/d, t/d and h_t/d combinations that could be achieved in the experimental setup.

The preliminary runs which were performed to determine the capabilities of the setup with one double screen arrangement are not included in Table 4.1. These runs were performed to determine limits of the upstream flow Froude numbers and tailwater gate heights both of which causes transitions between cases explained in conceptual frame section (section 3.1.1).

Table 4.1 The range of the experiments for ODSA

X	X/d	t/d	h_t/d
132	66	2D	0, 2.1, 3.9, 4.5
198	66	1.33D	0, 1.4, 3
	99	2D	0, 1.5, 2.1, 2.7, 3.25, 4.5, 5.1, 5.7, 6.3, 6.9
297	99	1.33D	0, 1.4, 2.6, 3

Table 4.2 X values and gate openings for ODSA

X	d(cm)	
132	2	
198	2	3
297	3	

Table 4.3 The range of the experiments for TDSA

X_1	X_1/d	t/d	X_2	X_2/d
198	66	1.33D	297	99
			399	133
	99	2D	297	149
			399	200
297	99	1.33D	399	133
	149	2D		200

Table 4.4 X values and gate openings for TDSA

X_1	X_2	$d(\text{cm})$	
198	297	2	3
	399	2	3
297	399	2	3

For each specified set of experiments, the location of the screen is arranged so that desirable X/d values are obtained. For a given location of the screen, the height of the sliding gate opening is changed providing proper experiment set and consistent t/d values. After the location of the screen and gate opening are fixed, discharge is regulated by means of the valve situated on the supply pipe between the pressure tank and the orifice meter. For each set of experiment, several Froude number values are adjusted between predetermined maximum and minimum Froude number values. The maximum Froude number value is determined as 16 but in some set of experiments this value is exceeded because the minimum Froude number value is high, and enough number of experiments for reasonable results can not be achieved in this range. The minimum Froude number value is determined as the water start to choke the gate for the specified discharge for one double screen arrangement. For two double screen arrangement the minimum Froude number value is determined as the effects of the upstream submerged jump can not be observed for the specified Froude number. The choking of the gate may start either by lowering the discharge

too much and hence the upstream flow Froude number or by raising the tailwater gate too much and increasing the tailwater depth for one double screen arrangement. In case of two double screen arrangement, the experiments are performed with the upstream sliding gate being submerged for a wide range of Froude numbers.

For each set of experiment, using the mercury manometer of the orifice meter, differential pressure head readings are taken. Then, the discharge values are calculated by using equation A.2 given in Appendix A using the mercury manometer readings. In addition, for each discharge value, depth measurements are taken on pre-determined sections, namely at points G, A, D, C₁, C₂ and E for one double screen arrangement and at points G, D, B₁, B₂, C₁, C₂ and E for two double screen arrangement, by means of a mobile point gage at three points along the width of the channel. The average of these readings is used in the calculations in order to be more accurate. All of the points are determined based on the observation of water surface behavior. Section A is the upstream section of the real or pseudo jump for one double screen arrangement. Point D is at just upstream of the screen for one double screen arrangement and it is at just upstream of the first screen for two double screen arrangement. Points B₁ and B₂ are at just downstream of the first screen and at just upstream of the second screen, respectively, for two double screen arrangement. Point C₁ is the vena contracta point at the downstream section of the screen (second screen for two double screen arrangement) before the secondary jump. Point C₂ is at the downstream section of the screen (second screen for two double screen arrangement) after the secondary jump. Point E is at upstream of the tailwater gate. As mentioned before, point G is located just downstream of the gate. Namely, for each set of experiment, manometer readings are taken for specified sliding gate openings, and depth measurements are taken at specified sections and all necessary calculations are performed. For the next tailwater gate height, all depth measurements and all calculations are repeated and the control gate opening is adjusted for the new series of experiments. Finally, the screen is moved to the next scheduled location and the same procedure is performed at the new location.

CHAPTER 5

RESULTS AND DISCUSSIONS

5.1 INTRODUCTION

The results of the experimental study are discussed in this Chapter. The original data are given in Appendix C. The reference key for the presentation of the experimental results of the present study for one double and two double screen arrangements are given below in Tables 5.1 and 5.2 respectively. D implies two screens of 1 cm thick each put together with a 2 cm space between them. The number preceding D is the ratio of total width of two screens with the space between them to the gate opening height, t/d . The numbers in reference key coming after relative screen thickness, t/d , are relative screen position, X/d , upstream flow Froude number, Fr_G , and relative tailwater gate height, h_t/d .

Table 5.1 Reference key for ODSA

Reference	t/d	X/d	Fr_G	h_t/d
2D-99-16.17-2.1	2 (double)	99	16.17	2.1
1.33D-66-14.15-3	1.33 (double)	66	14.15	3

Table 5.2 Reference key for TDSA

Reference	t/d	X_1/d	X_2/d	Fr_G
1.33D-66-99-12.97	1.33 (double)	66	99	12.97
2D-99-200-13.91	2 (double)	99	200	13.91

Yet, for the graphical representation of the data since variations are plotted against Fr_G , Froude number values were dropped out of the labels.

5.2 PERFORMANCE OF THE SYSTEM

As indicated before the total energy loss between just downstream of the gate (i.e. point G of Figures 3.1, 3.2, 3.3, 3.4 and 3.5) and just downstream of the screen (second screen for two double screen arrangement) (i.e. point C_1 of Figures 3.1, 3.2, 3.3, 3.4 and 3.5) is denoted as ΔE_{GC1} . This energy loss includes the friction losses, losses due to a pseudo, real jump or submerged jump and the screen loss. The relative energy loss defined as $\Delta E_{GC1}/E_G$ is used to analyze the system performance. The effects of relative screen thickness, t/d ; relative screen position, X/d (X_1/d and X_2/d for two double screen arrangement) and relative tailwater gate height, h_t/d on the system performance are presented in Figures 5.1 through 5.14.

5.2.1 PERFORMANCE OF THE SYSTEM AT LARGE

The main goal of the present study is to determine the effects of tailwater depth and multiple screens on the energy dissipation. Figures 5.1 through 5.14 are selected to show the variation of $\Delta E_{GC1}/E_G$ with Froude number at the downstream of the gate, Fr_G . On these figures, the relative energy loss that would occur if there were a conventional hydraulic jump at section G is also drawn as a solid line for comparison purposes.

From the figures, one may discern that

- i. All of the tests performed showed that energy dissipation is always more than that of a classical full jump that would have been forced to occur at the gate.
- ii. The relative energy loss, $\Delta E_{GC1}/E_G$ increases with increasing Froude number, Fr_G .
- iii. There is no apparent dependence of system performance observed on the relative screen thickness, t/d and on the relative screen position, X/d (X_1/d and X_2/d for two double screen arrangement).
- iv. Dependence on the relative tailwater gate height, h_i/d , being so weak, it influences the relative energy loss, $\Delta E_{GC1}/E_G$ in a negative way that as tailwater gate height increases $\Delta E_{GC1}/E_G$ decreases slightly for the same upstream flow Froude number.
- v. Using multiple screens (two double screen arrangement) dissipates more energy as compared to one double screen arrangement.

In Figure 5.1, best fit curve for the entire data of the present study for ODSA is shown emphasizing that all of the data exhibit a similar trend with increasing upstream Froude number, Fr_G , such that a best fit curve can easily describe that trend. Consequently, the equation of the best fit curve is of the following form obtained with a root mean square (rms) value of 0.078 and a correlation coefficient (r) of 0.960 indicating a good approximation of the data.

$$\frac{\Delta E_{GC1}}{E_G} = 0.92 + 0.0015 Fr_G - \frac{8.71}{Fr_G^2} \quad (5.1)$$

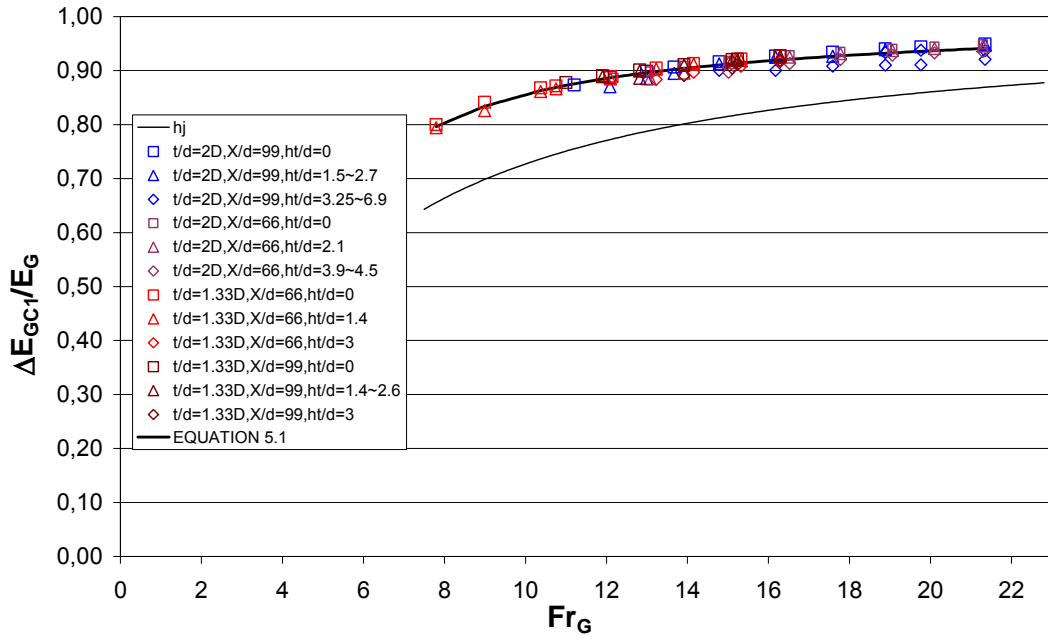


Figure 5.1 $\Delta E_{GC1}/E_G$ vs. Fr_G for ODSA and its best fit curve

In Figure 5.2a, best fit curve for the entire data of the present study for one double screen arrangement is shown for different relative tailwater gate height ranges emphasizing that all of the data exhibit a similar trend. The same data is plotted in Figure 5.2b with a larger scale of $\Delta E_{GC1}/E_G$. The equations of the best fit curves for $h_t/d = 0$, $h_t/d = 1.4\sim 2.7$ and $h_t/d = 3\sim 6.9$ are shown in equations 5.2, 5.3 and 5.4 with root mean square (rms) values of 0.012, 0.031, 0.035 and correlation coefficients (r) of 0.998, 0.987, 0.872, respectively.

$$\frac{\Delta E_{GC1}}{E_G} = 0.92 + 0.0022 Fr_G - \frac{8.45}{Fr_G^2} \quad (\text{for } h_t/d = 0) \quad (5.2)$$

$$\frac{\Delta E_{GC1}}{E_G} = 0.91 + 0.0028 Fr_G - \frac{8.49}{Fr_G^2} \quad (\text{for } h_t/d = 1.4\sim 2.7) \quad (5.3)$$

$$\frac{\Delta E_{GC1}}{E_G} = 0.98 + 0.0008 Fr_G - \frac{14.71}{Fr_G^2} \quad (\text{for } h_t/d = 3\sim 6.9) \quad (5.4)$$

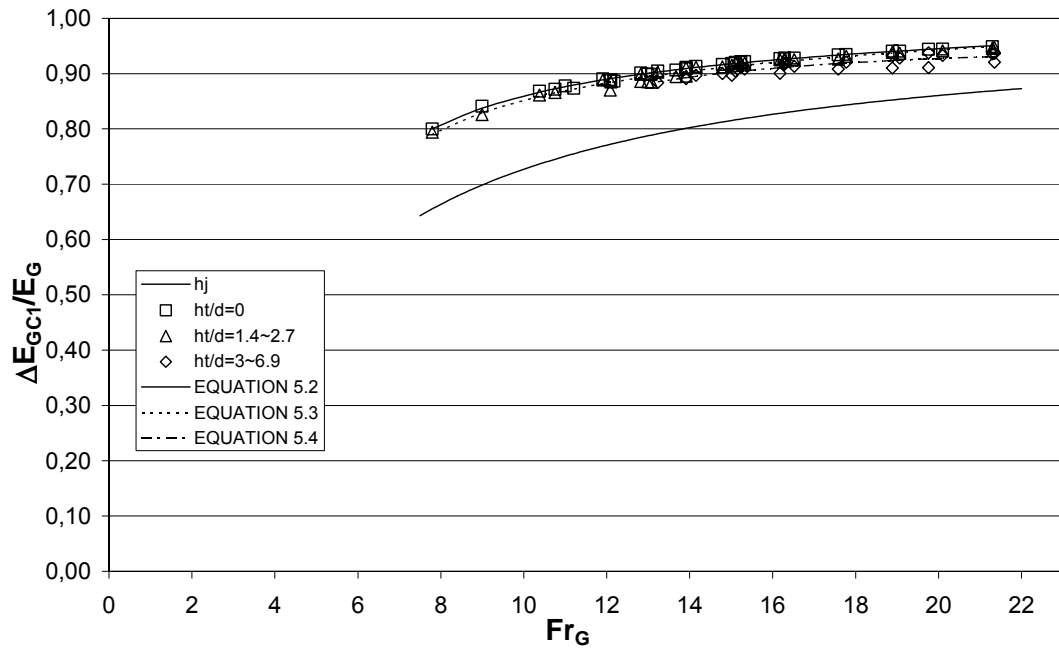


Figure 5.2a $\Delta E_{Gc1}/E_G$ vs. Fr_G for ODSA with different h_t/d and their best fit curves

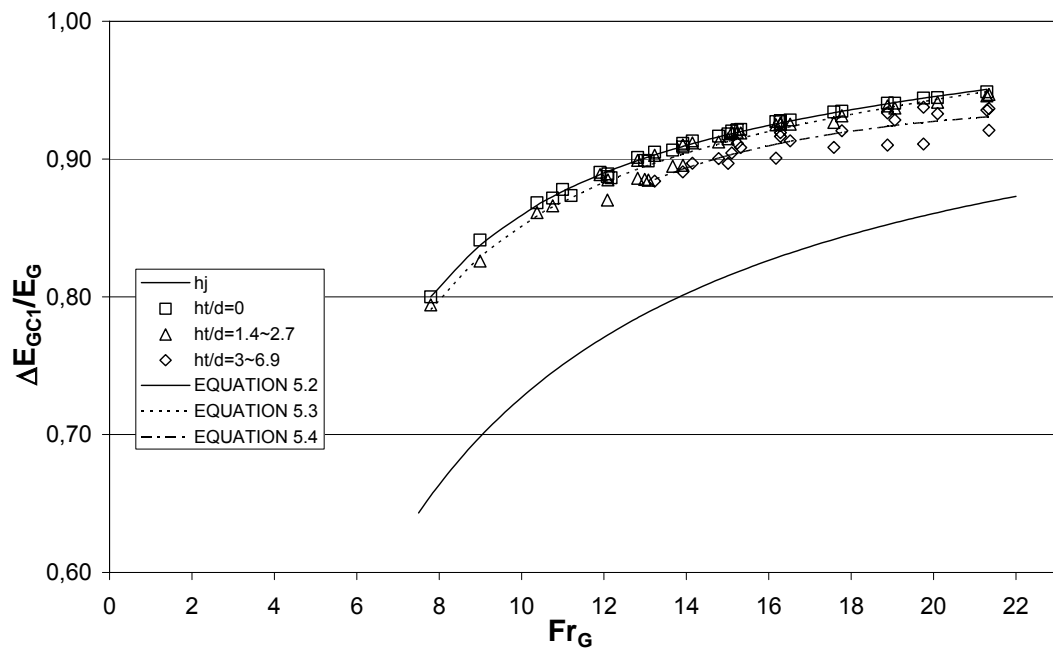


Figure 5.2b $\Delta E_{Gc1}/E_G$ vs. Fr_G for ODSA with different h_t/d and their best fit curves

In Figures 5.3 through 5.6 it is observed that there is no apparent dependence of $\Delta E_{GCl}/E_G$ both on the relative screen thickness, t/d and on the relative screen position, X/d for one double screen arrangement.

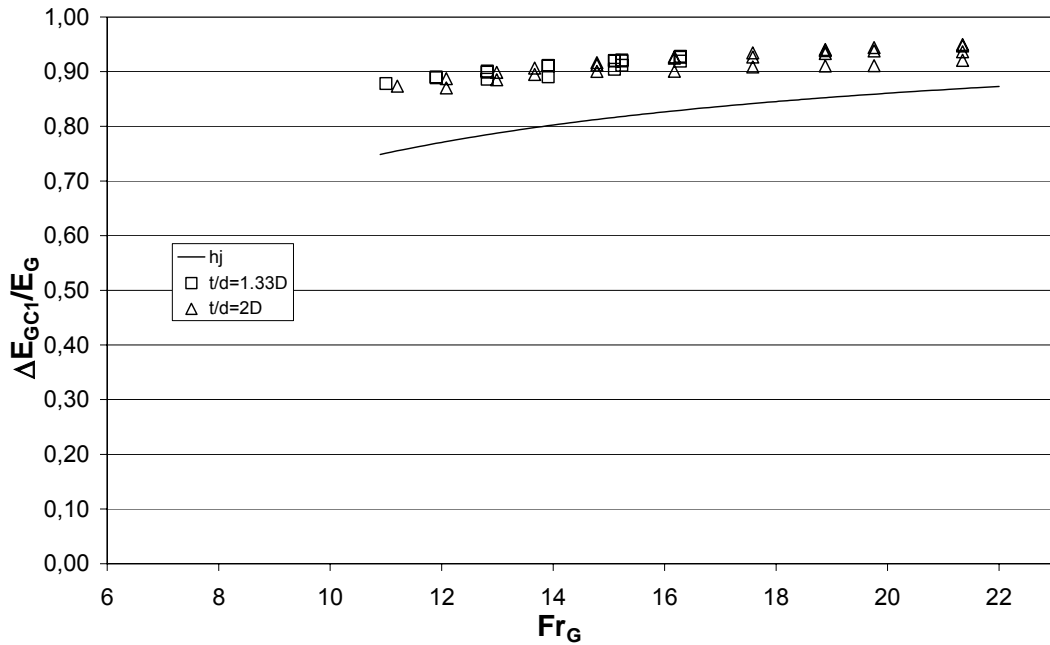


Figure 5.3 $\Delta E_{GCl}/E_G$ vs. Fr_G for ODSA with different t/d at $X/d = 99$

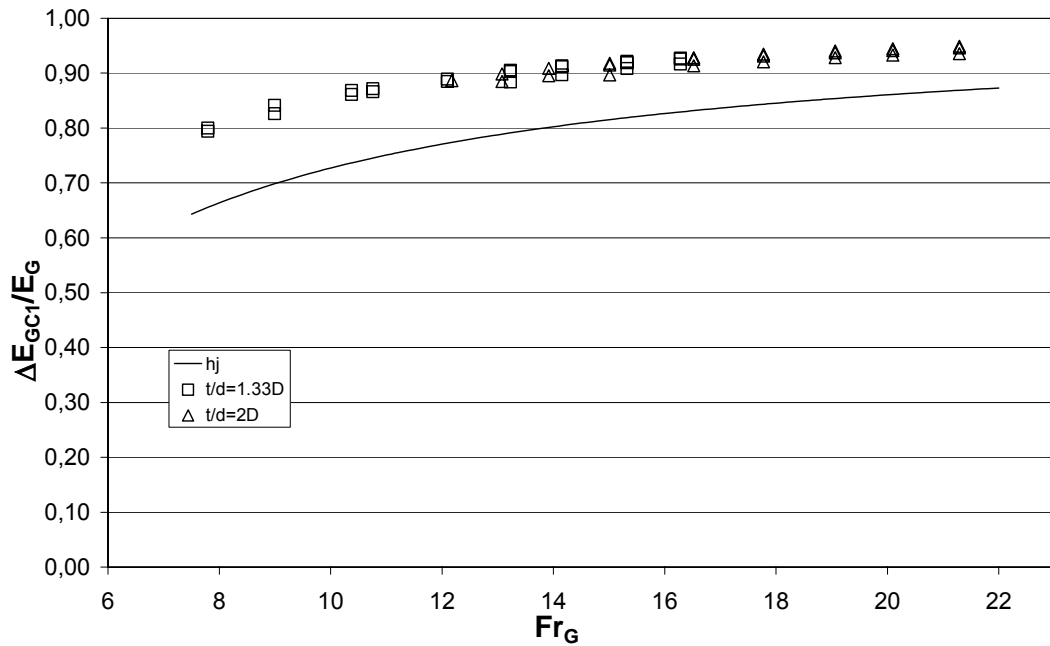


Figure 5.4 $\Delta E_{GCl}/E_G$ vs. Fr_G for ODSA with different t/d at $X/d = 66$

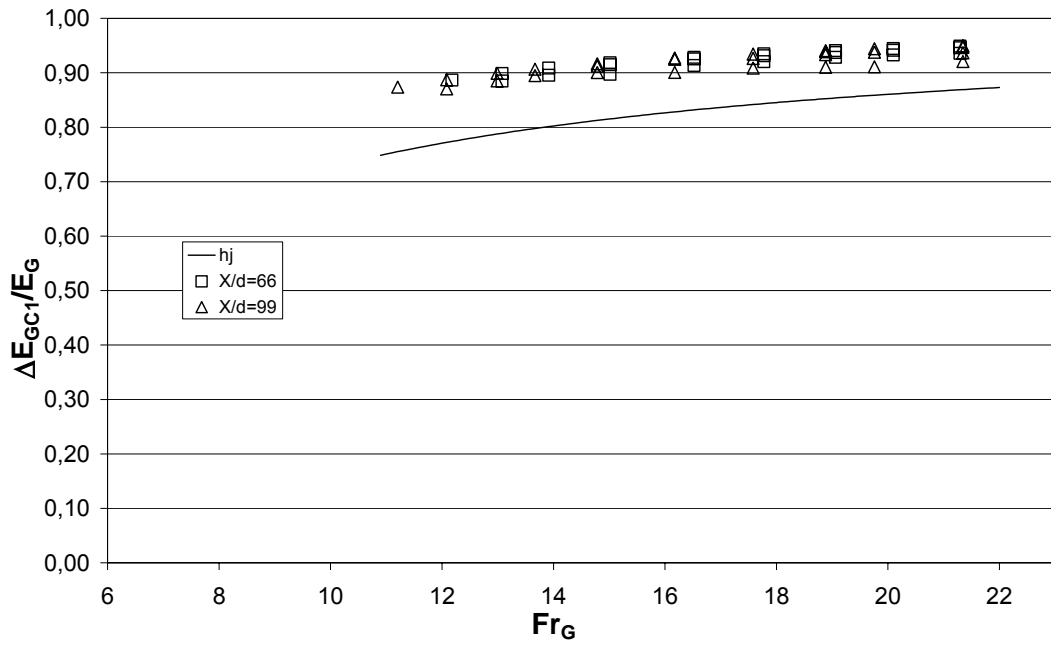


Figure 5.5 $\Delta E_{Gc1}/E_G$ vs. Fr_G for ODSA with different X/d for $t/d = 2D$

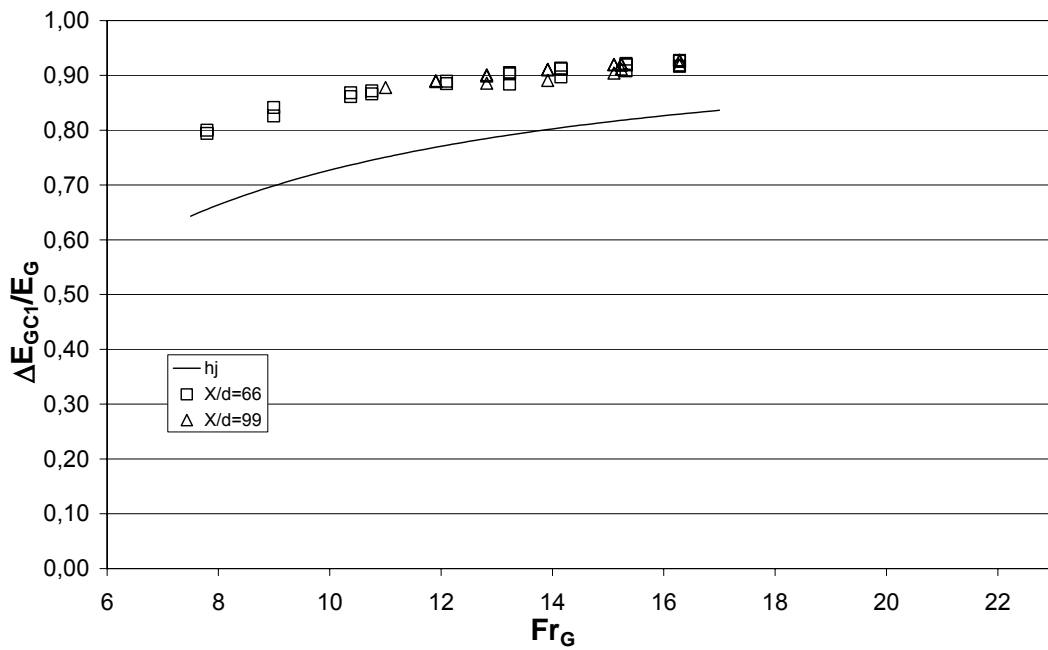


Figure 5.6 $\Delta E_{Gc1}/E_G$ vs. Fr_G for ODSA with different X/d for $t/d = 1.33D$

In Figure 5.7, best fit curve for the entire data of the present study for two double screen arrangement is shown emphasizing that all of the data exhibit the similar trend. The equation of the best fit curve is of the following form obtained with a root mean square (rms) value of 0.055 and a correlation coefficient (r) of 0.990 indicating a good approximation of the data.

$$\frac{\Delta E_{GC1}}{E_G} = 0.87 + 0.0046 Fr_G - \frac{4.28}{Fr_G^2} \quad (5.5)$$

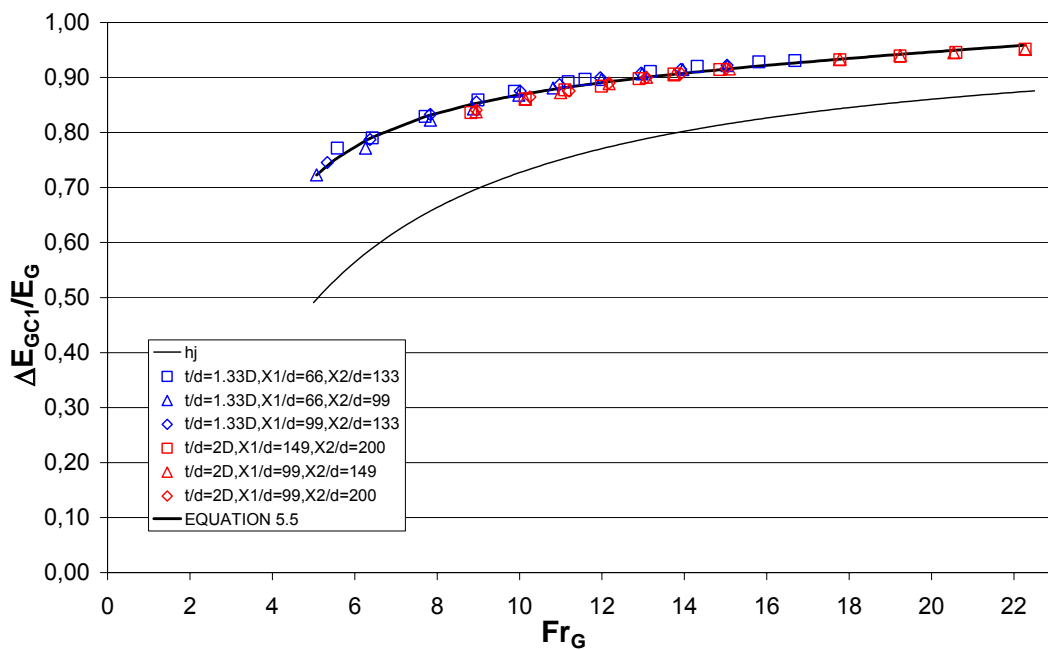


Figure 5.7 $\Delta E_{GC1}/E_G$ vs. Fr_G for TDSA and its best fit curve

In Figures 5.8 through 5.14 it is observed that there is no apparent dependence of $\Delta E_{GC1}/E_G$ both on the relative screen thickness, t/d and on the relative screen position, X/d for two double screen arrangement.

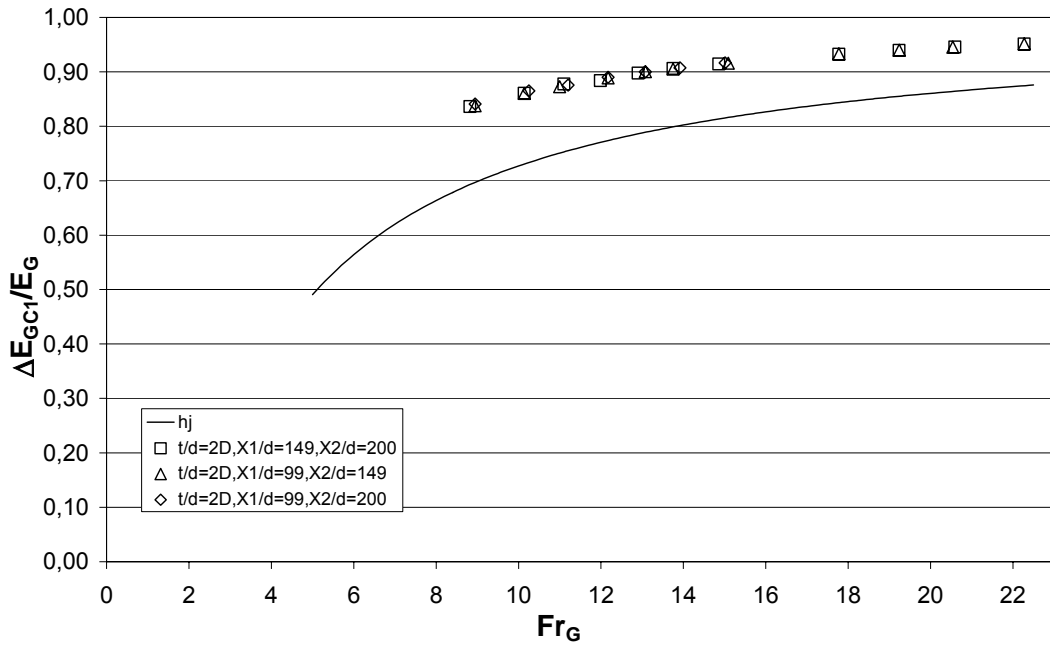


Figure 5.8 $\Delta E_{GC1}/E_G$ vs. Fr_G for TDSA for $t/d = 2D$

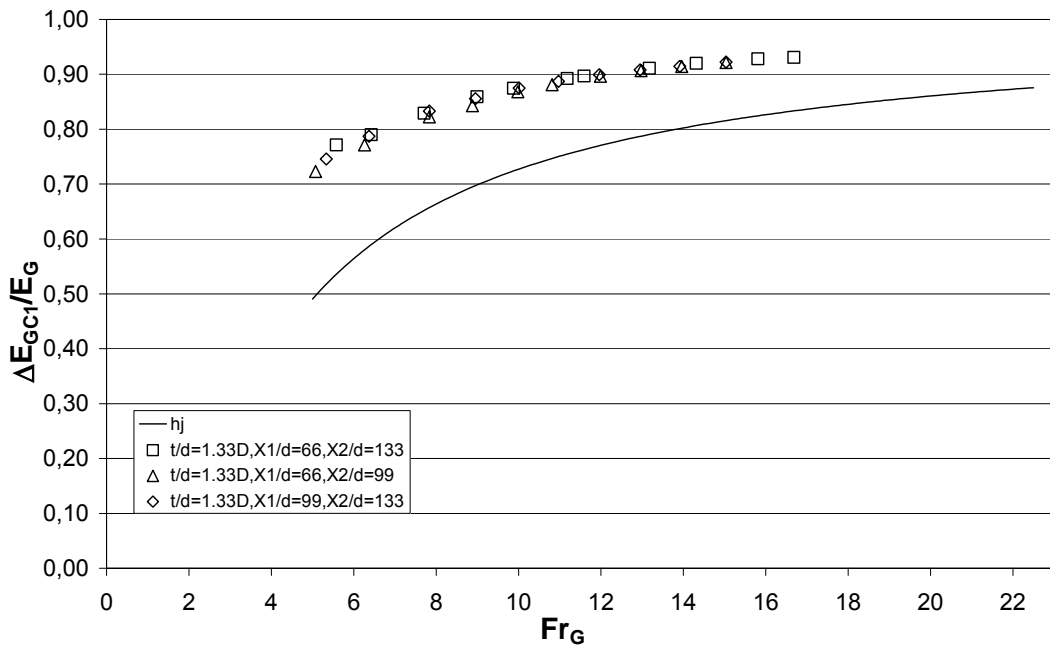


Figure 5.9 $\Delta E_{GC1}/E_G$ vs. Fr_G for TDSA for $t/d = 1.33D$

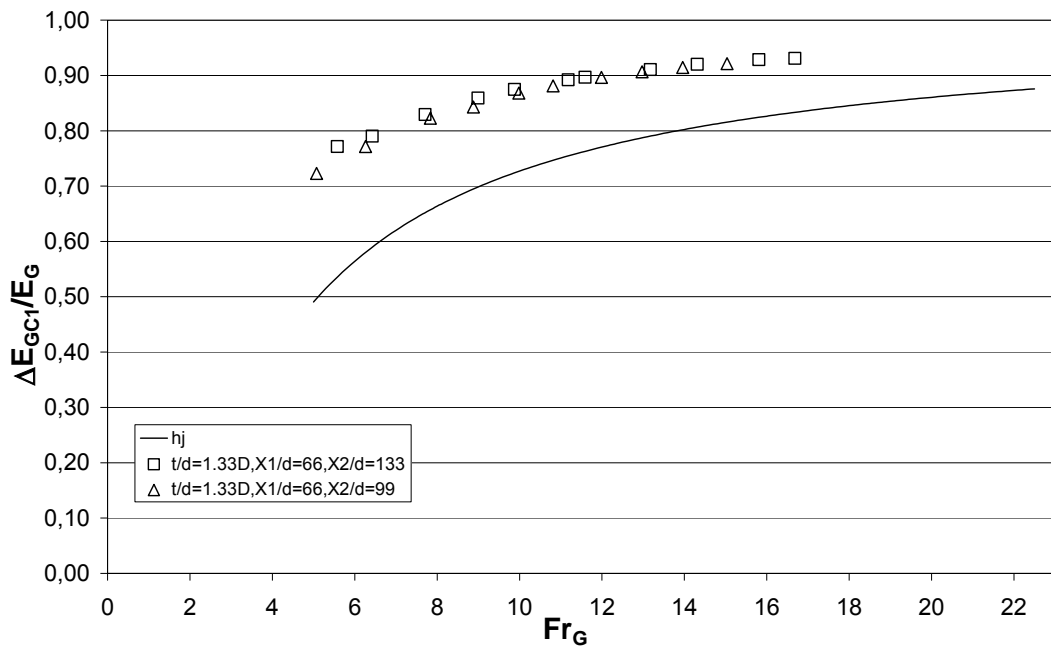


Figure 5.10 $\Delta E_{GCI}/E_G$ vs. Fr_G for TDSA at $X_1/d = 66$

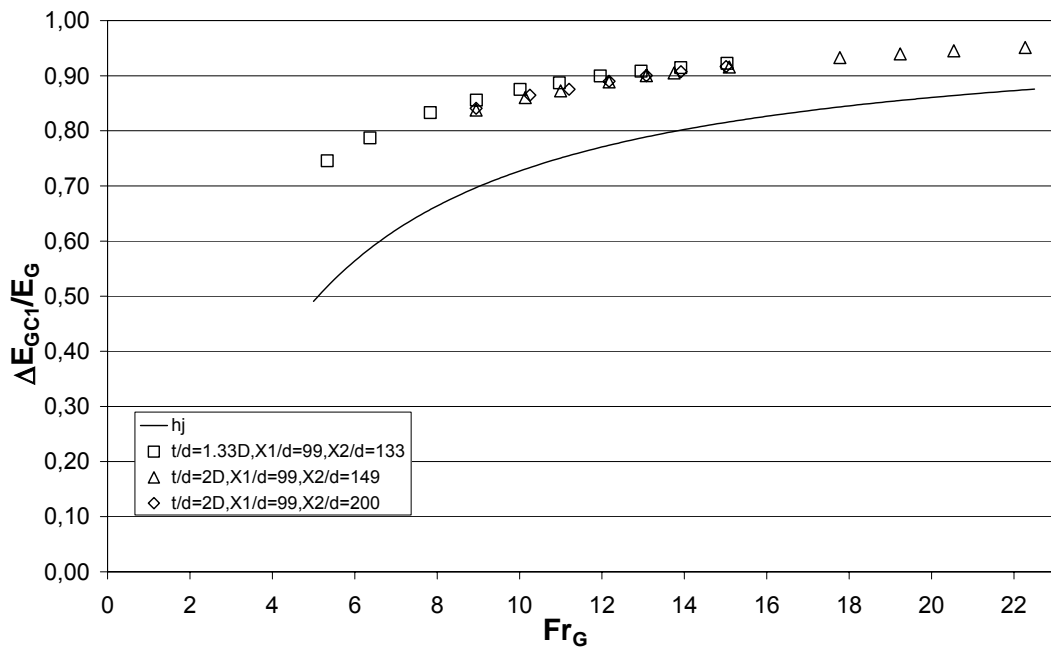


Figure 5.11 $\Delta E_{GCI}/E_G$ vs. Fr_G for TDSA at $X_1/d = 99$

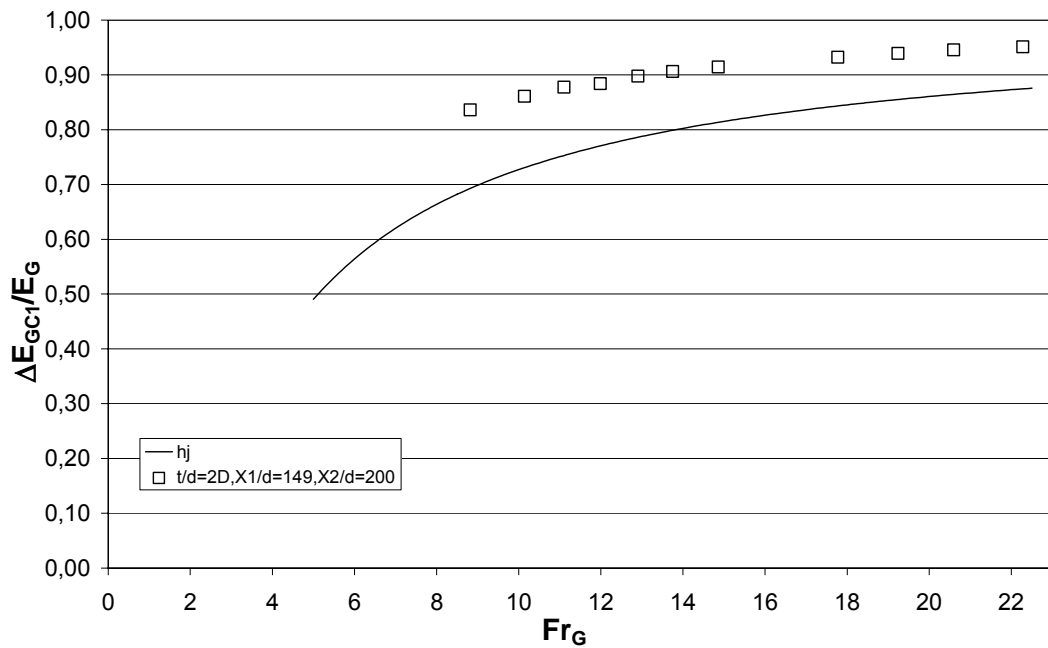


Figure 5.12 $\Delta E_{Gc1}/E_G$ vs. Fr_G for TDSA at $X_1/d = 149$

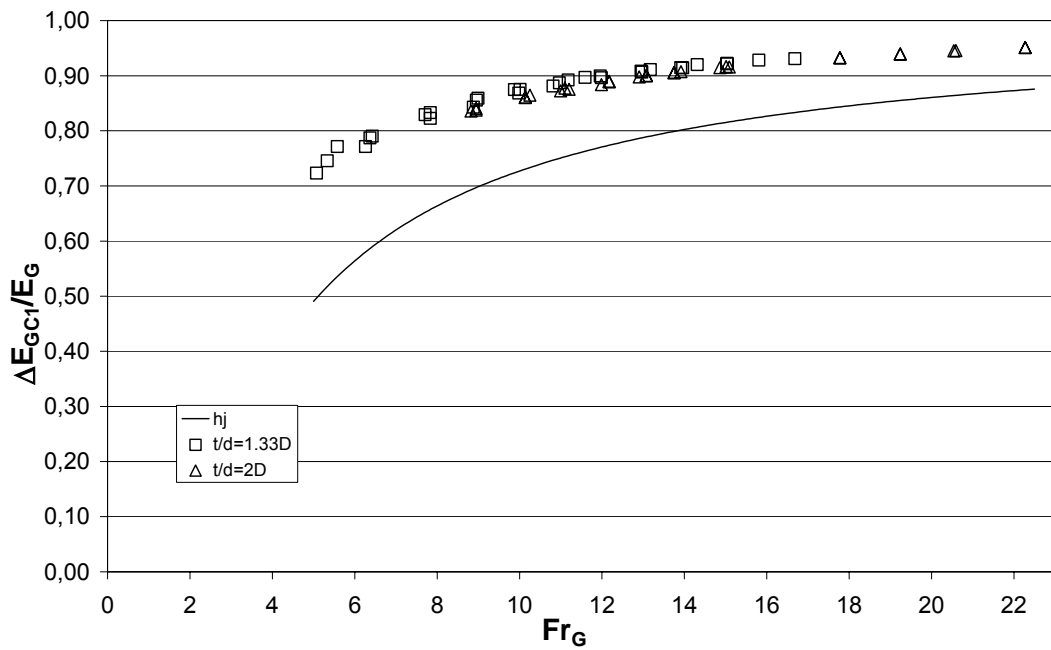


Figure 5.13 $\Delta E_{Gc1}/E_G$ vs. Fr_G for TDSA with different t/d values

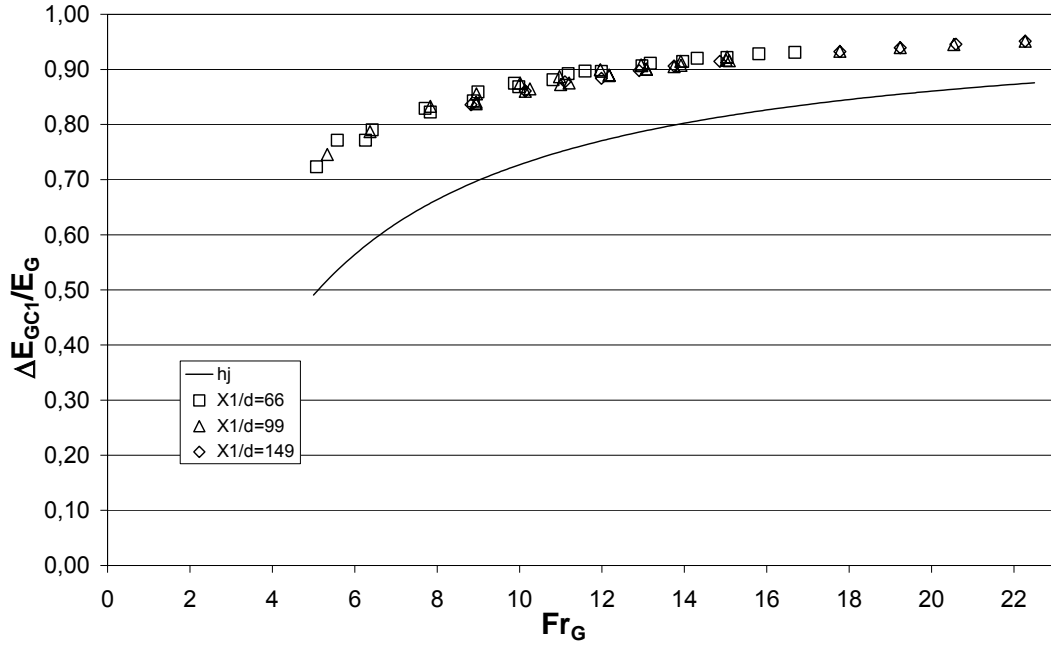


Figure 5.14 $\Delta E_{Gc1}/E_G$ vs. Fr_G for TDSA with different X_1/d values

5.2.2 COMPARISON OF THE PRESENT DATA WITH THAT OF PREVIOUS STUDIES

Güngör's (2005) and Balkış' (2004) results have shown that using either triangular screen configuration or various screens of different inclination angles like 60° , 75° and 90° both had no significant additional contribution on the energy dissipation over vertically placed screens. However, Çakır's studies showed that double screens dissipate energy more than single screens. Considering the fact that there is no appreciable differences for $t/d= 1D$, $2D$ and $1.33D$ cases on the energy dissipation and that the effects of inclination of the screens are insignificant, all available previous double screen data, data of Rajaratnam and Hurtig (2000), Çakır (2003), Balkış (2004) and Güngör (2005) are put into Equation 5.1 and 5.5, for ODSA and TDSA respectively, as depicted in Figures 5.15 and 5.16 in order to show the agreement between the present study and previous work. The rms value of the data of all the previous studies with double screens turns out to be equal to 0.260 and

0.423 and the correlation coefficient of all the previous data with that of the present work is (r) 0.977 and 0.973 with respect to Equations 5.1 and 5.5 derived from one double and two double screen arrangement data respectively. These results show the agreement between the present data and the previous studies performed by Rajaratnam and Hurtig (2000), Çakır (2003), Balkış (2004) and Güngör (2005). There is a high correlation between all of the previous data and the best fits obtained from the present work, that is, Equations 5.1 and 5.5. All double screen data including that of the present study are fitted as a best fit curve to show the amount of energy dissipation in general sense, as shown in Figure 5.17 with the following form

$$\frac{\Delta E_{GC_1}}{E_G} = 0.884 + 0.003Fr_G^2 - \frac{6.268}{Fr_G^2} \quad (5.6)$$

Since the present study focuses on use of vertically placed screens all double screen data of Çakır (2003) including that of the present study are fitted as a best fit curve to show the amount of energy dissipation by vertically placed screens in a general sense, as shown in Figures 5.18 and 5.19 for one double and two double screen arrangements with the following forms respectively

$$\frac{\Delta E_{GC_1}}{E_G} = 0.871 + 0.004Fr_G^2 - \frac{5.619}{Fr_G^2} \quad (5.7)$$

$$\frac{\Delta E_{GC_1}}{E_G} = 0.849 + 0.005Fr_G^2 - \frac{4.512}{Fr_G^2} \quad (5.8)$$

The r-values of the entire data, the data of Çakır (2003) with the present data for one double and two double screen arrangements separately are 0.934, 0.965, 0.953 respectively, conforming the significant agreement among the findings. The data from the previously conducted screen studies in METU hydraulics laboratory by Çakır (2003), Balkış (2004) and Güngör (2005) will be called previous METU data and they together with the present study data will be called the entire METU data thereafter.

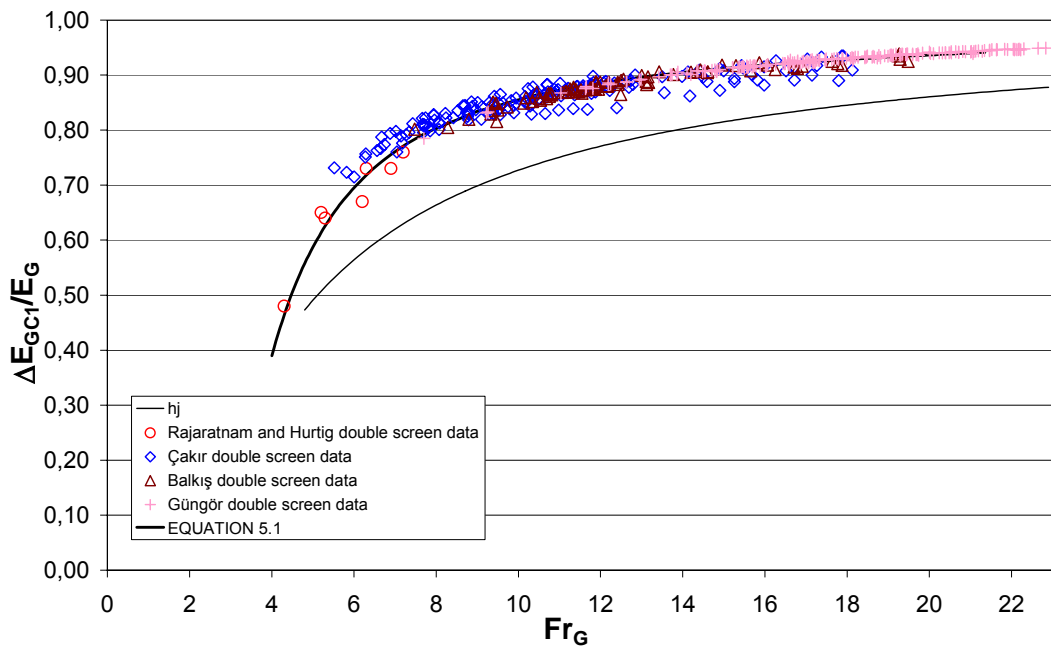


Figure 5.15 Data of previous studies and its curve based on Equation 5.1

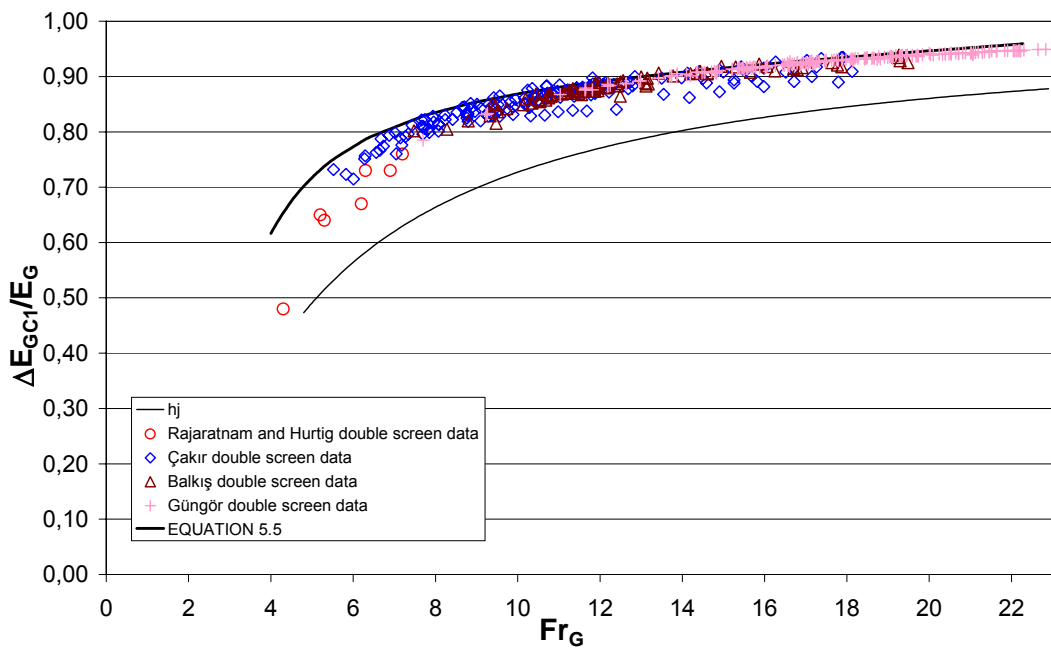


Figure 5.16 Data of previous studies and its curve based on Equation 5.5

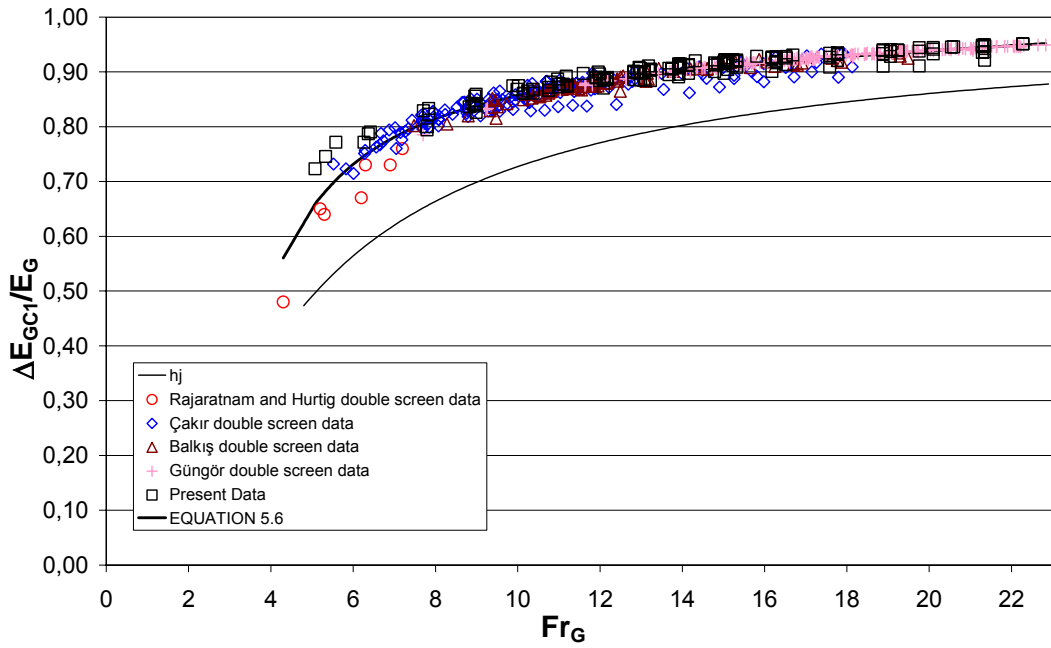


Figure 5.17 Data of all studies and its best fit curve

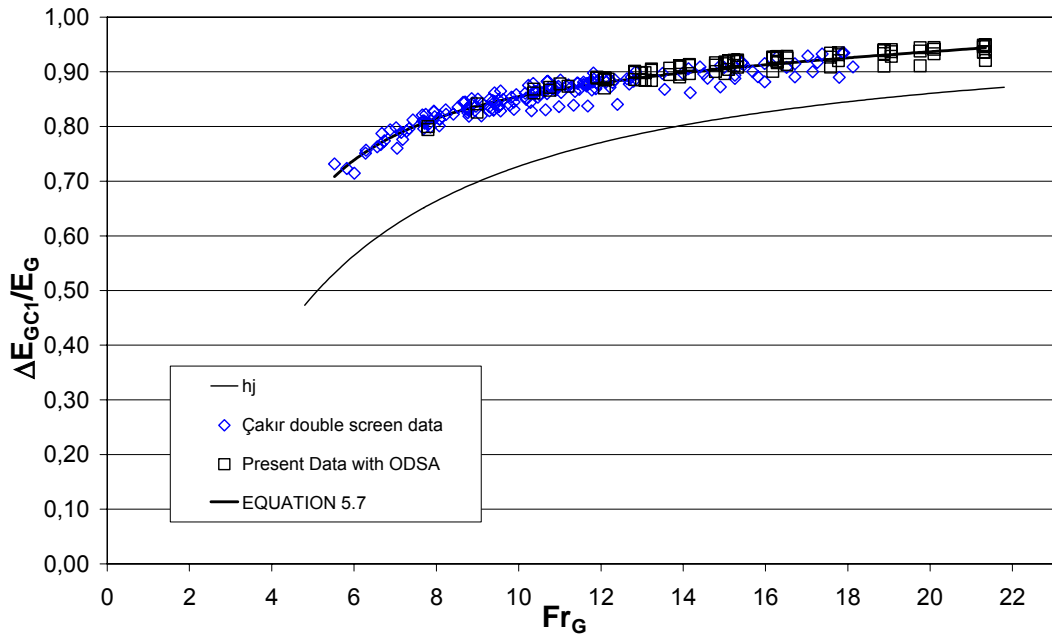


Figure 5.18 Çakır (2003) and ODSA data and its best fit curve

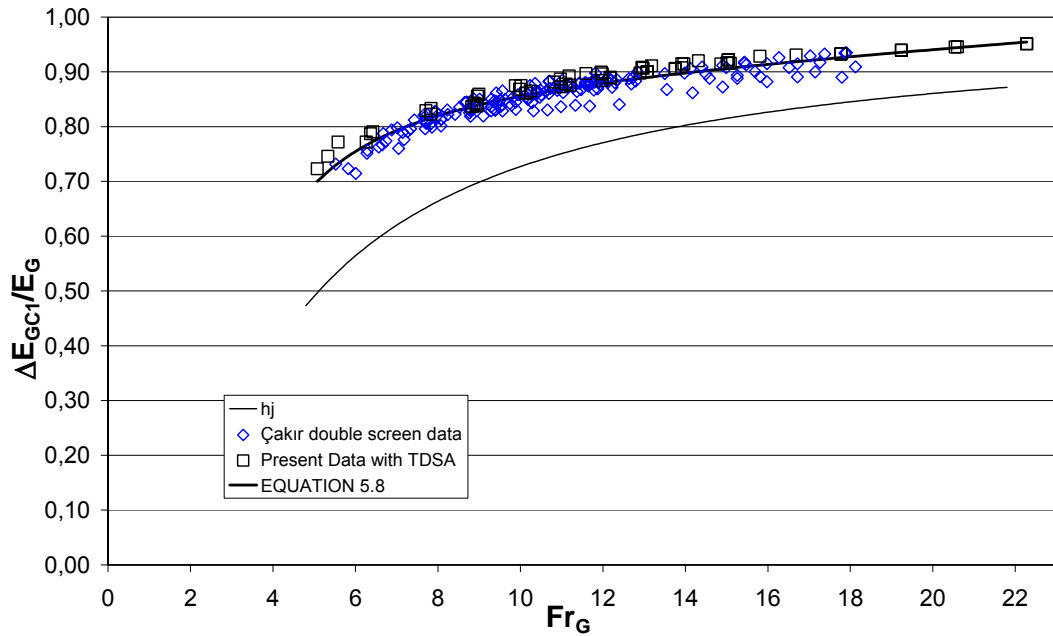


Figure 5.19 Çakır (2003) and TDSA data and its best fit curve

5.2.3 COMPARISON OF SYSTEM PERFORMANCES BETWEEN ODSA AND TDSA

The effect of using multiple screens is demonstrated in Figures 5.20 through 5.24. All the present data with one double and two double screen arrangements are given in Figure 5.20 with their best fit curves (Equations 5.1 and 5.5 respectively). The following figures are given to compare the effect of using multiple screens on the energy dissipation for different t/d and X/d values.

From the figures, one may discern that

- i. Two double screen arrangement is slightly more efficient compared to one double screen arrangement.

- ii. Efficiency of the two double screen arrangement becomes more pronounced with decreasing upstream flow Froude number, Fr_G .
- iii. There is no apparent dependence observed on the relative screen thickness, t/d and on the relative screen position, X/d (X_1/d and X_2/d for two double screen arrangement).

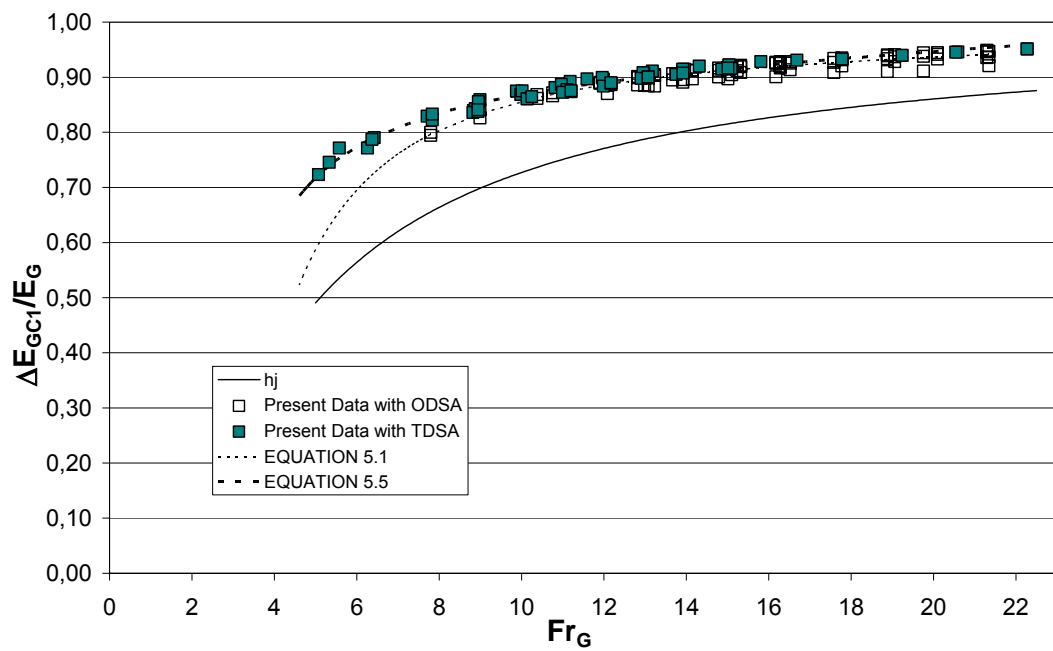


Figure 5.20 All the present data with ODSA and TDSA and their best fit curves.

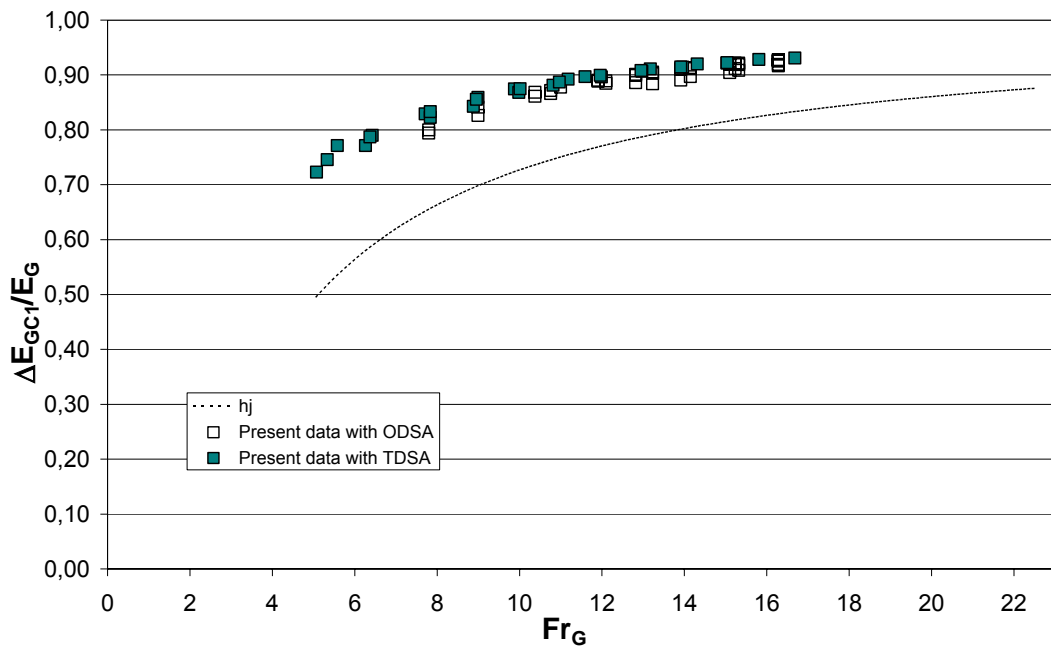


Figure 5.21 The present data with ODSA and TDSA for $t/d = 1.33D$

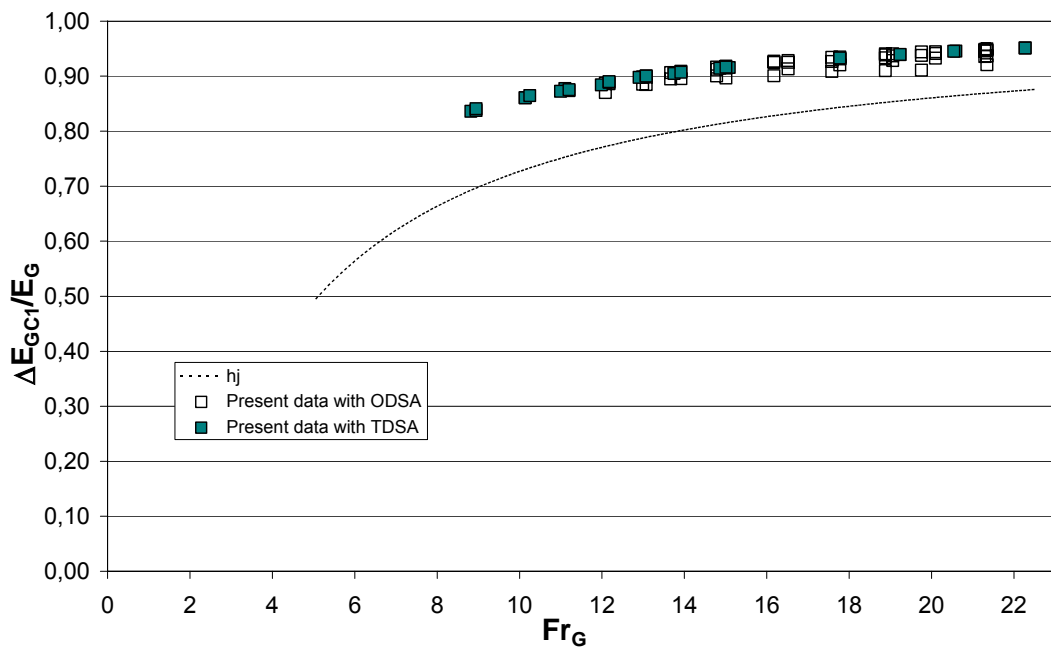


Figure 5.22 The present data with ODSA and TDSA for $t/d = 2D$

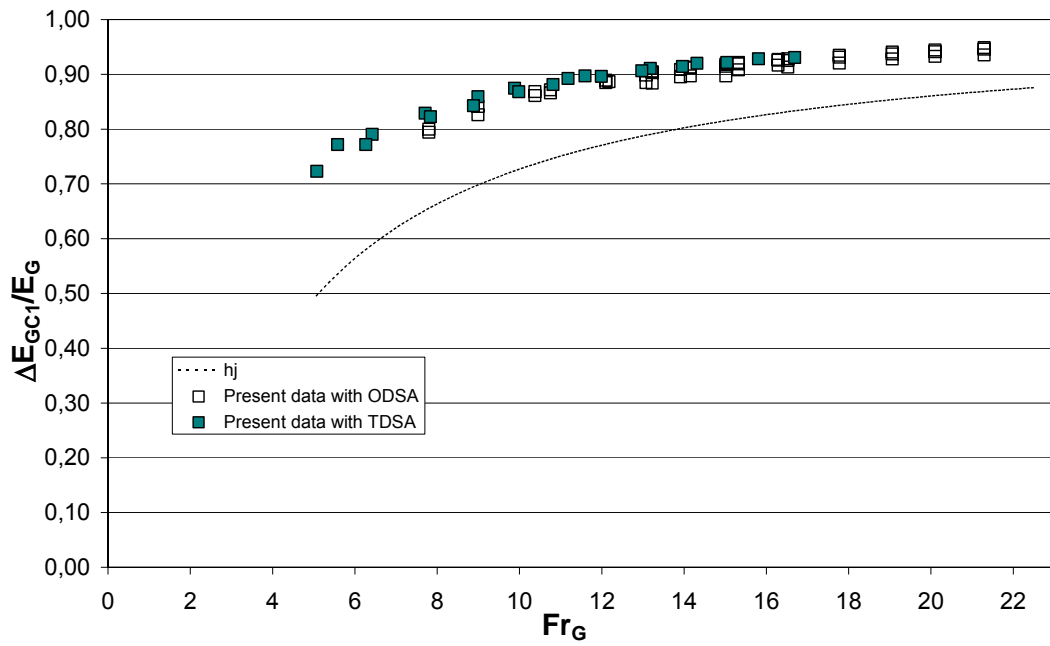


Figure 5.23 The present data with ODSA and TDSA at $X_1/d = 66$

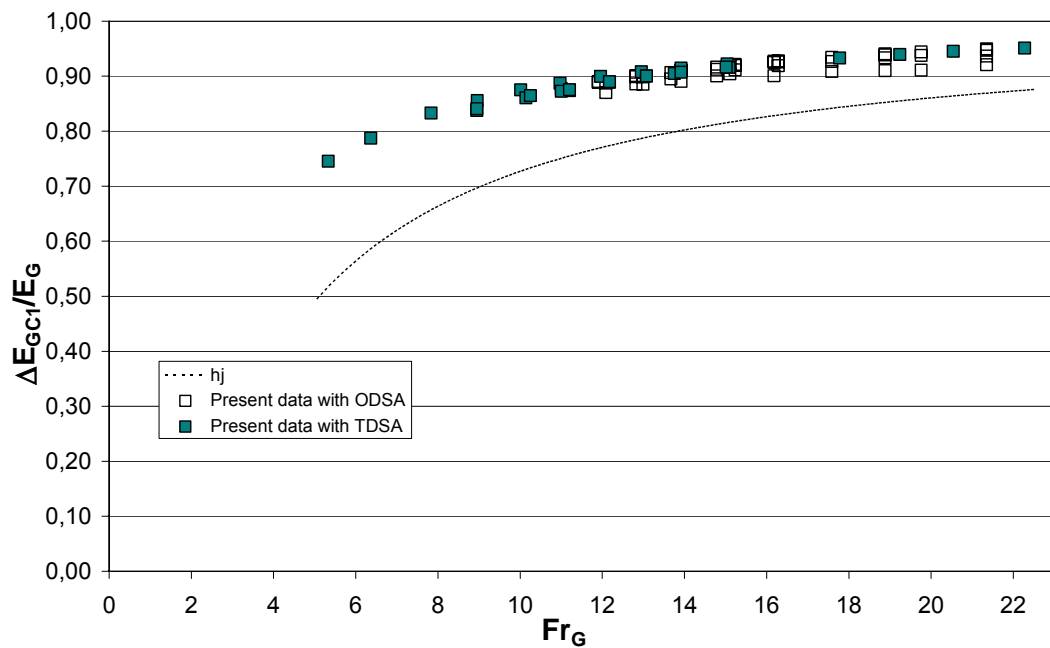


Figure 5.24 The present data with ODSA and TDSA at $X_1/d = 99$

5.3 PERFORMANCE OF THE SCREENS

As indicated before the energy loss at the screen is denoted as S . The relative energy loss S/E_G is formulated to represent the screen performance. The performance of the screens is not analyzed for TDSA because the flow parameters at section A can not be determined. Therefore, the screen efficiency is examined for only ODSA.

5.3.1 PERFORMANCE OF THE SCREENS AT LARGE

The variation of the screen performance, for ODSA is shown in Figures 5.25 through 5.29 for different relative tailwater gate heights.

In Figure 5.25, the best fit curve to all data of the present study for ODSA is shown. The equation of the best fit curve is

$$\frac{S}{E_G} = \frac{1}{(26.347 - 1.052Fr_G)} \quad (5.9)$$

The corresponding rms value and correlation coefficient are 0.604 and 0.651, respectively.

From the figures, one may discern that there is no significant dependence of the screen performance, S/E_G , on the relative screen position, X/d and on the relative screen thickness, t/d . As the upstream flow Froude number increases, S/E_G increases too. However, as the relative tailwater gate height h_t/d increases S/E_G decreases.

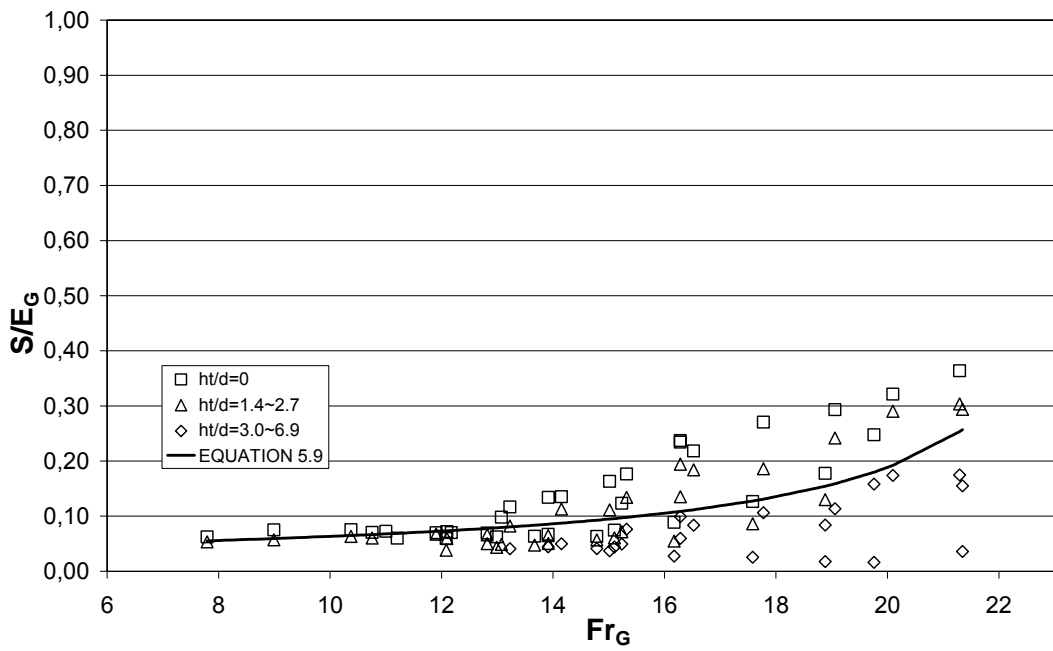


Figure 5.25 S/E_G vs. Fr_G for the ODSA data and its best fit curve

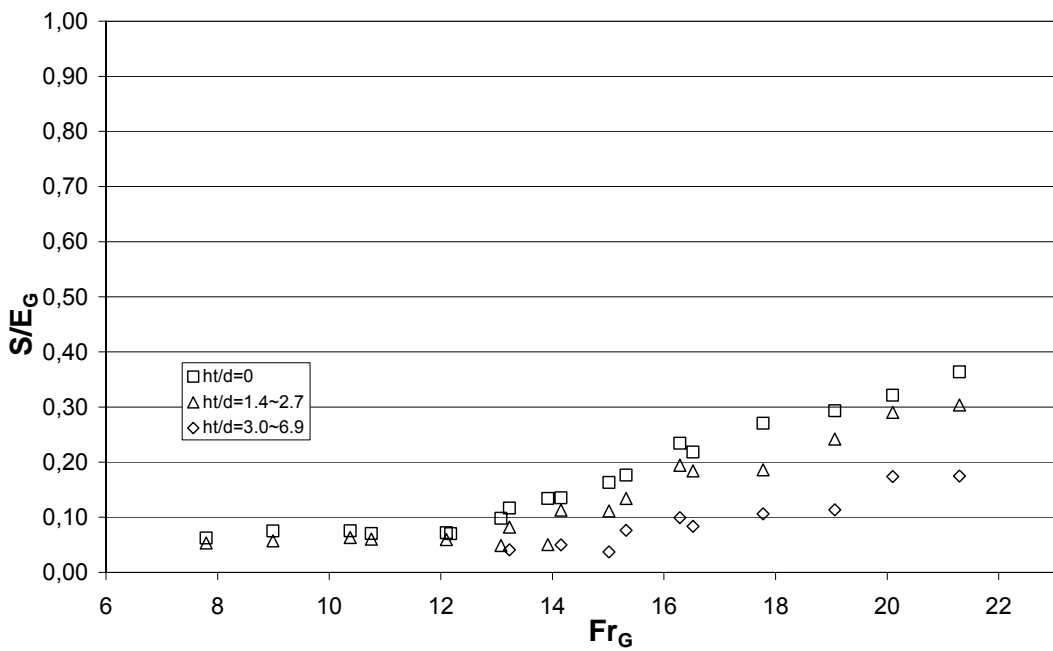


Figure 5.26 S/E_G vs. Fr_G for the ODSA data at $X/d = 66$

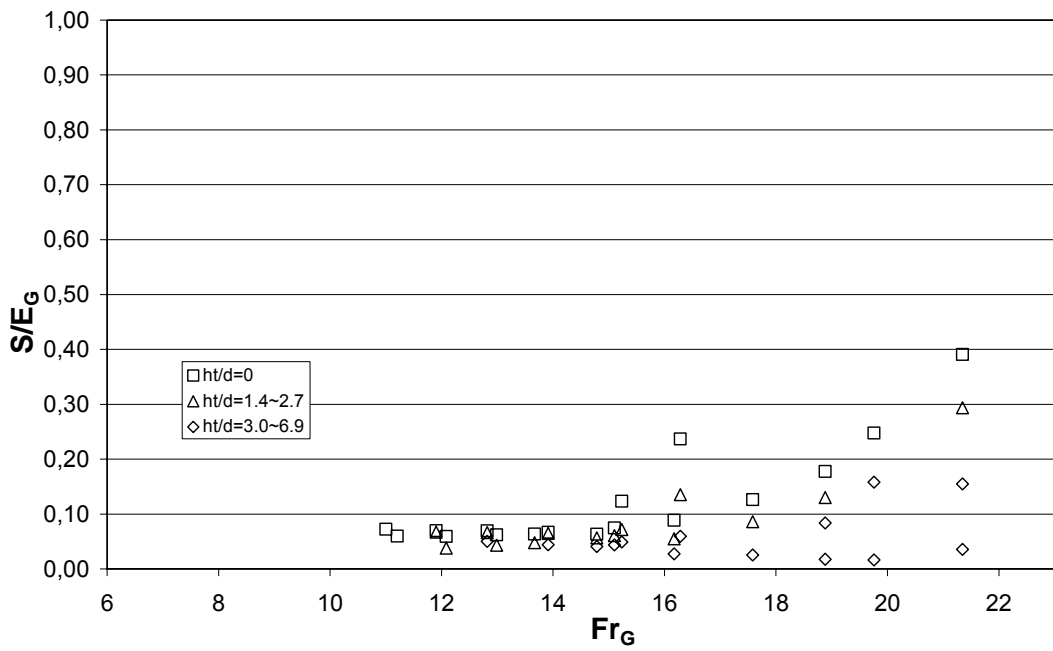


Figure 5.27 S/E_G vs. Fr_G for the ODSA data $X/d = 99$

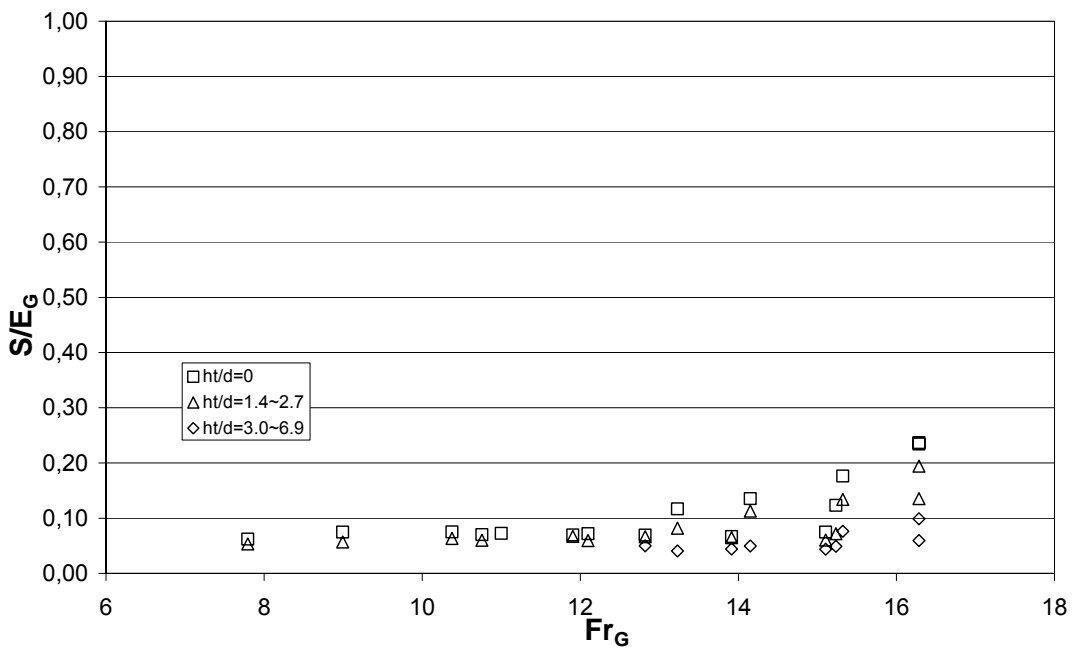


Figure 5.28 S/E_G vs. Fr_G for the ODSA data for $t/d = 1.33D$

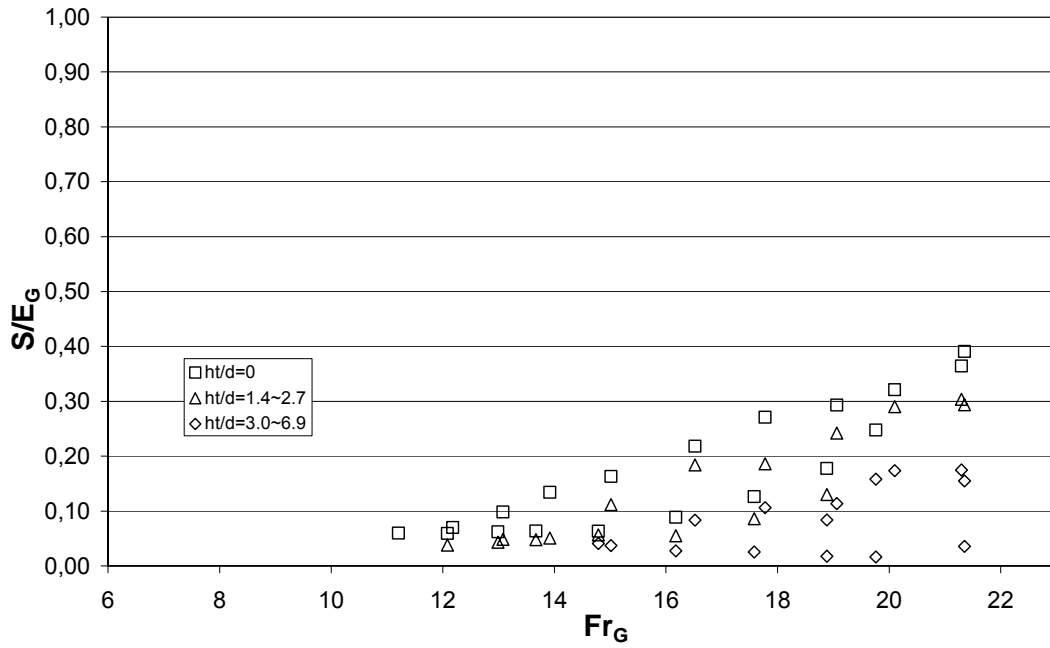


Figure 5.29 S/E_G vs. Fr_G for the ODSA data for $t/d = 2D$

Figures 5.30 through 5.41 show the relative energy loss between locations A and C_1 ($\Delta E_{AC_1}/E_A$) with respect to Froude number at location A, Fr_A . If Equation 3.11 is divided by the specific energy at location A (E_A) the following equation is obtained (Bozkuş et al. 2007);

$$\frac{S}{E_A} = \frac{\Delta E_{AC_1}}{E_A} - \frac{\Delta E_{AB}}{E_A} \quad (5.10)$$

Next, the relative energy loss term over the distance AC_1 is moved to the left side of Equation 5.10 to obtain

$$\frac{\Delta E_{AC_1}}{E_A} = \frac{S}{E_A} + \frac{\Delta E_{AB}}{E_A} \quad (5.11)$$

This form of the equation indicates that the relative energy loss over the distance AC_1 consists of two terms, namely the relative energy loss due to the screen

(thereafter called the screen contribution), and the relative energy loss over the distance AB. The contribution of the screen (S/E_A) to the relative energy loss over AC_1 is also shown in Figures 5.30 through 5.41. A line was approximated to each data group and the equation of each line is indicated in the figures. In the figures each data point at a fixed Froude number shown as a square represents how much of the original energy at location A is lost when going from A to C_1 . Similarly, each data point shown as a triangle indicates how much of this energy loss is achieved by the screen only. The data is handled separately for different relative tailwater gate heights. Despite the fact that the figures are drawn for various t/d and X/d values, the general trend in all of the figures is the same. That is, both $\Delta E_{AC_1}/E_A$ and S/E_A increase with an increase in the Froude number, Fr_A . However, the relative energy loss by the screen, S/E_A , increases at a greater rate. On the other hand, as the relative tailwater gate height h_t/d increases, the rate of increase in the relative energy loss by the screen, S/E_A , decreases.

For instance, the following observation can be made from Figure 5.30. At the point near Froude number 6 at Figure 5.30, about 74% of the energy at location A is dissipated going from A to C_1 and about 22% of that energy loss is due to the screen only (i.e. $0.16/0.74 = 0.22$). On the other hand, at the highest Froude number in Figure 5.30 (i.e. 13), about 82% of the energy loss is due to the screen only (i.e. $0.74/0.91 = 0.82$). Consequently, the energy dissipation of the screens is increasing linearly with an increase in the Froude number, as evident in Figures 5.30 through 5.41

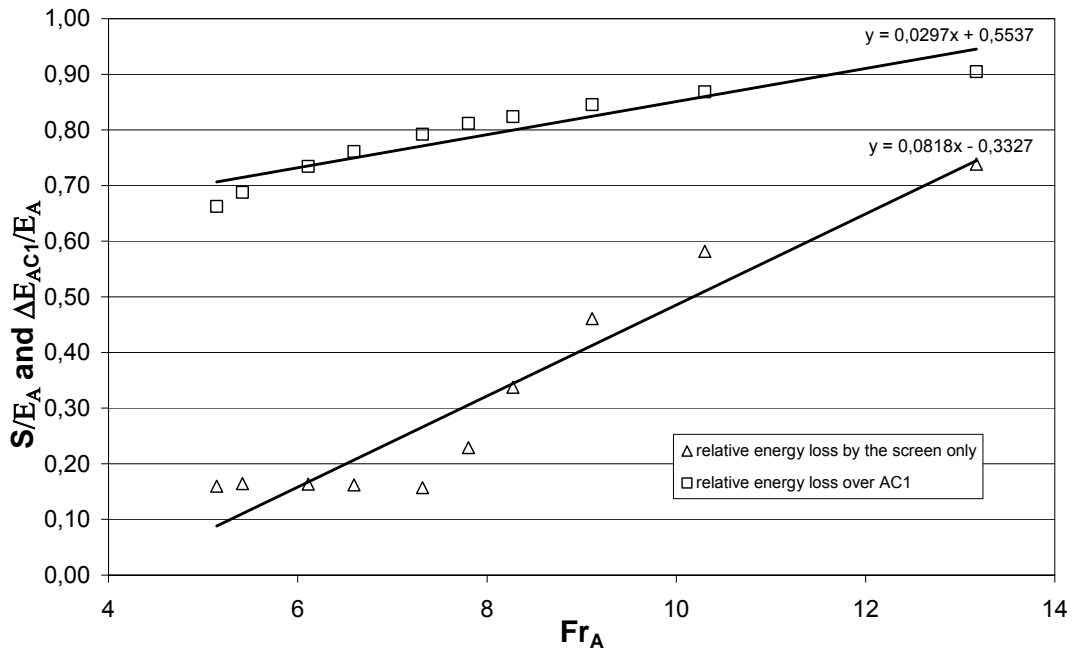


Figure 5.30 S/E_A and $\Delta E_{AC1}/E_A$ vs. Fr_A for $t/d=2D$, $X/d=99$ and $h_t/d=0$

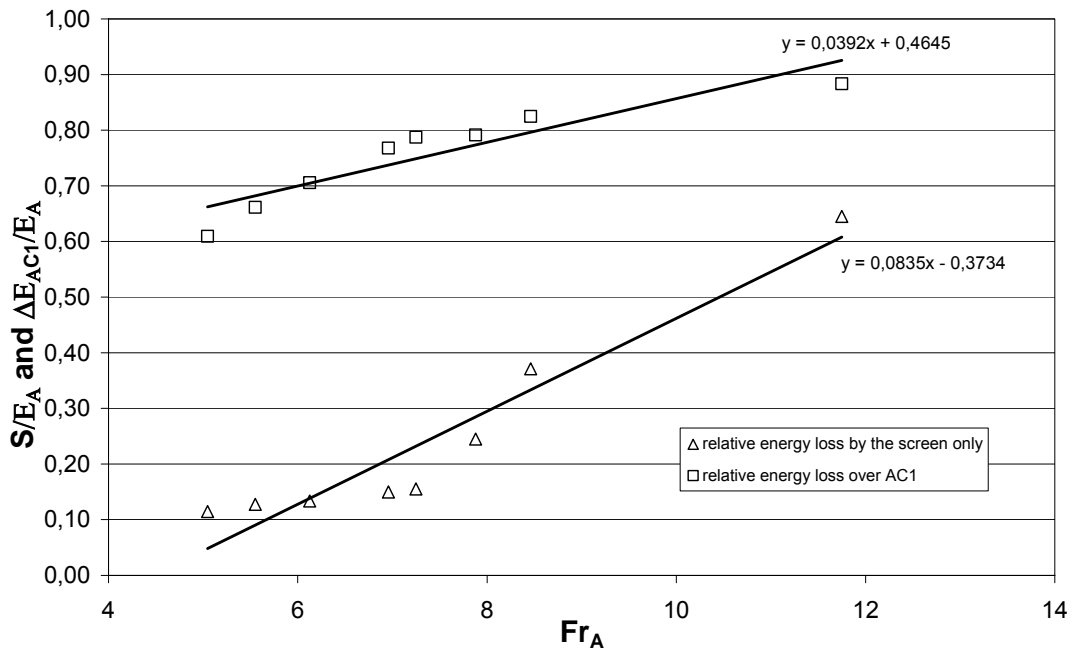


Figure 5.31 S/E_A and $\Delta E_{AC1}/E_A$ vs. Fr_A for $t/d=2D$, $X/d=99$ and $h_t/d=1.5\sim 2.7$

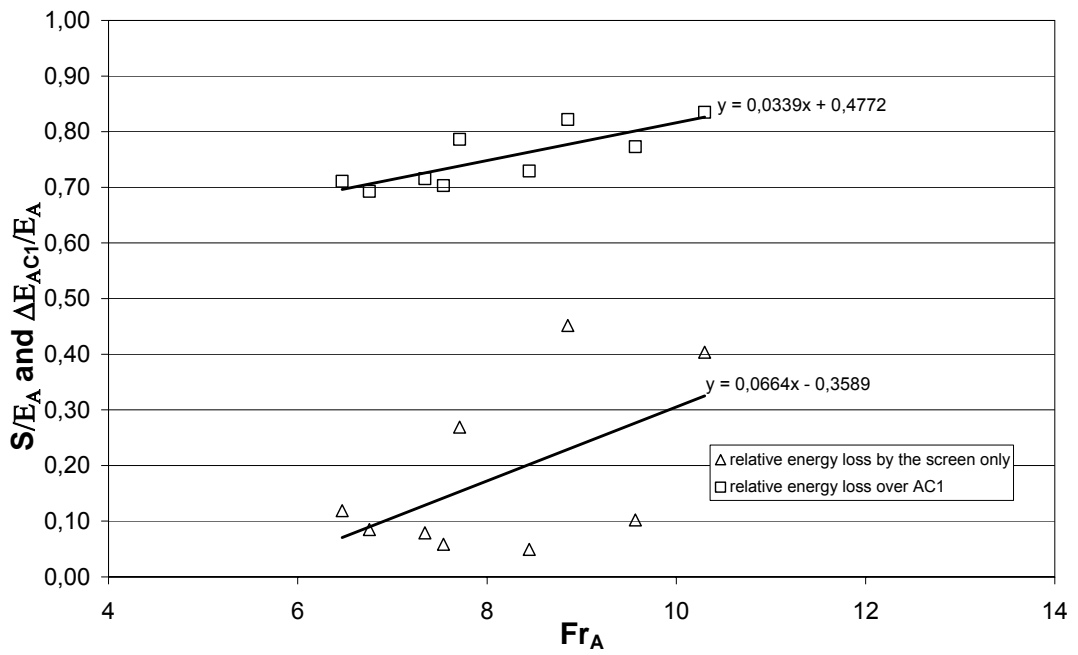


Figure 5.32 S/E_A and $\Delta E_{AC1}/E_A$ vs. Fr_A for $t/d=2D$, $X/d=99$ and $h_t/d=3.25\sim 6.9$

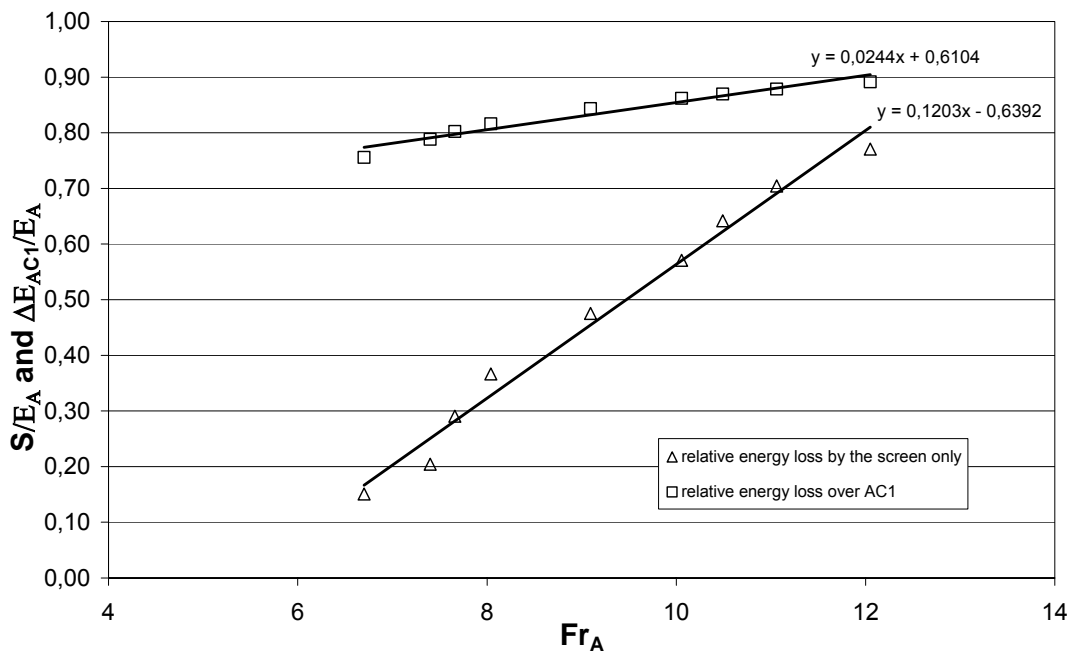


Figure 5.33 S/E_A and $\Delta E_{AC1}/E_A$ vs. Fr_A for $t/d=2D$, $X/d=66$ and $h_t/d=0$

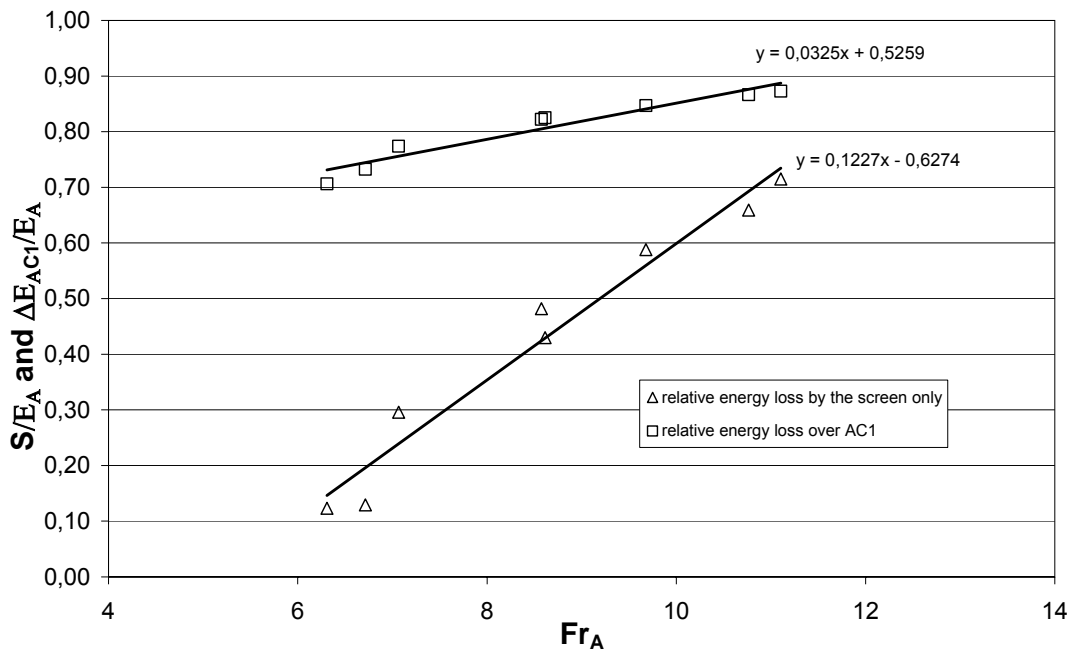


Figure 5.34 S/E_A and $\Delta E_{AC1}/E_A$ cs. Fr_A for $t/d=2D$, $X/d=66$ and $h_t/d=2.1$

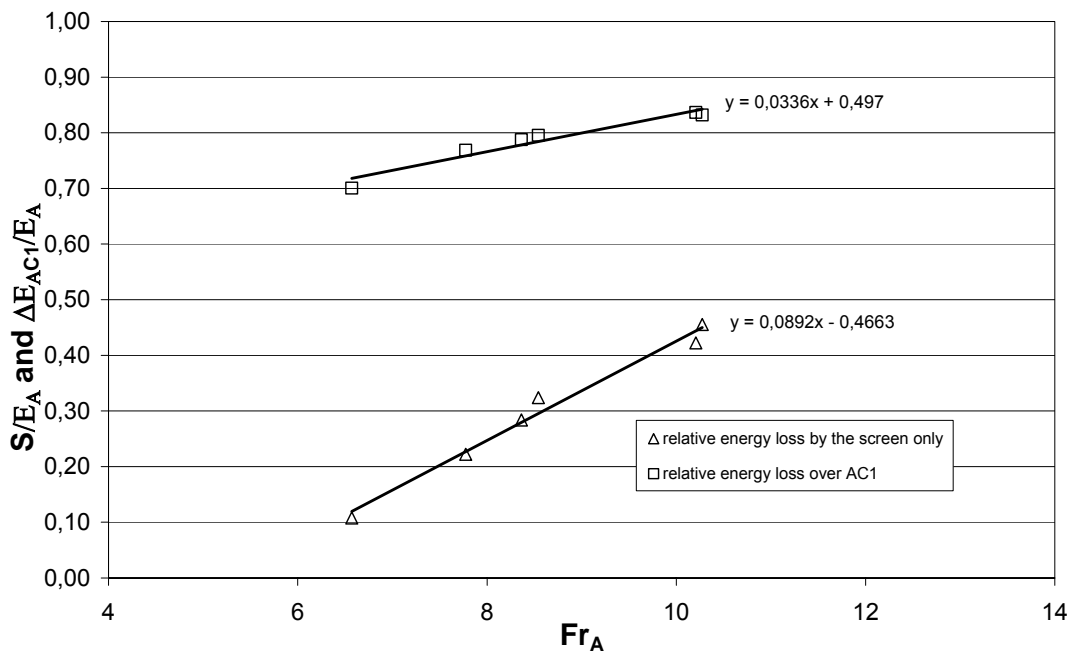


Figure 5.35 S/E_A and $\Delta E_{AC1}/E_A$ vs. Fr_A for $t/d=2D$, $X/d=66$ and $h_t/d=3.9\sim 4.5$

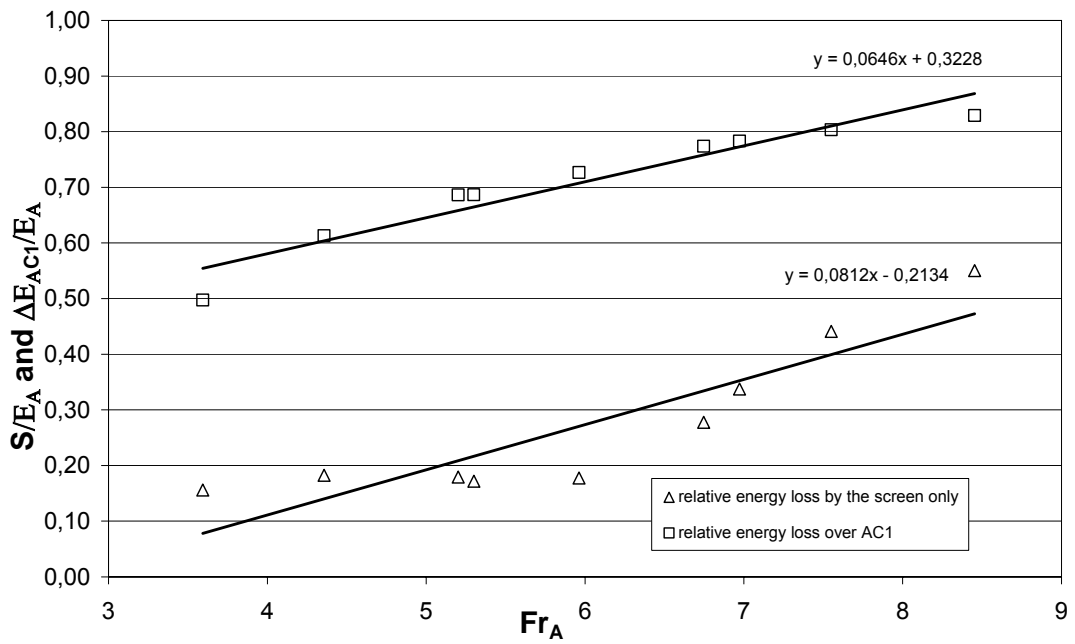


Figure 5.36 S/E_A and $\Delta E_{AC1}/E_A$ vs. Fr_A for $t/d=1.33D$, $X/d=66$ and $h_t/d=0$

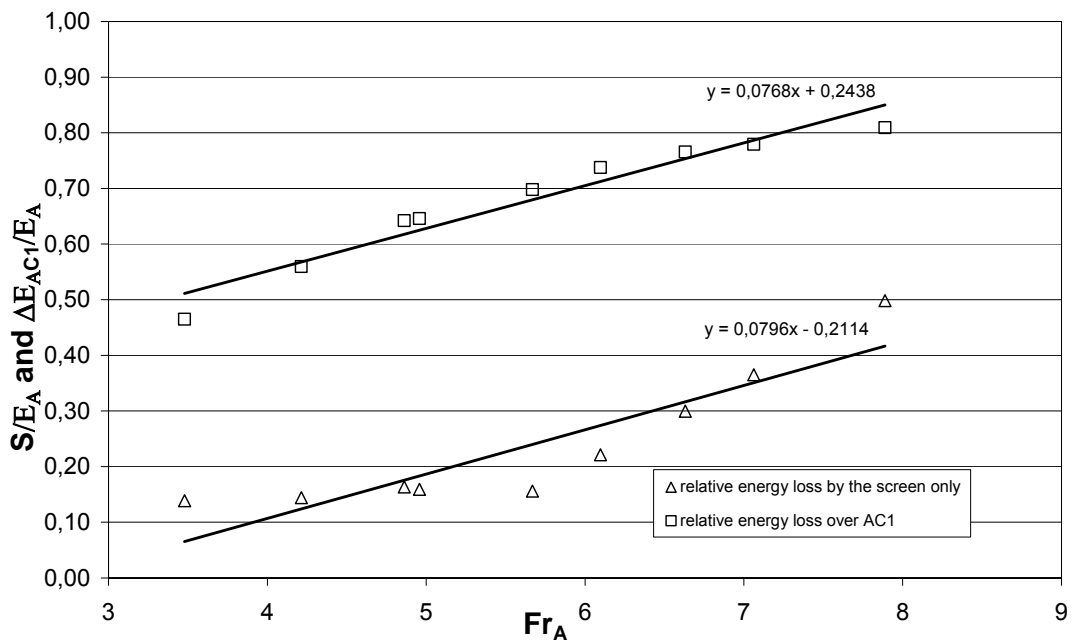


Figure 5.37 S/E_A and $\Delta E_{AC1}/E_A$ vs. Fr_A for $t/d=1.33D$, $X/d=66$ and $h_t/d=1.4$

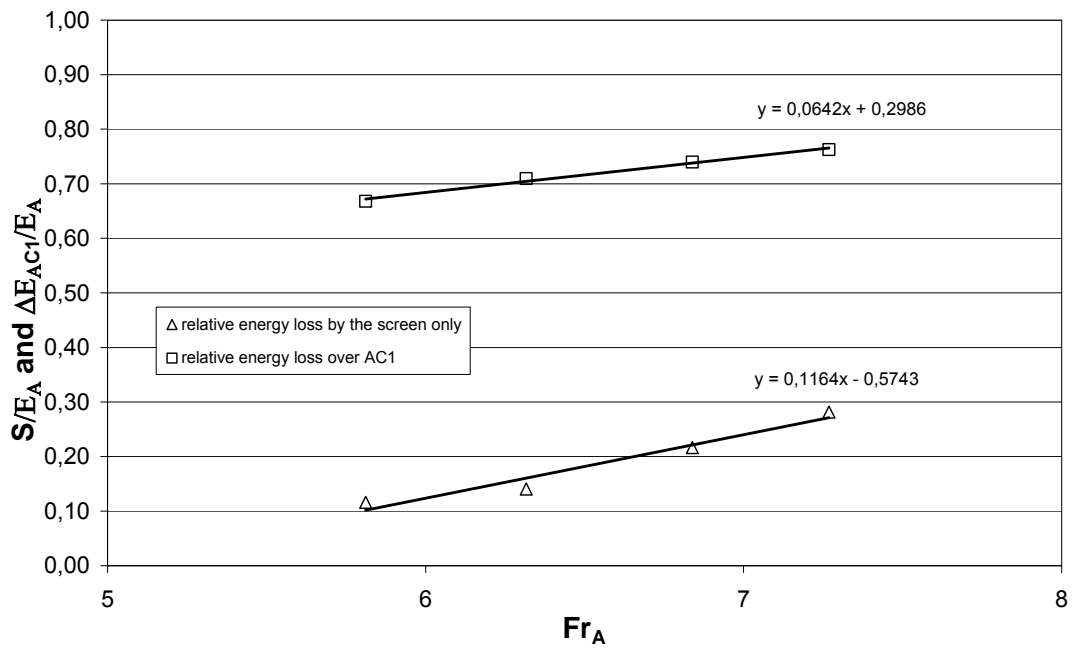


Figure 5.38 S/E_A and $\Delta E_{AC1}/E_A$ vs. Fr_A for $t/d=1.33D$, $X/d=66$ and $h_t/d=3.0$

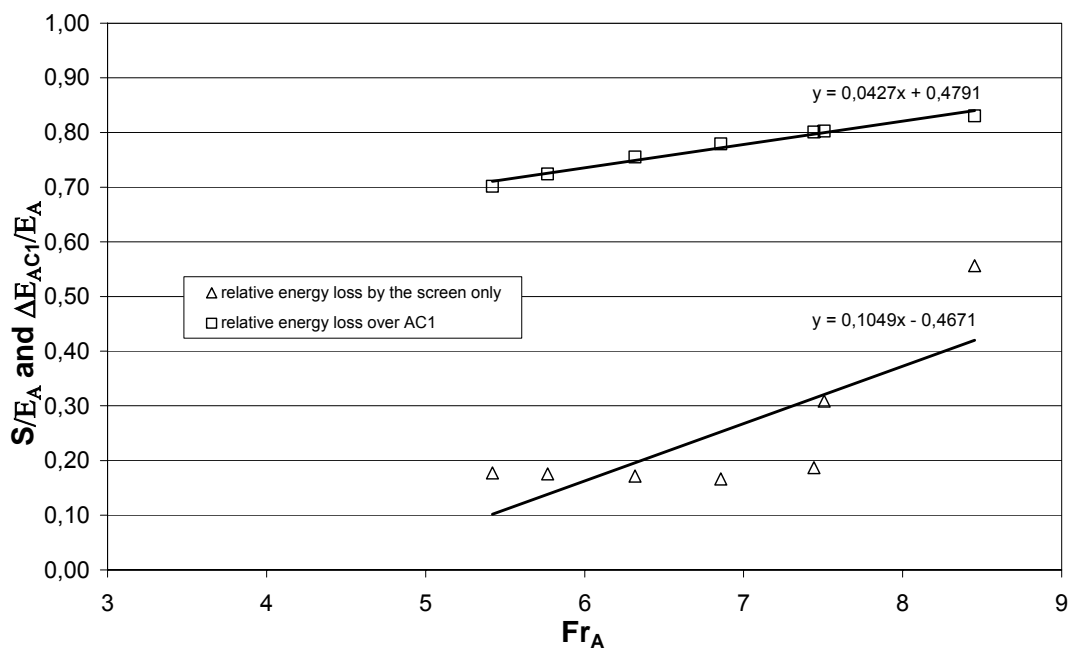


Figure 5.39 S/E_A and $\Delta E_{AC1}/E_A$ vs. Fr_A for $t/d=1.33D$, $X/d=99$ and $h_t/d=0$

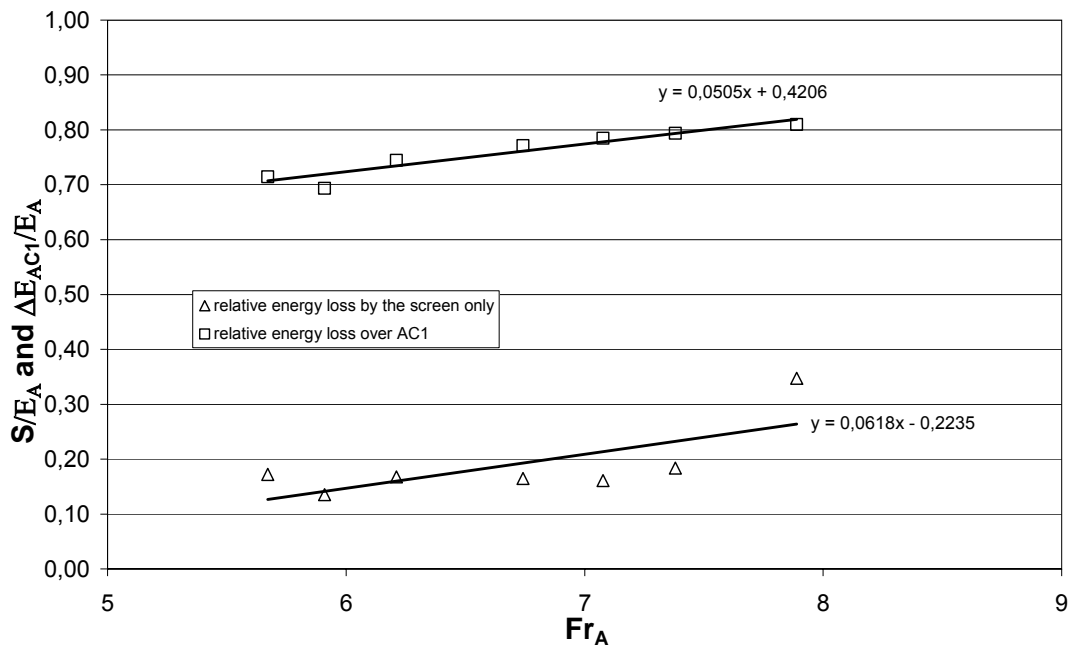


Figure 5.40 S/E_A and $\Delta E_{AC1}/E_A$ vs. Fr_A for $t/d=1.33D$, $X/d=99$ and $h_t/d=1.4\sim 2.6$

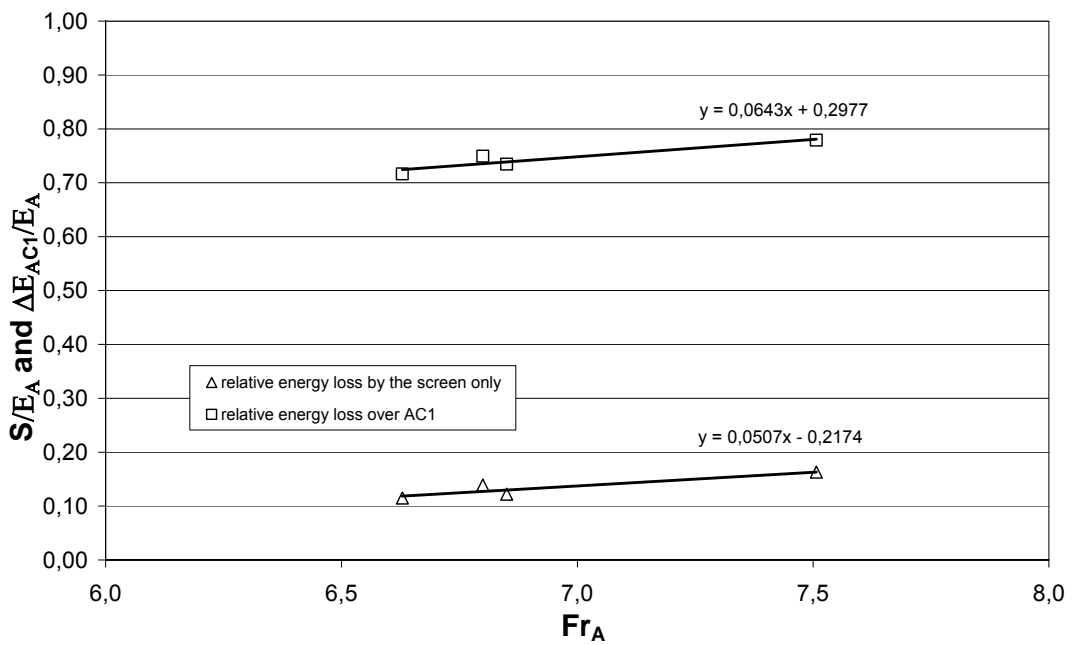


Figure 5.41 S/E_A and $\Delta E_{AC1}/E_A$ vs. Fr_A for $t/d=1.33D$, $X/d=99$ and $h_t/d=3.0$

5.4 SYSTEM EFFICIENCIES

The system efficiency is defined as the ratio of the difference between the system loss, ΔE_{GC1} and the energy loss that would occur if there were a full jump at section G, ΔE_{JG} to ΔE_{JG} as defined in Equations 3.13 and 3.18.

Figures 5.42 through 5.49 show the variations of the system efficiencies for one double and two double screen arrangements with different relative tailwater gate heights, h_t/d .

From the figures, one may discern that there is no significant dependence of the system efficiency, η_{sys} , on the relative screen position, X/d and on the relative screen thickness, t/d . However, as the relative tailwater gate height, h_t/d , increases, system efficiency decreases.

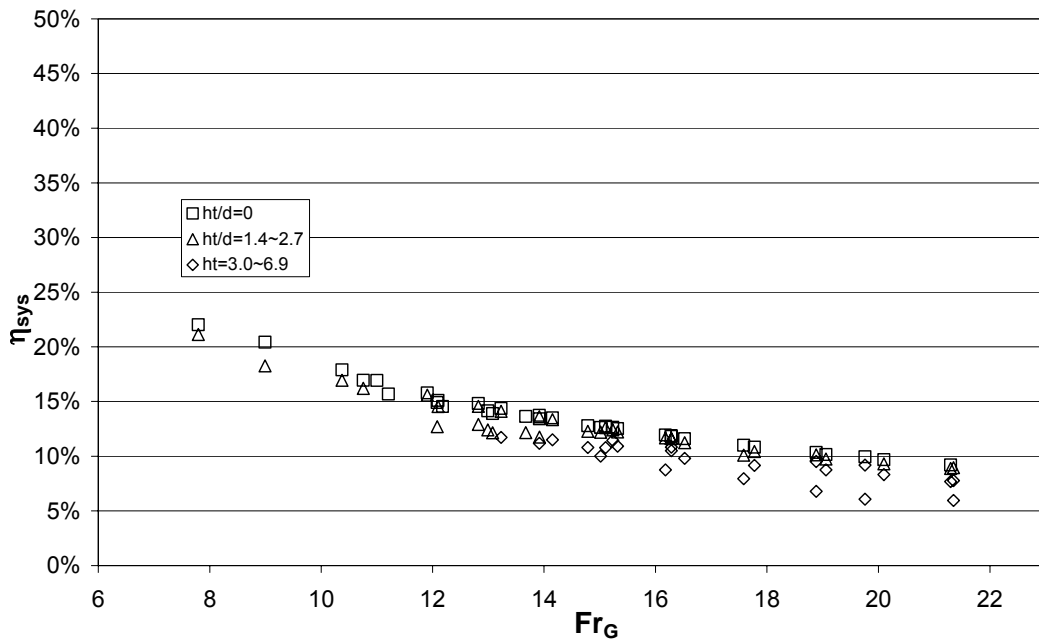


Figure 5.42 η_{sys} vs. Fr_G for ODSA with different h_t/d

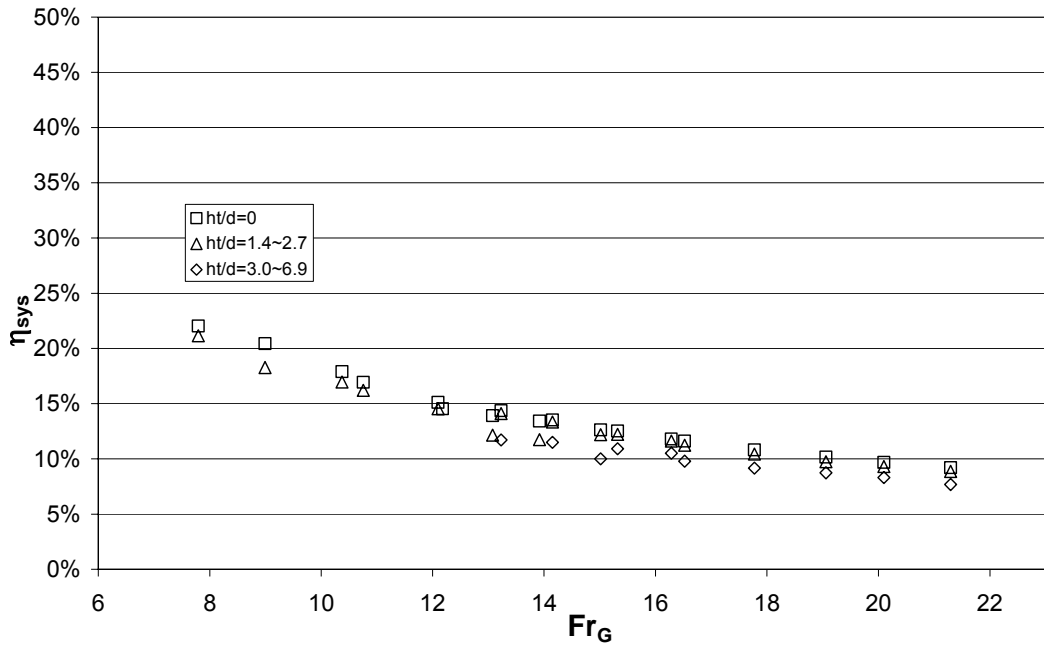


Figure 5.43 η_{sys} vs. Fr_G for ODSA with different h_t/d at $X/d = 66$

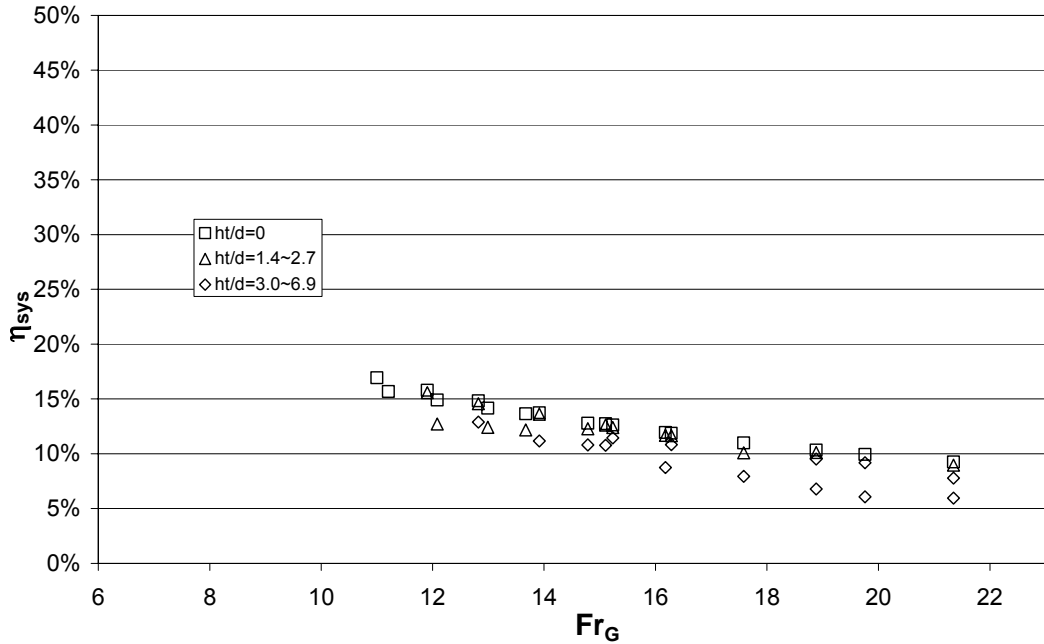


Figure 5.44 η_{sys} vs. Fr_G for ODSA with different h_t/d at $X/d = 99$

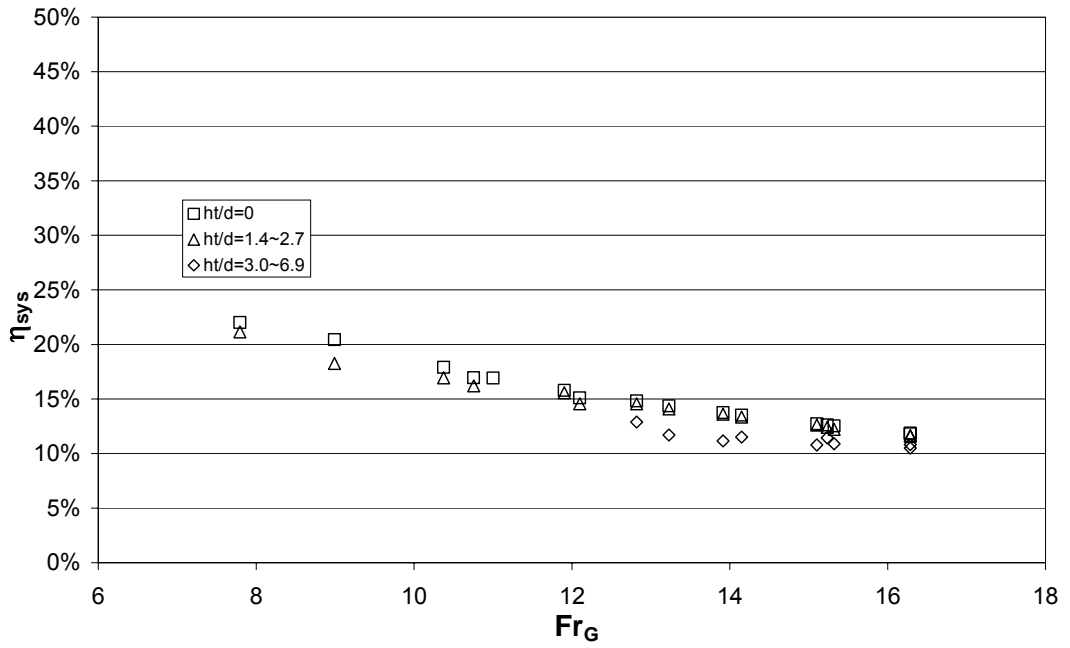


Figure 5.45 η_{sys} vs. Fr_G for ODSA with different h_t/d for $t/d = 1.33D$

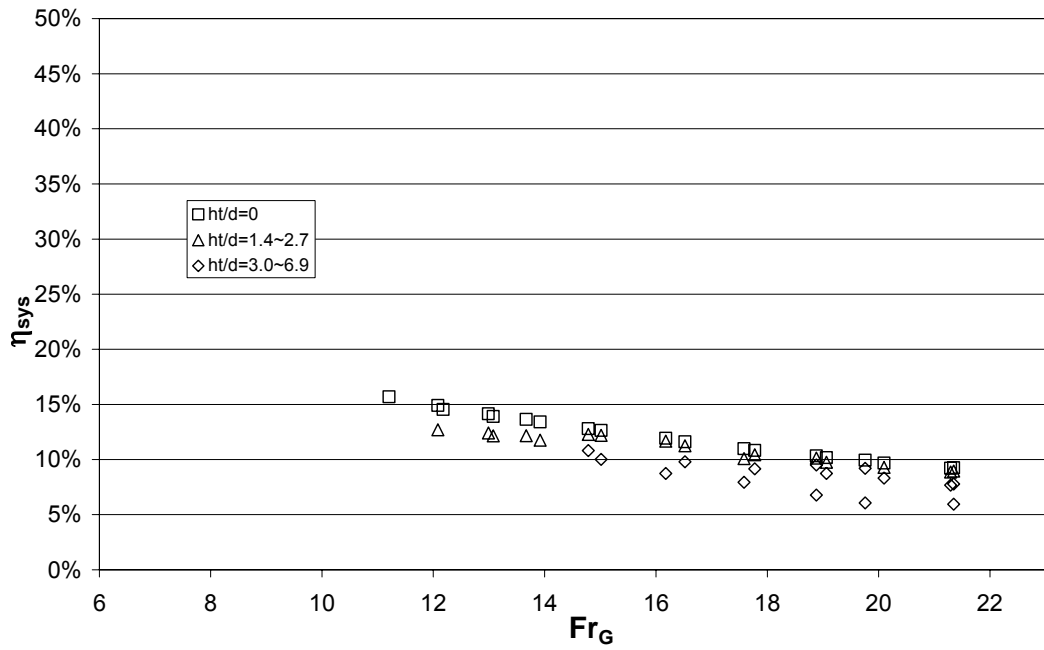


Figure 5.46 η_{sys} vs. Fr_G for ODSA with different h_t/d for $t/d = 2D$

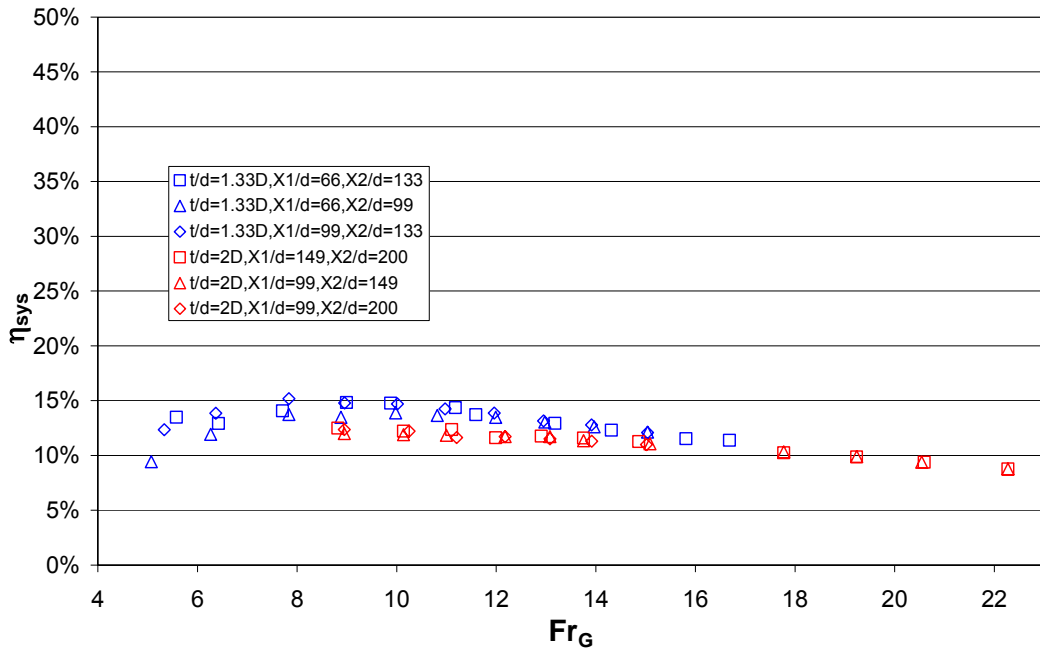


Figure 5.47 η_{sys} vs. Fr_G for TDSA

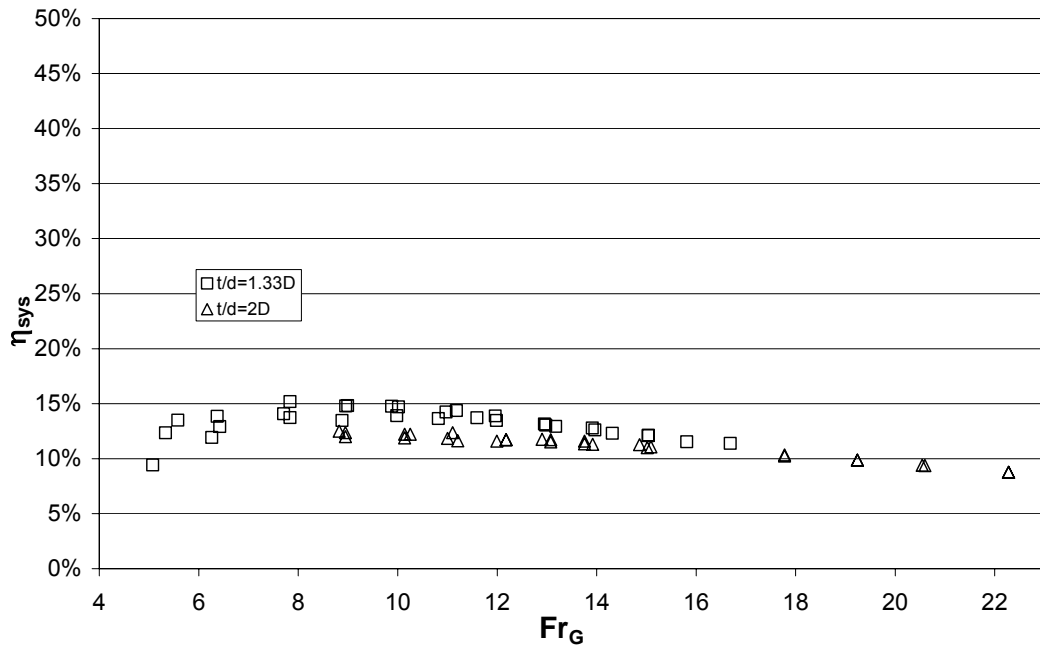


Figure 5.48 η_{sys} vs. Fr_G for TDSA with different t/d

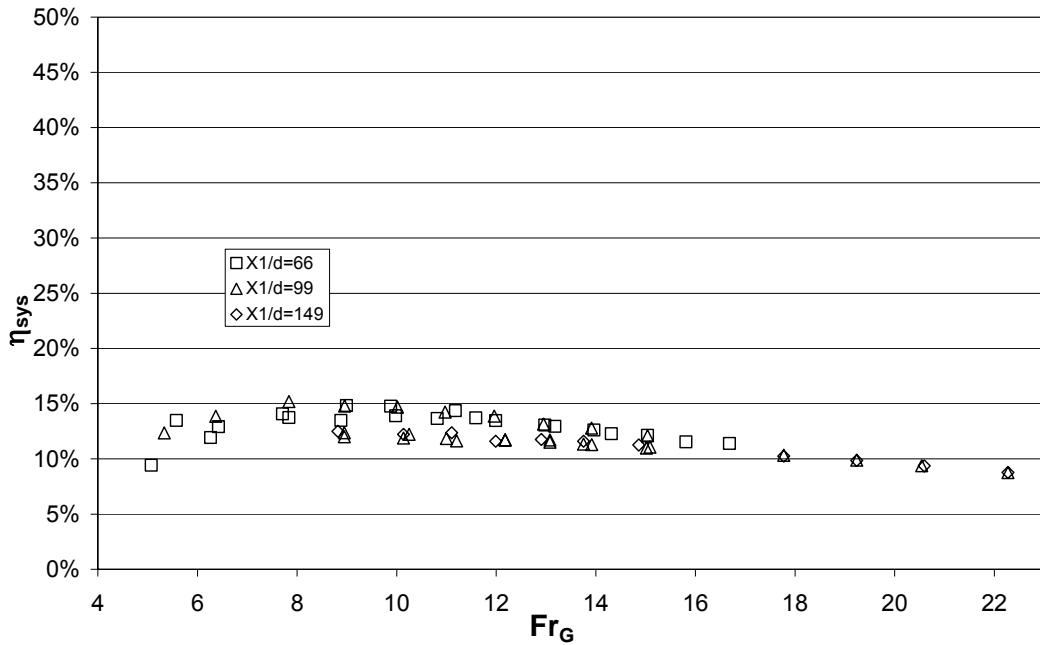


Figure 5.49 η_{sys} vs. Fr_G for TDSA with different X_1/d

5.4.1 COMPARISON OF SYSTEM EFFICIENCIES OF ODSA AND TDSA

The effect of using multiple screens is demonstrated in Figure 5.50. All the present data with one double and two double screen arrangements are given in Figure 5.50 with their best fit curves (Equations 5.12 and 5.13 respectively) with the following forms,

$$\eta_{sys} = \frac{1}{(0.282 + 0.542Fr_G)} \quad (5.12)$$

$$\eta_{sys} = \frac{1}{(6.279 + 0.158Fr_G)} \quad (5.13)$$

From the figure, one may discern that the rate of decreases of η_{sys} for one double screen arrangement with increasing upstream flow Froude number is greater than two double screen arrangement. Moreover, for relatively low upstream flow Froude numbers η_{sys} is greater for one double screen arrangement than two double screen arrangement. However, for relatively high upstream flow Froude numbers η_{sys} is greater for two double screen arrangement than one double screen arrangement. This result indicates that there is an optimum Froude number (around 15.5 from the Figure 5.50) at which the system efficiency, η_{sys} , is same for both one double and two double screen arrangements.

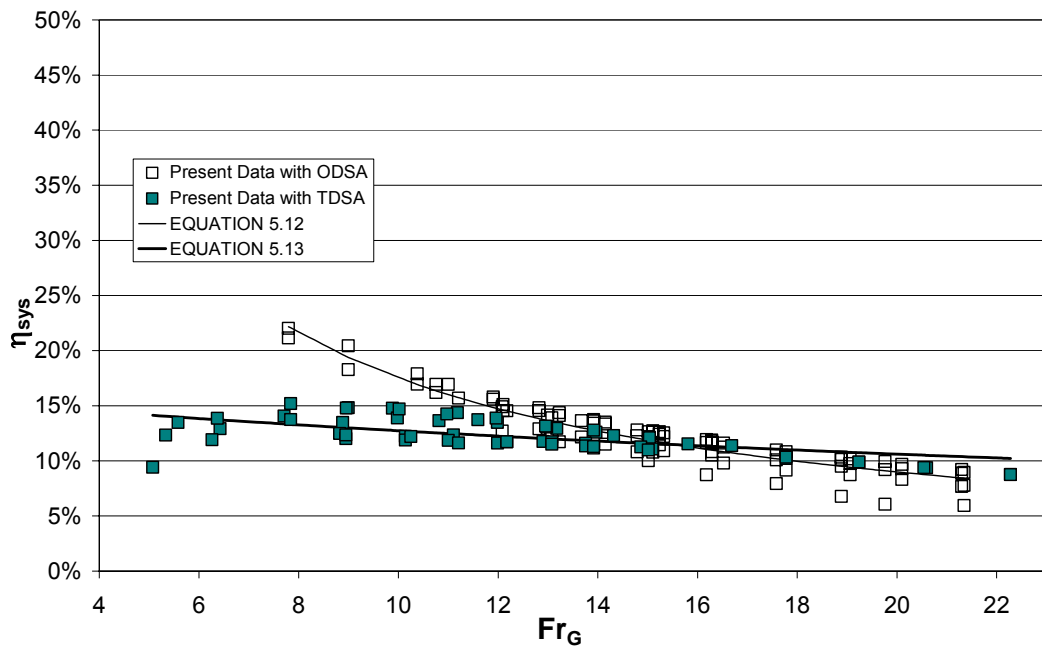


Figure 5.50 η_{sys} vs. Fr_G for ODSA and TDSA and their best fit curves

5.5 SCREEN EFFICIENCIES

Screen efficiency is defined as the ratio of the loss at the screen over the loss of a hypothetical jump at section G, as defined in Equation 3.14.

The screen efficiency is not analyzed for TDSA because the flow parameters at section A can not be determined. Therefore, the screen efficiency is examined for only ODSA.

Figures 5.51 through 5.55 show the variations of the screen efficiencies for one double screen arrangement with different relative tailwater gate heights, h_t/d .

From the figures, one may discern that there is no significant dependence of the screen efficiency, η_{scr} , on the relative screen position, X/d and on the relative screen thickness, t/d . As the upstream flow Froude number increases, η_{scr} increases too. However, as the relative tailwater gate height, h_t/d , increases, screen efficiency decreases.

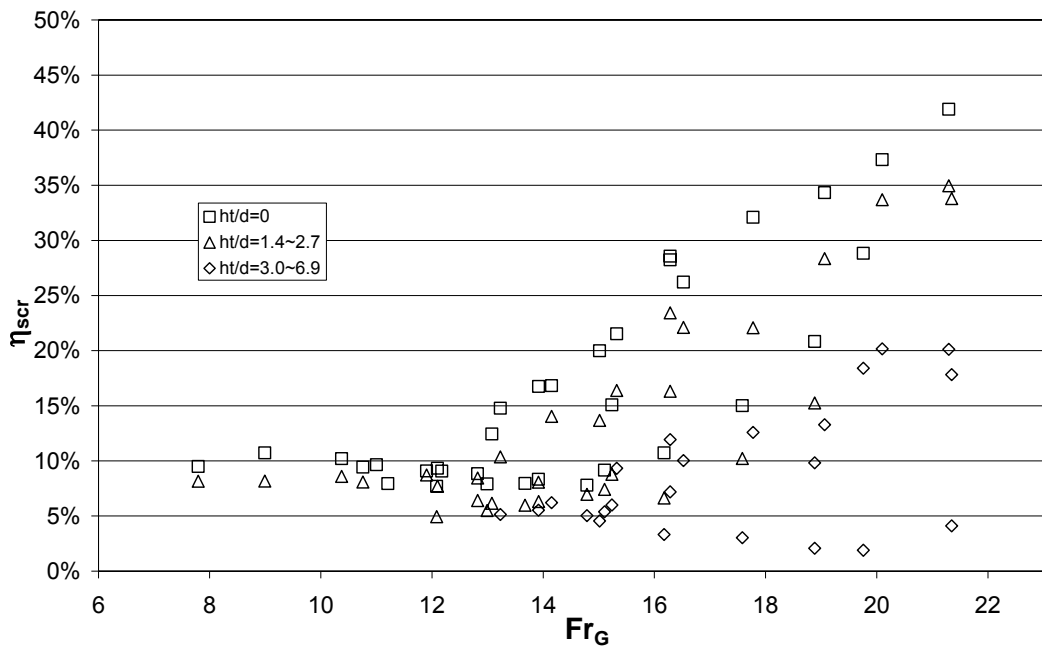


Figure 5.51 η_{scr} vs. Fr_G for ODSA

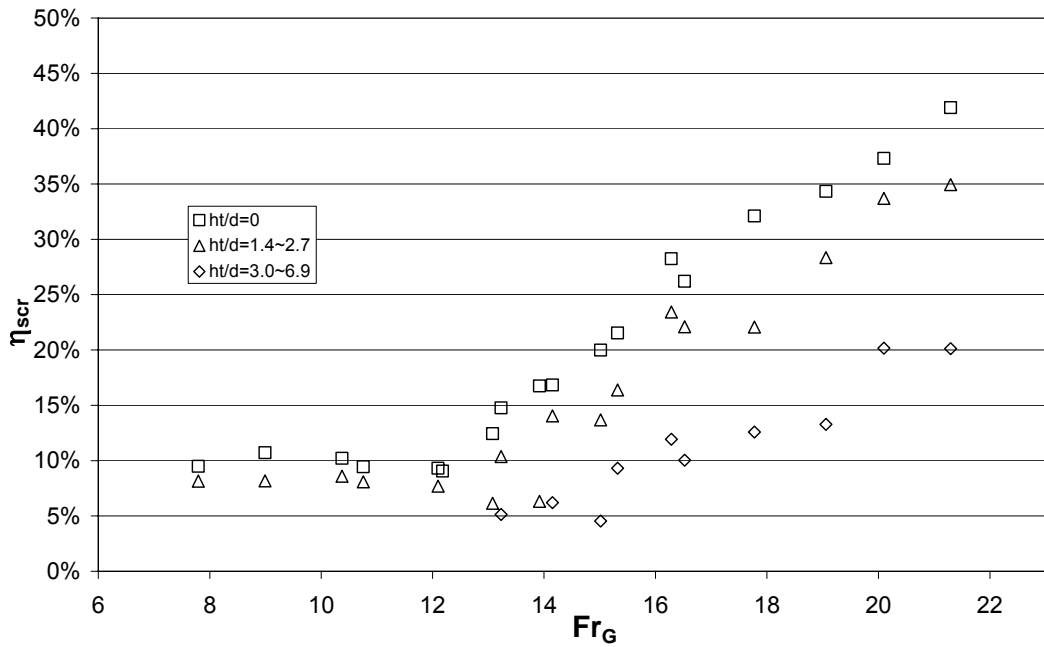


Figure 5.52 η_{scr} vs. Fr_G for ODSA with different h/d at $X/d = 66$

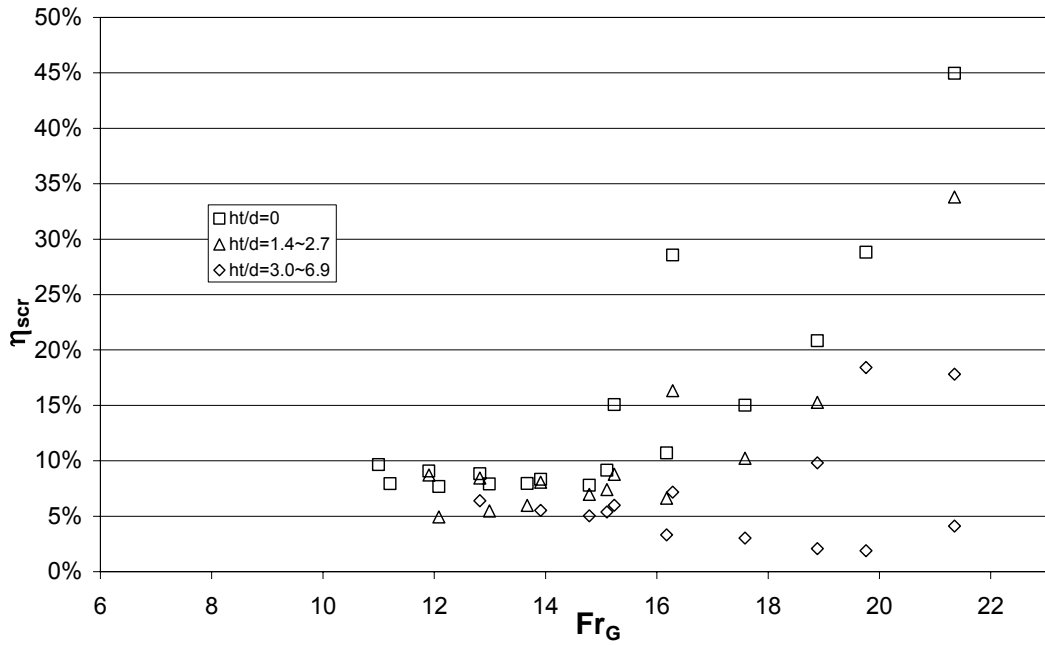


Figure 5.53 η_{scr} vs. Fr_G for ODSA with different h_t/d at $X/d = 99$

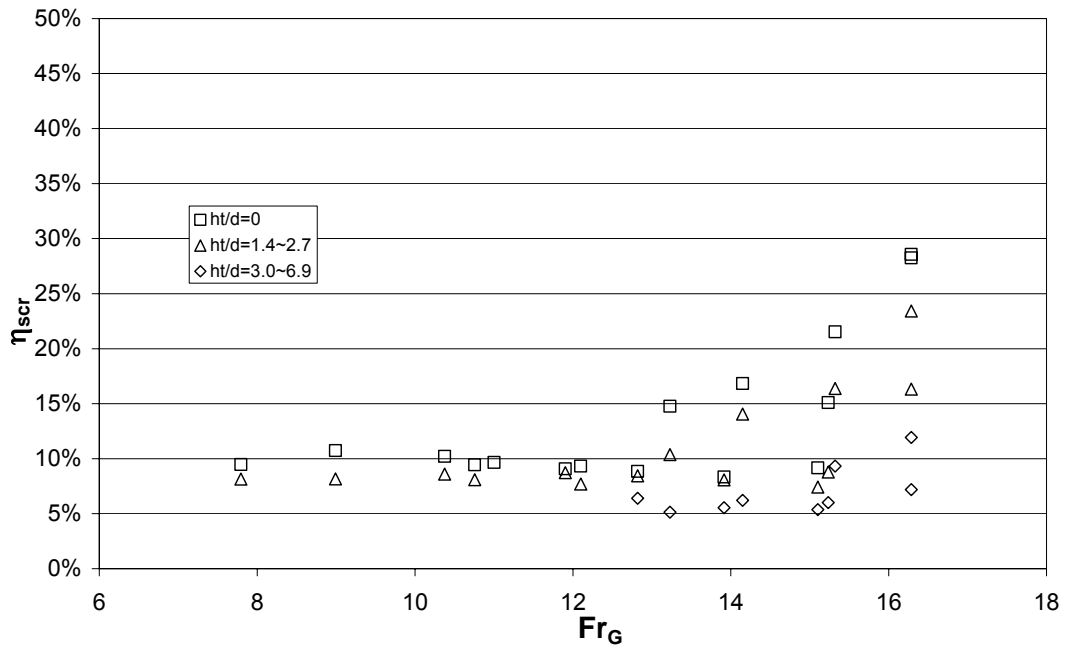


Figure 5.54 η_{scr} vs. Fr_G for ODSA with different h_t/d for $t/d = 1.33D$

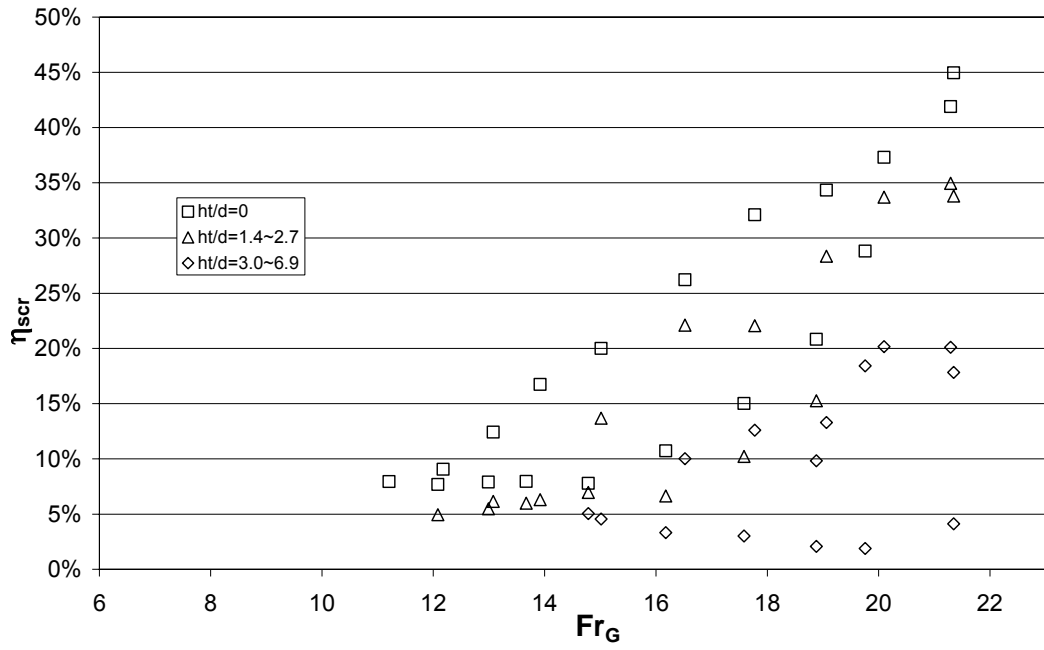


Figure 5.55 η_{scr} vs. Fr_G for ODSA with different h_t/d for $t/d = 2D$

CHAPTER 6

CONCLUSIONS AND RECOMMENDATIONS

In the present thesis work, the effects of tailwater depth and multiple screen usage upon efficiency of screens on the energy dissipation is analyzed experimentally. As indicated in the previous chapters, vertically placed double screens with a porosity of 40% are utilized in one double screen and two double screen arrangements for the experiments. Froude number range covered during the study is from 5.0 to 22.5. The gate opening simulating a hydraulic structure is adjusted at heights of 2 cm and 3 cm in accordance with t/d , X/d and h_t/d relation specified in the dimensional analysis.

The conclusions drawn from the analysis of the experimental data are as follows;

- i. All of the experiments performed showed that energy dissipation is always more than that of a classical full hydraulic jump for the same Froude number as shown in Figures 5.1 and 5.7,
- ii. There is a general trend that the system performance decrease with increasing h_t/d (shown in Figure 5.2),
- iii. System performance of two double screen arrangement is better than one double screen arrangement (shown in Figure 5.20),
- iv. There is a general trend that both the system and screen performances increase with increasing Fr_G (shown in Figures 5.1, 5.7 and 5.25),

- v. Screen performance decrease with increasing h_t/d (shown in Figures 5.25 through 5.29),
- vi. The relative energy loss over the distance AC_1 , $\Delta E_{AC1}/E_A$, and contribution of the screen, S/E_A , increase with an increase in the Froude number, Fr_A (shown in Figures 5.30 through 5.41),
- vii. System efficiency decrease with increasing Fr_G (shown in Figures 5.42 and 5.47),
- viii. System efficiency decrease with increasing h_t/d (shown in Figures 5.42 through 5.46),
- ix. The rate of decrease of η_{sys} for one double screen arrangement with increasing upstream flow Froude number is greater than two double screen arrangement (shown in Figure 5.50),
- x. Screen efficiency increase with increasing Fr_G (shown in Figure 5.51),
- xi. Screen efficiency decrease with increasing h_t/d (shown in Figures 5.51 through 5.55),
- xii. In the range studied, the relative screen thickness, t/d , and relative screen position, X/d , have no significant effect on the system performance, screen performance, screen efficiency and system efficiency.
- xiii. The entire screen configurations studied at METU indicated that no configuration has any substantial superiority over the rest for the effectiveness of the screens in energy dissipation. Therefore, it is

recommended that the vertical screen be used in practice since it is cheaper and easier to build it.

Present study can be further developed by considering the followings;

- Thicker screens
- Different functions for β parameter
- Different hole geometry

Before putting into practice the screen-type energy dissipaters, real life factors such as vibration or debris accumulation behind the screen that could plug the holes should be investigated extensively.

REFERENCES

Balkış, G. (2004). “Experimental Investigation of Energy Dissipation Through Inclined Screens”. MSc Thesis Department of Civil Engineering Middle East Technical University, Ankara, Turkey.

Bozkuş, Z., Çakır, P., Ger, M. and Özeren, Y.(2004) “Energy Dissipation Through Screens “, Proceedings of ASCE World Water & Environmental Resources Conference 2004 ,Salt Lake City, Utah, U.S.A.

Bozkuş, Z., Balkış, G. and Ger, M. (2005) “Effect of Inclination of Screens on Energy Dissipation Downstream of Small Hydraulic Structures“, Proceedings of the 17th Canadian Hydrotechnical Conference, Edmonton, Alberta, Canada.

Bozkuş, Z., Güngör, E. and Ger, M. (2006) “Energy Dissipation by Triangular Screens“, Proceedings of the Seventh International Congress on Advances in Civil Engineering, Yıldız Technical University, İstanbul, Turkey.

Bozkuş, Z., Çakır, P. and Ger, M. (2007) “Energy Dissipation by Vertically Placed Screens“, Canadian Journal of Civil Engineering, Vol. 34, No. 4, 557-564.

Çakır, P. (2003). “Experimental Investigation of Energy Dissipation Through Screens”. MSc Thesis Department of Civil Engineering Middle East Technical University, Ankara, Turkey.

French, R. H. (1986). “Open Channel Hydraulics.” McGraw-Hill Book Company, Singapore.

Güngör, E. (2005). "Experimental Investigation of Energy Dissipation Through Triangular Screens". MSc Thesis Department of Civil Engineering Middle East Technical University, Ankara, Turkey.

Henderson, F. M. (1966). "Open Channel Flow." Macmillan Publishing Co. Inc., New York, U.S.A.

Munson, B.R., Young, D. F. and Okiishi, T. H. (1994). "Fundamentals of Fluid Mechanics." John Wiley and Sons, Inc., Toronto, Canada.

Rajaratnam, N., Subramanya, K. (1967). "Flow Immediately Below Submerged Sluice Gate." Journal of the Hydraulics Division, Vol. 93, No. HY4, 57-77.

Rajaratnam, N. (1977). "Free Flow Immediately Below Sluice Gates." Journal of the Hydraulics Division, Vol. 103, No. HY4, 345-351.

Rajaratnam, N., Hurtig, K. I. (2000). "Screen-Type Energy Dissipater for Hydraulic Structures." Journal of Hydraulic Engineering, Vol. 126, No. 4, 310-312.

Simon, A. L. (1981). "Practical Hydraulics." John Wiley and Sons, Inc., Toronto, Canada.

APPENDIX A

ORIFICE METER DETAILS

An orifice meter whose design is made according to the Institution of Turkish Standards (TSE) specifications (Figure A.1) is constructed on the pipe serving as a link between the constant head tank and the pressurized tank. A 30 degree inclined mercury manometer, used for the discharge measurements, is connected to the orifice meter.

The principle of the orifice is based on reduction of the cross section of the flowing stream in passing through the orifice which causes an increase in velocity that is accompanied by a decrease in pressure. The reduction in pressure between the taps is measured by the manometer. Bernoulli's equation provides a basis for correlating the increase in velocity head with the decrease in pressure head and this correlation provides a way of measuring the flowrate (Manson, Young, and Okiishi (1994)).

Assuming the flow is horizontal, steady, inviscid and incompressible between points (1) and (2), then Energy equation becomes

$$\frac{p_1}{\gamma} + \frac{V_1^2}{2g} = \frac{p_2}{\gamma} + \frac{V_2^2}{2g} + h_L \quad (\text{A.1})$$

Ideally hydraulic losses, $h_L=0$. However, non-ideal case occurs for two reasons. Firstly, the vena contracta area, A_2 , is less than the area of the hole, A_0 , by an unknown amount. Thus, $A_2=C_c A_0$, where C_c is the contraction coefficient ($C_c < 1$).

Secondly, a head loss occurs due to the swirling flow and turbulent motion near the orifice plate that cannot be calculated theoretically. Therefore, to account for those losses an orifice discharge coefficient, C_0 , is utilized. As a result, the equation by which the discharge is calculated becomes:

$$Q = C_0 Q_{ideal} = C_0 A_0 \sqrt{\frac{2(p_1 - p_2)}{\rho(1 - \phi^4)}} \quad (\text{A.2})$$

where $\phi = 0.5$ is defined as $\phi = D_0/D_1$ with D_0 being the orifice meter throat diameter and D_1 is the pipe inside diameter on which the orifice meter is located, and $A_0 = \pi D_0^2/4$ is the area of the hole in the orifice plate. The coefficient, C_0 is a function of $\phi = D_0/D_1$ and the Reynolds number $Re = \rho V_t D_t / \mu$ with $V_t = Q/A_t$. The value of C_0 depends on the specific construction of the orifice meter.

For the determination of the value of C_0 , the distinct values specified by TSE are used by adapting a proper trend curve for the discharge calculations (Figure A.2).

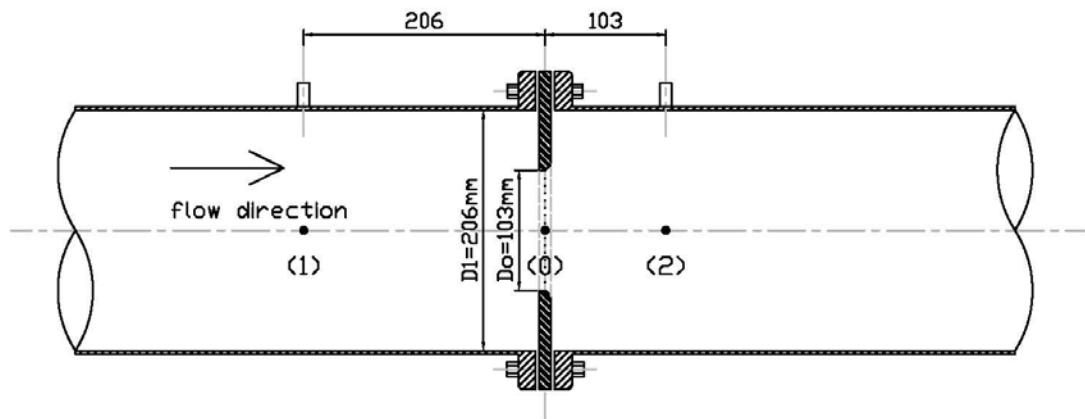


Figure A.1 Orifice-meter details

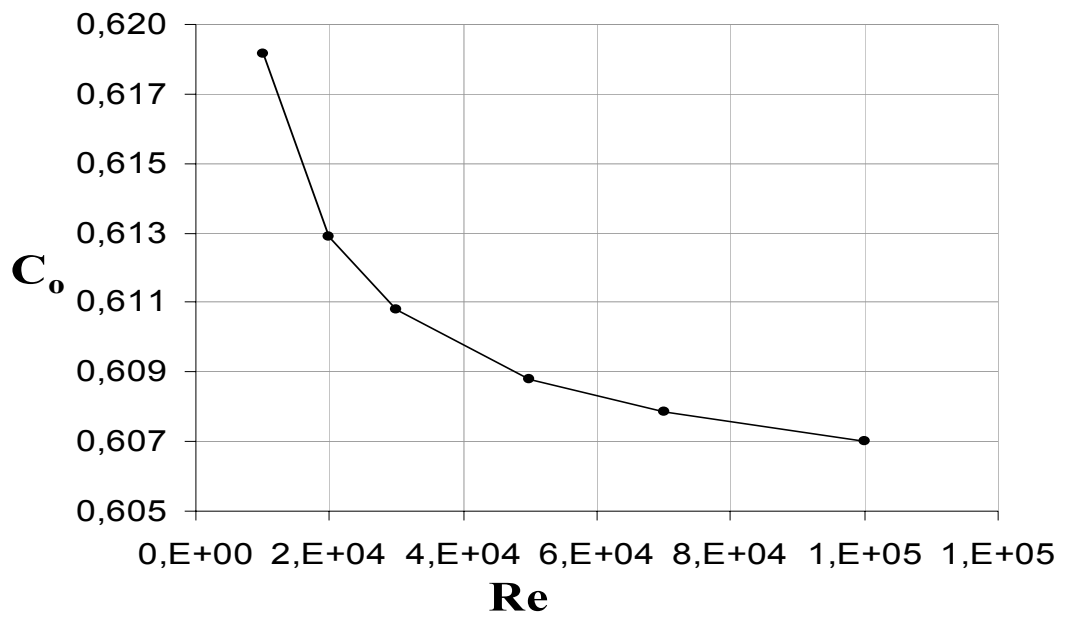


Figure A.2 Variation of C_0 with respect to Reynolds number

APPENDIX B

UNCERTAINTY ANALYSIS OF EXPERIMENTAL DATA

Since no measurements are perfect, a mechanism is necessitated to determine the rate of the errors made during measurements. As a common agreement in engineering, uncertainty analysis is the appropriate concept to express the errors. Therefore, uncertainty analysis was performed for Q, E_{GC1} and S values by using the following basic definitions;

$$\delta R = \left\{ \sum_1^n ((\partial R / \partial x_i) \delta x_i)^2 \right\}^{\frac{1}{2}} \quad (\text{B.1})$$

$$\delta R = \left\{ \sum_1^n [R(x_i + \delta x_i) - R(x_i)]^2 \right\}^{\frac{1}{2}} \quad (\text{B.2})$$

where R denotes the result computed from the n measurements $x_1, \dots, x_i, \dots, x_n$. δR is the overall uncertainty interval of R and δx_i is the precision error associated with x_i .

B.1 UNCERTAINTY ANALYSIS FOR Q

Equation A.2 used for the discharge calculation can be rewritten as follows;

$$Q = C_0 Q_{ideal} = \frac{C_0 A_0}{(1 - \phi^4)^{\frac{1}{2}}} \sqrt{2g\Delta h} \quad (\text{B.3})$$

In the present study, discharge, Q is computed from one measurand, that is, Δh . Then, Equation B.2 becomes

$$\delta Q = Q(\Delta h + \delta\Delta h) - Q(\Delta h) \quad (\text{B.4})$$

$$\delta Q = \frac{C_0 A_0}{(1 - \phi^4)^{\frac{1}{2}}} \sqrt{2g(\Delta h + \delta\Delta h)} - \frac{C_0 A_0}{(1 - \phi^4)^{\frac{1}{2}}} \sqrt{2g(\Delta h)} \quad (\text{B.5})$$

where $\delta\Delta h$ is the precision error associated with Δh . Since the minimum segment of the instrument used for Δh measurements is ± 0.001 m, $\delta\Delta h$ can be taken as 0.002 m.

Overall uncertainty values for the discharge, δQ_j can be normalized by the corresponding discharge values, Q_j as depicted in Figure B.1. (where j is the measurement number for Q values taken for the present study.)

From the figure, one may discern that the relative uncertainty decreases as the Reynolds number increases.

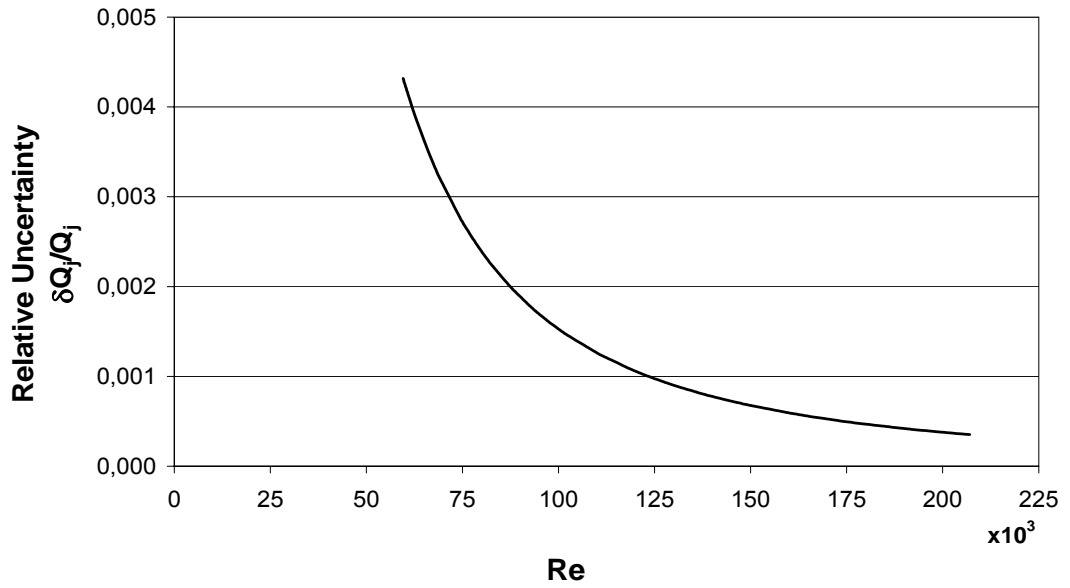


Figure B.1 Relative Uncertainty for Q_j values vs. Re

B.2 UNCERTAINTY ANALYSIS FOR ΔE_{GC1}

ΔE_{GC1} is calculated as follows;

$$\Delta E_{GC1} = \left(y_G + \frac{V_G^2}{2g} \right) - \left(y_{C1} + \frac{V_{C1}^2}{2g} \right) \quad (B.6)$$

In present study, ΔE_{GC1} is computed from three measurands; Δh , y_{C1} and y_G . Then, Equation B.2 becomes

$$\delta \Delta E_{GC1} = \left\{ \sum_1^3 \left[\Delta E_{GC1}(x_i + \delta x_i) - \Delta E_{GC1}(x_i) \right]^2 \right\}^{\frac{1}{2}} \quad (B.7)$$

Then, Equation B.7 can be also written as follows;

$$\delta\Delta E_{Gd} = \left\{ (\Delta E_{Gd}(\Delta h + \delta\Delta h) - \Delta E_{Gd}(\Delta h))^2 + (\Delta E_{Gd}(y_{C1} + \delta y_{C1}) - \Delta E_{Gd}(y_{C1}))^2 + (\Delta E_{Gd}(y_G + \delta y_G) - \Delta E_{Gd}(y_G))^2 \right\}^{1/2} \quad (\text{B.8})$$

where $\delta\Delta h$, δy_{C1} , δy_G are the precision errors associated with Δh , y_{C1} , y_G , respectively. Since the minimum segment of the instrument used for Δh , y_{C1} , y_G measurements are $\pm 0.001\text{m}$, $\pm 0.0001\text{m}$ and $\pm 0.0001\text{m}$ respectively, random errors for $\delta\Delta h$, δy_{C1} , δy_G can be taken as $\pm 0.002\text{m}$, $\pm 0.0002\text{m}$ and $\pm 0.0002\text{m}$ respectively.

Overall uncertainty values of $\delta\Delta E_{GC1}$ can be normalized by the corresponding ΔE_{GC1} values as depicted in Figure B.2.

From the figure, one may discern that the relative uncertainty interval of ΔE_{GC1} is in the range of 0.017 - 0.035.

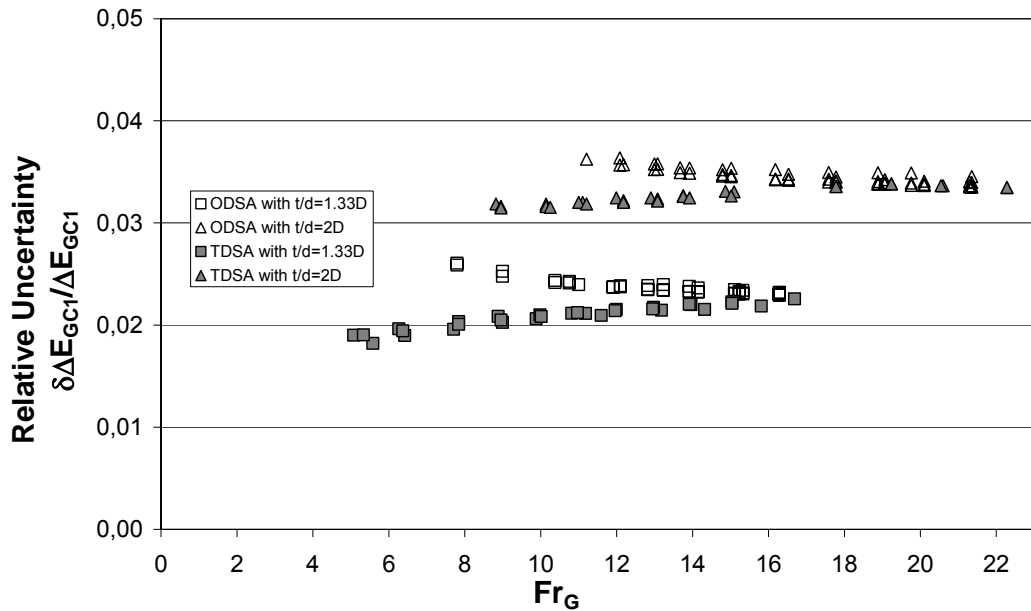


Figure B.2 $\delta\Delta E_{GC}/\Delta E_{GC}$ vs. Fr_G for the present data

B.3 UNCERTAINTY ANALYSIS FOR S

S is calculated as follows;

$$S = \left(y_A + \frac{V_A^2}{2g} \right) - \left(y_{C1} + \frac{V_{C1}^2}{2g} \right) - \beta \Delta E_{jA} \quad (\text{B.9})$$

In the present study, S is computed from four measurands; x, Δh, y_A and y_{C1}. (β is computed from one measurand; x, V_A is computed from two measurands; Δh and y_A, and V_{C1} is computed from two measurands Δh and y_{C1}.) Then, Equation B.2 becomes

$$\delta S = \left\{ \sum_1^4 [S(x_i + \delta x_i) - S(x_i)]^2 \right\}^{\frac{1}{2}} \quad (\text{B.10})$$

where x₁=x and δx₁= δx (the precision error associated with x and equal to ±0.002m), x₂=Δh and δx₂= δΔh (the precision error associated with Δh and equal to ±0.002m), x₃=y_A and δx₃=δy_A (the precision error associated with y_A and equal to ±0.0002m), x₄=y_{C1} and δx₄=δy_{C1} (the precision error associated with y_{C1} and equal to ±0.0002m).

Overall uncertainty values of δS can be normalized by the corresponding S values as depicted in Figure B.3.

From the figure, one may discern that the relative uncertainty interval of S is in the range of 0.01 - 0.07.

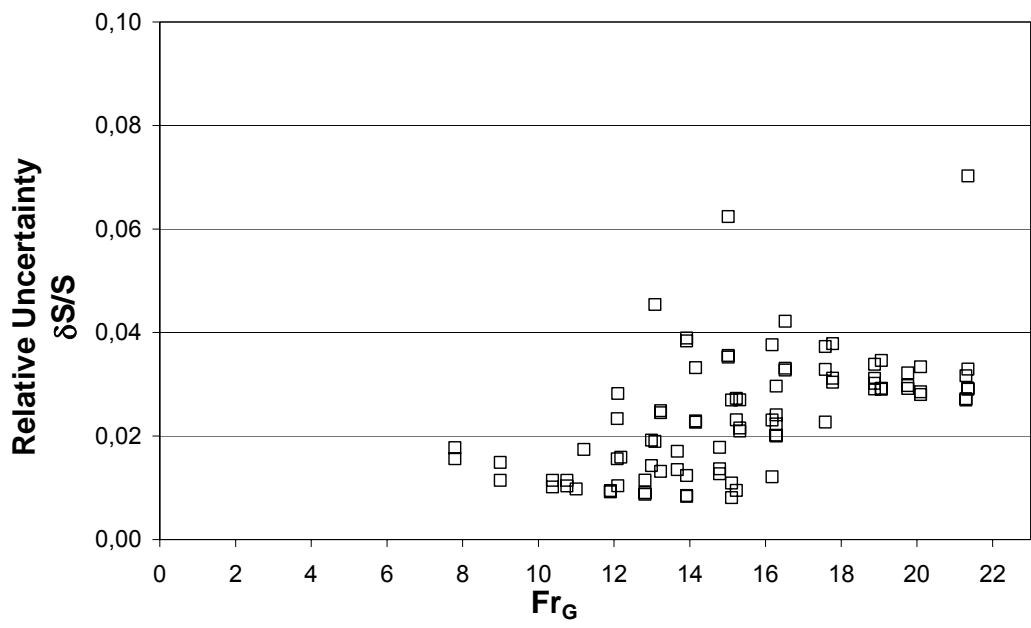


Figure B.3 $\delta S/S$ vs. Fr_G for the present data

APPENDIX C

EXPERIMENTAL DATA

The measurements taken with ODSA are given in Table C.1.

Table C.1 Experimental Data with ODSA

Reference	Q (m ³ /s)	y _{C1} (cm)	y _A (cm)	S/E _A	ΔE _{GC1} /E _G
2D-99-21,34-0	0,026	9,283	1,683	0,739	0,950
2D-99-21,34-2,1	0,026	11,883	1,817	0,645	0,947
2D-99-21,34-4,5	0,026	16,083	1,983	0,404	0,937
2D-99-21,34-6,9	0,026	21,183	2,083	0,102	0,921
2D-99-19,75-0	0,024	8,883	1,883	0,582	0,944
2D-99-19,75-3,25	0,024	12,717	2,083	0,452	0,938
2D-99-19,75-6,3	0,024	20,483	2,150	0,049	0,911
2D-99-18,88-0	0,023	9,183	1,983	0,461	0,940
2D-99-18,88-1,5	0,023	10,483	2,083	0,371	0,939
2D-99-18,88-3,25	0,023	12,483	2,217	0,269	0,933
2D-99-18,88-5,7	0,023	18,717	2,250	0,058	0,910
2D-99-17,58-0	0,022	9,117	2,017	0,338	0,934
2D-99-17,58-2,7	0,022	11,983	2,083	0,245	0,927
2D-99-17,58-5,1	0,022	16,317	2,183	0,079	0,908
2D-99-16,17-0	0,020	8,117	1,983	0,229	0,927
2D-99-16,17-2,1	0,020	9,383	2,083	0,155	0,925
2D-99-16,17-4,5	0,020	14,917	2,183	0,085	0,901
2D-99-14,78-0	0,018	8,483	1,950	0,157	0,916
2D-99-14,78-1,5	0,018	9,683	2,017	0,150	0,912
2D-99-14,78-3,25	0,018	12,050	2,117	0,119	0,900

Table C.1 Experimental Data with ODSA (continued)

Reference	Q (m ³ /s)	y _{C1} (cm)	y _A (cm)	S/E _A	DE _{GCI} /E _G
2D-99-13,67-0	0,017	8,317	1,983	0,162	0,907
2D-99-13,67-2,1	0,017	10,617	2,083	0,134	0,895
2D-99-12,98-0	0,016	8,317	2,017	0,163	0,899
2D-99-12,98-2,1	0,016	10,583	2,150	0,128	0,885
2D-99-12,08-0	0,015	8,217	2,083	0,164	0,887
2D-99-12,08-2,1	0,015	10,517	2,183	0,115	0,870
2D-99-11,20-0	0,014	8,117	2,050	0,160	0,873
2D-66-21,29-0	0,026	10,483	1,783	0,771	0,949
2D-66-21,29-2,1	0,026	12,317	1,883	0,715	0,946
2D-66-21,29-4,5	0,026	16,383	1,983	0,455	0,936
2D-66-20,09-0	0,025	10,217	1,817	0,705	0,945
2D-66-20,09-2,1	0,025	12,017	1,850	0,659	0,941
2D-66-20,09-4,5	0,025	15,017	1,917	0,423	0,933
2D-66-19,06-0	0,023	9,883	1,817	0,642	0,940
2D-66-19,06-2,1	0,023	11,583	1,917	0,588	0,937
2D-66-19,06-3,9	0,023	14,383	2,083	0,324	0,928
2D-66-17,77-0	0,022	9,483	1,783	0,571	0,935
2D-66-17,77-2,1	0,022	10,883	1,983	0,482	0,931
2D-66-17,77-3,9	0,022	13,917	2,017	0,284	0,921
2D-66-16,52-0	0,020	8,883	1,817	0,475	0,928
2D-66-16,52-2,1	0,020	10,117	1,883	0,430	0,925
2D-66-16,52-3,9	0,020	13,117	2,017	0,222	0,913
2D-66-15,01-0	0,018	8,517	1,850	0,367	0,918
2D-66-15,01-2,1	0,018	9,617	2,017	0,296	0,915
2D-66-15,01-3,9	0,018	13,117	2,117	0,108	0,897
2D-66-13,91-0	0,017	8,417	1,817	0,291	0,909
2D-66-13,91-2,1	0,017	11,050	1,983	0,129	0,895
2D-66-13,07-0	0,016	8,617	1,783	0,205	0,899
2D-66-13,07-2,1	0,016	10,850	1,983	0,123	0,885
2D-66-12,17-0	0,015	8,583	1,817	0,151	0,886

Table C.1 Experimental Data with ODSA (continued)

Reference	Q (m ³ /s)	y _{C1} (cm)	y _A (cm)	S/E _A	DE _{GCI} /E _G
1,33D-66-16,28-0	0,037	12,933	2,833	0,550	0,927
1,33D-66-16,28-1,4	0,037	14,033	2,967	0,498	0,926
1,33D-66-16,28-3	0,037	17,867	3,133	0,282	0,917
1,33D-66-15,32-0	0,034	12,033	2,933	0,441	0,922
1,33D-66-15,32-1,4	0,034	13,767	3,067	0,365	0,919
1,33D-66-15,32-3	0,034	17,533	3,133	0,216	0,908
1,33D-66-14,15-0	0,032	11,133	2,933	0,337	0,913
1,33D-66-14,15-1,4	0,032	12,267	3,033	0,300	0,912
1,33D-66-14,15-3	0,032	16,933	3,133	0,141	0,897
1,33D-66-13,22-0	0,030	10,833	2,867	0,278	0,905
1,33D-66-13,22-1,4	0,030	12,067	3,067	0,221	0,903
1,33D-66-13,22-3	0,030	16,933	3,167	0,116	0,884
1,33D-66-12,09-0	0,027	11,867	2,933	0,178	0,889
1,33D-66-12,09-1,4	0,027	12,967	3,033	0,156	0,885
1,33D-66-10,75-0	0,024	10,767	2,933	0,172	0,872
1,33D-66-10,75-1,4	0,024	11,933	3,067	0,159	0,866
1,33D-66-10,37-0	0,023	9,733	2,900	0,179	0,868
1,33D-66-10,37-1,4	0,023	11,367	3,033	0,163	0,861
1,33D-66-8,993-0	0,020	8,967	2,967	0,182	0,841
1,33D-66-8,993-1,4	0,020	11,233	3,033	0,144	0,826
1,33D-66-7,794-0	0,018	9,367	3,067	0,156	0,800
1,33D-66-7,794-1,4	0,018	9,933	3,133	0,139	0,794
1,33D-99-16,28-0	0,037	11,733	2,833	0,557	0,928
1,33D-99-16,28-1,4	0,037	13,933	2,967	0,347	0,926
1,33D-99-16,28-3	0,037	16,933	3,067	0,163	0,919
1,33D-99-15,23-0	0,034	11,233	2,933	0,309	0,921
1,33D-99-15,23-1,4	0,034	13,167	2,967	0,184	0,919
1,33D-99-15,23-3	0,034	16,267	3,133	0,139	0,912
1,33D-99-15,10-0	0,034	11,133	2,933	0,187	0,920
1,33D-99-15,10-1,4	0,034	12,533	3,033	0,161	0,919

Table C.1 Experimental Data with ODSA (continued)

Reference	Q (m³/s)	y_{C1}(cm)	y_A(cm)	S/E_A	DE_{GCI}/E_G
1,33D-99-15,10-3	0,034	17,967	3,100	0,122	0,904
1,33D-99-13,91-0	0,031	10,667	2,933	0,166	0,911
1,33D-99-13,91-1,4	0,031	11,867	2,967	0,165	0,910
1,33D-99-13,91-3	0,031	17,667	3,000	0,115	0,891
1,33D-99-12,82-0	0,029	10,333	2,933	0,172	0,901
1,33D-99-12,82-1,4	0,029	11,667	2,967	0,167	0,899
1,33D-99-12,82-2,6	0,029	15,167	3,067	0,135	0,886
1,33D-99-11,90-0	0,027	10,433	2,967	0,175	0,890
1,33D-99-11,90-1,4	0,027	11,133	3,000	0,172	0,889
1,33D-99-11,00-0	0,025	10,133	2,933	0,177	0,878

The measurements taken with TDSA are given in Table C.2.

Table C. 2 Experimental Data with TDSA

Reference	Q (m ³ /s)	y _G [*] (cm)	y _{Cl} (cm)	DE _{GCl} /E _G
1,33D-66-133-16,68	0,038	5,367	11,183	0,931
1,33D-66-133-15,81	0,036	12,867	11,483	0,928
1,33D-66-133-14,31	0,032	15,333	11,083	0,920
1,33D-66-133-13,17	0,030	15,133	11,483	0,911
1,33D-66-133-11,59	0,026	17,033	11,083	0,897
1,33D-66-133-11,18	0,025	15,333	10,517	0,892
1,33D-66-133-9,880	0,022	16,467	10,583	0,875
1,33D-66-133-8,993	0,020	16,867	10,583	0,859
1,33D-66-133-7,707	0,017	17,233	10,617	0,829
1,33D-66-133-6,422	0,014	16,367	10,117	0,790
1,33D-66-133-5,579	0,013	15,467	8,817	0,771
1,33D-66-99-15,03	0,034	9,133	12,567	0,922
1,33D-66-99-13,96	0,031	11,533	12,367	0,914
1,33D-66-99-12,97	0,029	13,300	12,133	0,907
1,33D-66-99-11,98	0,027	14,267	12,067	0,896
1,33D-66-99-10,81	0,024	15,733	12,167	0,881
1,33D-66-99-9,981	0,022	15,767	11,967	0,868
1,33D-66-99-8,880	0,020	15,567	12,167	0,843
1,33D-66-99-7,837	0,018	15,633	11,267	0,823
1,33D-66-99-6,262	0,014	15,067	10,567	0,772
1,33D-66-99-5,074	0,011	14,100	9,567	0,723
1,33D-99-133-15,03	0,034	10,400	12,250	0,922
1,33D-99-133-13,91	0,031	11,100	11,817	0,915
1,33D-99-133-12,94	0,029	14,133	11,583	0,908
1,33D-99-133-11,95	0,027	14,533	10,917	0,900
1,33D-99-133-10,97	0,025	14,967	11,217	0,887
1,33D-99-133-10,01	0,023	15,833	10,817	0,875
1,33D-99-133-8,955	0,020	16,033	10,817	0,856
1,33D-99-133-7,837	0,018	15,633	10,183	0,833
1,33D-99-133-6,369	0,014	15,067	9,817	0,787

Table C.2 Experimental Data with TDSA (continued)

Reference	Q (m ³ /s)	y _G *(cm)	y _{Cl} (cm)	DE _{GCl} /E _G
1,33D-99-133-5,333	0,012	13,933	9,117	0,746
2D-149-200-22,27	0,027	1,220	11,283	0,951
2D-149-200-20,59	0,025	1,220	11,000	0,945
2D-149-200-19,23	0,024	1,220	10,960	0,939
2D-149-200-17,77	0,022	4,000	10,950	0,932
2D-149-200-14,86	0,018	7,633	10,283	0,914
2D-149-200-13,75	0,017	9,333	9,983	0,906
2D-149-200-12,90	0,016	10,167	9,883	0,898
2D-149-200-11,98	0,015	10,433	10,117	0,884
2D-149-200-11,10	0,014	11,000	9,250	0,878
2D-149-200-10,13	0,012	11,233	9,183	0,861
2D-149-200-8,819	0,011	10,783	8,583	0,836
2D-99-149-22,27	0,027	1,220	11,433	0,951
2D-99-149-20,54	0,025	1,220	11,033	0,945
2D-99-149-19,23	0,024	1,220	10,867	0,940
2D-99-149-17,77	0,022	4,000	10,667	0,933
2D-99-149-15,08	0,018	7,867	10,467	0,916
2D-99-149-13,75	0,017	9,867	10,267	0,905
2D-99-149-13,07	0,016	10,467	9,833	0,900
2D-99-149-12,17	0,015	10,967	9,900	0,889
2D-99-149-11,00	0,013	11,267	9,667	0,873
2D-99-149-10,13	0,012	11,833	9,333	0,860
2D-99-149-8,948	0,011	11,333	8,833	0,838
2D-99-200-15,01	0,018	9,533	10,383	0,916
2D-99-200-13,91	0,017	10,267	10,217	0,907
2D-99-200-13,07	0,016	11,233	9,983	0,900
2D-99-200-12,17	0,015	11,433	9,817	0,890
2D-99-200-11,20	0,014	11,767	9,817	0,876
2D-99-200-10,25	0,013	11,833	9,117	0,865
2D-99-200-8,948	0,011	11,433	8,617	0,841